Inaugural dissertation

for

obtaining the doctoral degree

of the

Combined Faculty of Mathematics, Engineering and Natural Sciences

of the

Ruprecht – Karls – University

Heidelberg

Presented by

M. Sc. Sabrina Schütz

born in Dieburg, Germany

Oral examination: 15.09.2023

Characterization of cancer-associated fibroblast heterogeneity in squamous cell carcinoma progression using single-cell RNA sequencing

Abstract

Cutaneous squamous cell carcinoma (cSCC) is a keratinocyte cancer with a rapidly increasing incidence and one of the most common cancer types in the fair-skinned population. Chronic exposure to ultraviolet radiation (UVR) is its main risk factor and can lead to the development of a premalignant skin lesion, actinic keratosis (AK), which might further progress into cSCC. In addition, invasive cSCC can also develop from the *in situ* carcinoma Bowen's disease (BD). During this progression, resident dermal fibroblasts are transformed into cancer-associated fibroblasts (CAFs) that are known to promote tumorigenesis. However, a detailed characterization of cSCC-related CAFs with respect to their fibroblast subpopulation-specific origin, heterogeneity, and tumor-promoting functions was still missing. Therefore, in this thesis, more than 115,000 single-cell transcriptomes from healthy human skin, BD and cSCC samples were analyzed. The results revealed two main CAF subpopulations with distinct functions and origins. Inflammatory CAFs (iCAFs) seemed to develop mainly from pro-inflammatory fibroblasts and presented immunoregulatory functions, including cellular interactions with immune cells in the tumor microenvironment (TME). On the other hand, myofibroblastic CAFs (myCAFs) were observed to originate mainly from healthy mesenchymal fibroblasts and were involved in extracellular matrix (ECM) remodeling processes. Furthermore, multiplexed RNA fluorescence *in situ* hybridization (FISH) assays not only confirmed both CAF subpopulations in human BD and cSCC, but also provided valuable information about the time window of CAF activation, as no CAFs could be observed in AK tissue sections. Interestingly, these findings could not be transferred to basal cell carcinoma (BCC), the second major keratinocyte cancer. Taken together, this thesis provides novel insights into CAF development, stratification, and functions during cSCC initiation and progression.

Zusammenfassung

Das kutane Plattenepithelkarzinom (PEK) gehört zu den häufigsten Krebsformen der hellhäutigen Bevölkerung mit stark steigenden Inzidenzen weltweit. Der größte Risikofaktor stellt dabei die chronische Exposition mit Ultraviolettstrahlung dar, was zunächst zur Entstehung einer aktinischen Keratose (AK) führen kann, die als präkanzeröse Hautläsion definiert wird. Unbehandelt kann sich daraus jedoch ein PEK entwickeln. Außerdem kann auch aus einem *in situ* Karzinom, dem sogenannten Morbus Bowen (MB), ein invasives PEK entstehen. Während der Entwicklung eines PEKs, werden dermale Fibroblasten zu Krebs-assoziierten Fibroblasten (cancer-associated fibroblasts, CAFs) transformiert, die bekanntermaßen die Tumorentwicklung unterstützen. Allerdings gab es bis jetzt noch keine detaillierte Charakterisierung dieser CAFs in PEKs, mit Bezug auf deren Ursprung, Heterogenität und ihre Tumor-unterstützenden Funktionen. Daher wurden in dieser Dissertation mehr als 115.000 Transkriptome einzelner Zellen aus gesunder menschlicher Haut, sowie aus MB und PEK Proben analysiert. Die Ergebnisse zeigten zwei CAF Gruppen mit unterschiedlichen Funktionen und zellulären Ursprüngen. Inflammatorische CAFs (iCAFs) scheinen sich aus gesunden pro-inflammatorischen Fibroblasten zu entwickeln und zeigen immunregulatorische Funktionen, einschließlich zellulärer Interaktionen mit Immunzellen im Tumorgewebe. Andererseits wurde beobachtet, dass myofibroblastische CAFs (myCAFs) von gesunden mesenchymalen Fibroblasten abstammen und an der Organisation von extrazellulärer Matrix beteiligt sind. Darüber hinaus bestätigten Multiplex RNA Fluoreszenz *in situ* Hybridisierungsexperimente nicht nur das Vorhandensein beider CAF Gruppen in menschlichen MB und PEK Schnittpräparaten, sondern lieferten auch wertvolle Informationen über das Zeitfenster der CAF-Aktivierung, da in AK Proben keine klaren iCAFs und myCAFs detektiert wurden. Interessanterweise konnten diese Ergebnisse nicht auf das Basalzellkarzinom übertragen werden. Insgesamt bietet diese Dissertation neue Einblicke in die Entwicklung und die Eigenschaften von CAFs während der PEK Entstehung und seines Fortschreitens.

Table of Contents

List of Figures

List of Tables

List of Abbreviations

2/3D	Two/three-dimensional
6-4PP	Pyrimidine-6,4-pyrimidone dimer
%	Percent
°C	Degree Celsius
μm	Micrometer
α-SMA	Alpha smooth muscle actin
ACTA2	Actin Alpha 2, Smooth Muscle
ADM	Adrenomedullin
AK	Actinic keratosis
ALA-PDT	5-aminolevulinic acid-mediated photodynamic therapy
ANGPTL2	Angiopoietin Like 2
ANOVA	Analysis of variance
apCAF	Antigen-presenting CAF
APCDD1	APC Down-Regulated 1
APOE	Apolipoprotein E
APM	Arrector pili muscle
ASPN	Asporin
BCC	Basal cell carcinoma
BD	Bowen's disease
BGN	Biglycan
BM-MSC	Bone marrow-derived mesenchymal stem cell
BMP	Bone Morphogenetic Protein
bp	Base pair
C3	Complement C3
CAF	Cancer-associated fibroblast
CAF_{adi}	Adipogenic CAF
CAF_{ap}	Antigen-presenting CAFs
CAF_{EndMT}	Endothelial-mesenchymal transition CAF
CAF_{infla}	Inflammatory CAF
CAF_{myo}	Myofibroblastic CAF
CAF_{PN}	Peripheral nerve-like CAF
CALCR(L)	Calcitonin Receptor (Like Receptor)
CCA	Canonical correlation analysis
cCAF	Cycling CAF
CCDC80	Coiled-Coil Domain Containing 80

CCL19	C-C Motif Chemokine Ligand 19
CCN5	Cellular Communication Network Factor 5
CD3D	CD3 Delta Subunit Of T-Cell Receptor Complex
CDKN2A	Cyclin Dependent Kinase Inhibitor 2A
cDNA	Coding DNA
chr	Chromosome
CLDN5	Claudin 5
cm^2	Square centimeter
CNV	Copy number variation
COL11A1	Collagen Type XI Alpha 1 Chain
COL13A1	Collagen Type XIII Alpha 1 Chain
COL14A1	Collagen Type XIV Alpha 1 Chain
COL18A1	Collagen Type XVIII Alpha 1 Chain
COL1A1/2	Collagen Type I Alpha 1/2 Chain
COL23A1	Collagen Type XXIII Alpha 1 Chain
COL24A1	Collagen Type XXIV Alpha 1 Chain
COL3A1	Collagen Type III Alpha 1 Chain
COL5A1/2	Collagen Type V Alpha 1/2 Chain
COL6A1	Collagen Type VI Alpha 1 Chain
CPA3	Carboxypeptidase A3
CPD	Cyclobutane pyrimidine dimer
CRYAB	Crystallin Alpha B
cSCC	Cutaneous squamous cell carcinoma
CTHRC1	Collagen Triple Helix Repeat Containing 1
CTNNB1	Catenin Beta 1
CXCL1/2/3/12/13	C-X-C Motif Chemokine Ligand 1/2/3/12/13
CXCR4	C-X-C Motif Chemokine Receptor 4
DAPI	4′,6-diamidino-2-phenylindole
dCAF	Development-associated CAF
DCN	Decorin
DIO2	Iodothyronine Deiodinase 2
DKFZ	Deutsches Krebsforschungszentrum
DNA	Deoxyribonucleic acid
DP	Dermal papilla
Dr.	Doctor
DS	Dermal sheath
DWAT	Dermal white adipose tissue

e.g.	For example (exempli gratia)
EC	Endothelial cell
ECM	Extracellular matrix
EDC	Electrodessication and curettage
EFEMP1	EGF Containing Fibulin Extracellular Matrix Protein 1
EGF(R)	Epidermal Growth Factor (Receptor)
EH	Chronically UVR-exposed healthy
EMT	Epithelial-mesenchymal transition
EndMT	Endothelial-mesenchymal transition
ERK1/2	Extracellular Signal-Regulated Kinase 1/2
ESCC	Esophageal squamous cell carcinoma
ESG	Eccrine sweat gland
EV	Extracellular vesicle
FAK	Focal Adhesion Kinase
FAP	Fibroblast Activation Protein Alpha
FFPE	Formalin-fixed paraffin-embedded
FGF	Fibroblast Growth Factor
FN1	Fibronectin 1
FSP1	Fibroblast-Specific Protein-1
G1	Gap 1
G2	Gap 2
GEM	Gel bead-in-emulsion
GEO	Gene Expression Omnibus
GLI1	GLI Family Zinc Finger 1
GO	Gene ontology
GPC3	Glypican 3
GSEA	Gene set enrichment analysis
h	Hour
H2AK119ub	Ubiquitination of histone H2A at lysine 119
H&E	Hematoxylin and eosin
HBA1	Hemoglobin Subunit Alpha 1
HCC	Hepatocellular carcinoma
HES1	Hes Family BHLH Transcription Factor 1
HGD-IPMN	High-grade intraductal papillary mucinous neoplasm
HGF	Hepatocyte Growth Factor
HIP1	Huntingtin Interacting Protein 1
HSP90AA1	Heat Shock Protein 90 Alpha Family Class A Member 1

HSPA1A	Heat Shock Protein 70 Family Member 1A
i.e.	That is (id est)
iCAF	Inflammatory CAF
ID1	Inhibitor Of DNA Binding 1
IF	Immunofluorescence
IFI6	Interferon Alpha Inducible Protein 6
IGF1	Insulin Like Growth Factor 1
IGLL5	Immunoglobulin Lambda Like Polypeptide 5
IL1β/6/17A/22	Interleukin 1 Beta/6/17A/22
IL7R	Interleukin 7 Receptor
ITGA5	Integrin Subunit Alpha 5
ITGB1	Integrin Subunit Beta 1
JAK	Janus Kinase
JUN(D)	Jun(D) Proto-Oncogene, AP-1 Transcription Factor Subunit
KC	Keratinocyte carcinoma
KNN	K-nearest neighbor
KRT	Keratin
LGD-IPMN	Low-grade intraductal papillary mucinous neoplasm
LOX	Lysyl Oxidase
LRIG1	Leucine Rich Repeats And Immunoglobulin Like Domains 1
LUM	Lumican
LYZ	Lysozyme
M	Mitosis
MAPK	Mitogen-Activated Protein Kinase
MCAM	Melanoma Cell Adhesion Molecule
meCAF	Metabolic CAF
med.	Medicinae
MFAP5	Microfibril Associated Protein 5
MGP	Matrix Gla Protein
MHC II	Major histocompatibility class II
min	Minute
MIR203	miRNA 203
MIR21	miRNA 21
miRNA	Micro RNA
MLANA	Melan-A
MMP1/9/11	Matrix Metallopeptidase 1/9/11
MMS	Mohs micrographic surgery

mRNA	Messenger RNA
MSigDB	Molecular Signature Database
mTOR	Mechanistic Target Of Rapamycin
myCAF	Myofibroblastic CAF
MYL4/9	Myosin Light Chain 4/9
N/A	Not available
NCT	National Center for Tumor Diseases
NF-κB	Nuclear Factor Kappa B
NGS	Next generation sequencing
nm	Nanometer
NOTCH1/2/3	Neurogenic locus notch homolog protein 1/2/3
NREP	Neuronal Regeneration Related Protein
OPN	Osteopontin
OSCC	Oral squamous cell carcinoma
p	*p*-value
PBST	Phosphate-buffered saline with Tween-20
PCA	Principal component analysis
PCK	Phosphoenolpyruvate Carboxykinase
PD	PrivatdozentIn
PDAC	Pancreatic ductal adenocarcinoma
PDGF	Platelet-Derived Growth Factor
PDGFRA/B	PDGF Receptor Alpha/Beta
PDPN	Podoplanin
pH	Potential hydrogen
PH	UVR-protected healthy
PI3K	Phosphatidylinositol 3-Kinase
POSTN	Periostin
Prof.	Professor
PTCH1	Patched 1
PTGDS	Prostaglandin D2 Synthase
PTK7	Protein Tyrosine Kinase 7 (Inactive)
RGS5	Regulator Of G Protein Signaling 5
RNA	Ribonucleic acid
RNA FISH	RNA fluorescence *in situ* hybridization
RNA-seq	RNA sequencing
ROS	Reactive oxygen species
RT	Room temperature

S	Synthesis
S100A4/7/9	S100 Calcium Binding Protein A4/7/9
SCC	Squamous cell carcinoma
scOpen Lab	Single-cell Open Lab
SCRG1	Stimulator Of Chondrogenesis 1
scRNA-seq	Single-cell RNA sequencing
SD	Standard deviation
SDC1/4	Syndecan 1/4
SELE	Selectin E
SFRP1	Secreted Frizzled Related Protein 1
SG	Sebaceous gland
SHH	Sonic Hedgehog
SLPI	Secretory Leukocyte Peptidase Inhibitor
SMO	Smoothened, Frizzled Class Receptor
SNP	Single nucleotide polymorphism
SOX9	SRY-Box Transcription Factor 9
SRC	SRC Proto-Oncogene, Non-Receptor Tyrosine Kinase
SSC	Saline-sodium citrate
STAT	Signal Transducer And Activator Of Transcription
SUFU	SUFU Negative Regulator Of Hedgehog Signaling
SULF1	Sulfatase 1
TAGLN	Transgelin
TDO2	Tryptophan 2,3-Dioxygenase
TET2	Tet Methylcytosine Dioxygenase 2
TGF-β1/3	Transforming Growth Factor Beta 1/3
TGFB(R)	Transforming Growth Factor Beta (Receptor)
TIMP	Tissue inhibitor of metallopeptidases
TME	Tumor microenvironment
TNF-α	Tumor Necrosis Factor Alpha
TNN	Tenascin N
TP53	Tumor Protein P53
TPM1	Tropomyosin 1
Treg	Regulatory T cell
TSC22D3	TSC22 Domain Family Member 3
TSPAN8	Tetraspanin 8
UMAP	Uniform manifold approximation and projection
UMI	Unique molecular identifier

UVR	Ultraviolet radiation
v	Version
vCAF	Vasculature-associated CAF
VCAN	Versican
VEGF	Vascular Endothelial Growth Factor
VIM	Vimentin
VWF	Von Willebrand Factor
WIF1	WNT Inhibitory Factor 1
WISP2	WNT1 Inducible Signaling Pathway Protein 2
WNT5A	Wnt Family Member 5A
XBP1	X-Box Binding Protein 1

1. Introduction

1.1 Human skin – General structure

The skin is one of the major sensory organs of the human body and it is constantly exposed to environmental conditions. Therefore, it acts as a physical barrier and fulfills essential functions, such as protection against external pathogens, the synthesis of vitamin D, as well as the regulation of temperature and water content of the organism (Dabrowska *et al.*, 2018; Giacomoni *et al.*, 2009). In general, the skin is composed of the outermost epidermis containing mostly keratinocytes and the subjacent dermis with fibroblasts as the main cell type. Both layers are separated via the basement membrane. In the dermis also vasculature and nerves are located, as well as extracellular matrix (ECM) comprising structural proteins and a hydrated gel of molecules, such as glycosaminoglycans and proteoglycans (Kendall and Feghali-Bostwick, 2014; Ravikanth *et al.*, 2011). The hypodermis or dermal white adipose tissue (DWAT) at the lower end of the skin consists of adipocytes filled with lipids (Figure 1). Furthermore, skin harbors different specialized structures, for example hair follicles, sebaceous glands, and sweat glands (Rognoni and Watt, 2018).
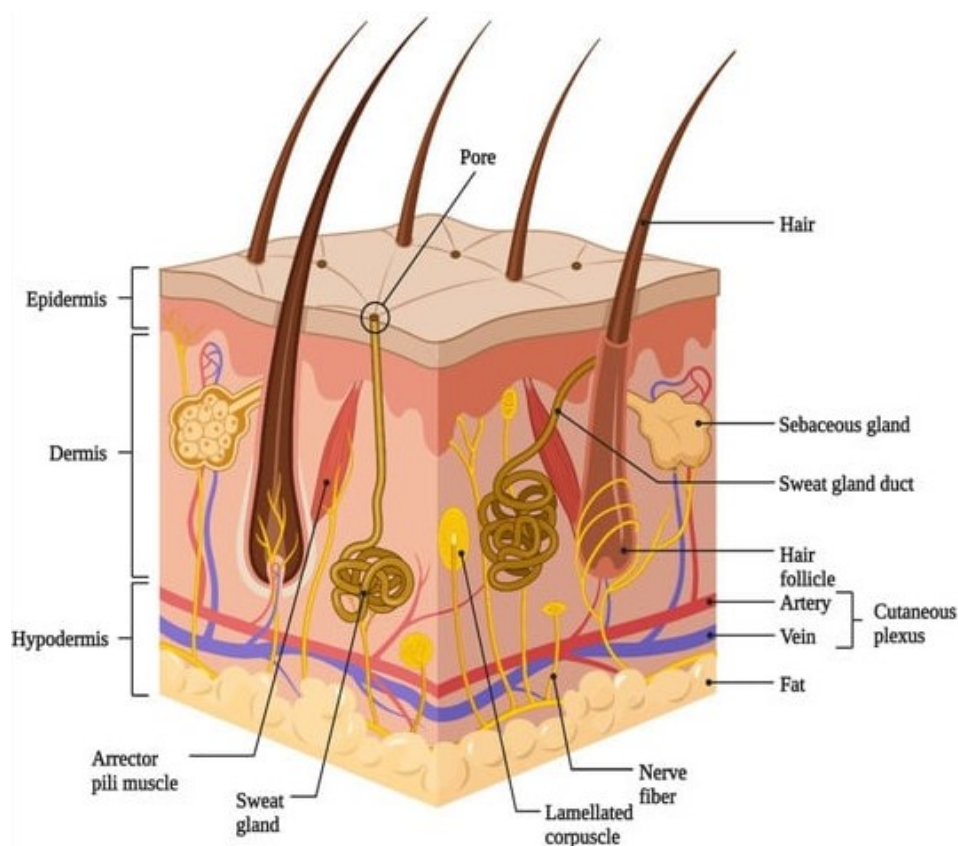
Figure 1. Structure of human skin. Schematic model showing the overall structure of human skin with the main layers epidermis and dermis, as well as the subjacent hypodermis. Specialized structures, such as hair follicles, glands, and sensory nerves, are also depicted (Kolimi *et al.*, 2022).

1.1.1 Differences between male and female skin

Several studies already investigated sex-associated differences for many organs in health and disease (Giacomoni *et al.*, 2009; Regitz-Zagrosek and Kararigas, 2017; Sorge and Totsch, 2017). Understanding this variance is not only important for medical research (e.g. design of clinical trials), but in the case of skin differences also for the cosmetic industry (Rahrovan *et al.*, 2018).

As a steroidogenic tissue, the human skin metabolizes sex hormones, such as testosterone, estrogen, as well as progesterone and also responds to them (Chen *et al.*, 2002; Thiboutot *et al.*, 2003). These processes differ between males and females and, for example aberrant levels of testosterone can lead to androgenic-dependent alopecia in females, as well as hair loss (Chen *et al.*, 2002) and slower healing rates (Gilliver *et al.*, 2007) in males. Also non-sexual hormones can influence human skin, such as urinary cortisol. Its elevated level in males was associated with enriched cutaneous stress, delayed wound healing (Gilliver *et al.*, 2007), and increased ultraviolet radiation (UVR) sensitivity, resulting in immune-suppression and a higher probability of skin cancer development (Damian *et al.*, 2008; Lasithiotakis *et al.*, 2008).

Male and female skin also show differences in sebaceous and sweat gland activities that can be increased by androgenic hormonal stimulation. For males, higher sebum production and increased sweating during exercise was observed, influencing skin surface pH (Green *et al.*, 2000; Jacobi *et al.*, 2005). This can result in a diverse cutaneous microbiome for males and females (Marples, 1982). Furthermore, differences in the ECM and collagen synthesis of male and female dermis lead to thicker skin in males (Shuster *et al.*, 1975).

All these sex-dependent differences in the structure and functions of human skin cause an increased risk of developing autoimmune and inflammatory diseases for females and higher susceptibility to bacterial and viral infections, as well as an elevated skin cancer incidence for males (Damian *et al.*, 2008; Dao and Kazin, 2007; Lasithiotakis *et al.*, 2008).

1.1.2 Skin aging

Human aging is a rapid developing research area with around 300,000 published articles during the last decade, since it is the major cause of many pathologies, especially degenerative diseases (López-Otín *et al.*, 2023a). Furthermore, aging is the most important risk factor for several tumor entities, resulting in raising cancer incidence with age (López-Otín *et al.*, 2023b).

Skin aging is a particularly complex and interesting field because it is not only affected by endogenous factors but also by exogenous factors due to the high environmental exposure of skin (Tobin, 2017). Therefore, it is an appropriate model system to study intrinsic (also known as chronological or physiological) aging and extrinsic aging (Gu *et al.*, 2020). Every part of

human skin undergoes chronological aging over time, influenced by changes in gene expression and the neuroendocrine system or by the development of skin diseases (Bocheva *et al.*, 2019). In addition, external factors, such as UVR, air pollution, and cigarette smoke accelerate skin aging depending on exposure duration and body part (Figure 2). All these components result in a decreased structural integrity and physiological dysfunctions in skin, and can finally lead to the development of skin cancer (Durai *et al.*, 2012; Kammeyer and Luiten, 2015).
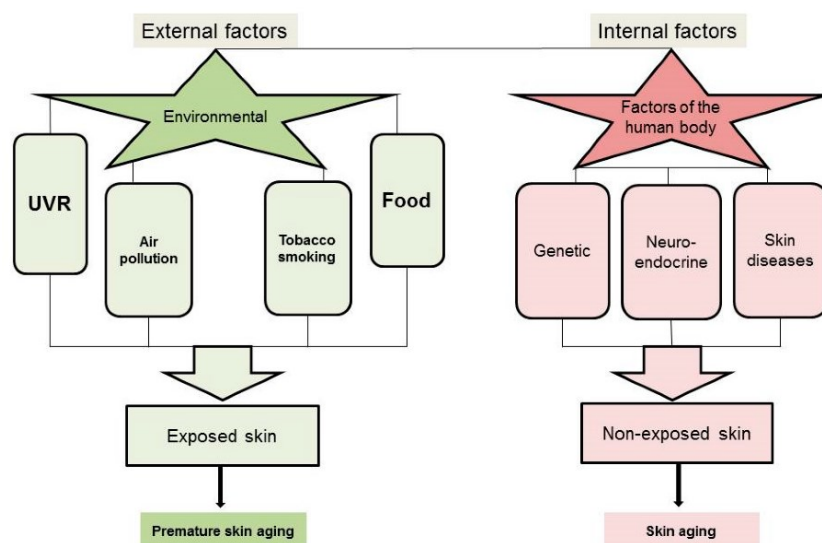
Figure 2. External and internal factors affecting skin aging. Schematic model visualizing different factors accounting for chronological and environment-induced skin aging. Internal factors, such as genetic, the neuroendocrine system, and diseases lead to physiological changes, resulting in skin aging. Depending on body area and exposure time, this chronological aging can be accelerated by the external factors ultraviolet radiation (UVR), air pollution, smoking, and nutrition (Bocheva *et al.*, 2019).

Phenotypic changes of chronological aging are thinner skin, dryness, less elasticity, benign tumors, and fine wrinkles. Moreover, senescent cells accumulate, keratinocytes and fibroblasts show less activity and proliferation, and the ECM structure gets more loose with thinner elastic fibers and less collagen type I/III (Gu *et al.*, 2020; Rittié and Fisher, 2015).

Extrinsic aging, also known as photoaging, is responsible for more than 80% of facial aging with chronic UVR exposure as the main factor (Cavinato and Jansen-Dürr, 2017; Friedman, 2005). It accelerates intrinsic skin aging and promotes hyperpigmentation, deep and thick wrinkles, as well as benign and malignant tumors. Furthermore, degradation of collagen fibers and abnormal deposition of elastic fibers were observed, and slower keratinocyte renewal processes result in a worse skin barrier (Gu *et al.*, 2020).

Another important factor influencing skin aging is the production of reactive oxygen species (ROS) during the mitochondrial metabolism of oxygen (Gu *et al.*, 2020). By intrinsic processes, around 1.5-5% of the cutaneous oxygen consumption is converted to ROS (Poljšak *et al.*, 2012) and antioxidant systems, including vitamin C and E, maintain a dynamic balance

between ROS production and clearance (Obrador *et al.*, 2019). However, UVR exposure can alter these mechanisms, leading to oxidative stress (Figure 3). High levels of ROS can cause direct cellular damage and also activate distinct pathways, such as MAPK and NF-κB signaling (Gu *et al.*, 2020). They then lead to increased expression of matrix metallopeptidases (MMPs), which act as proteolytic enzymes, as well as inflammation mediating cytokines (Kammeyer and Luiten, 2015; Lephart, 2016; Wang *et al.*, 2019b). These molecular changes result in reduced collagen production, increased ECM degradation, and different inflammatory responses, ultimately promoting premature skin aging, as well as skin tumorigenesis (Calcinotto *et al.*, 2019; Kammeyer and Luiten, 2015).
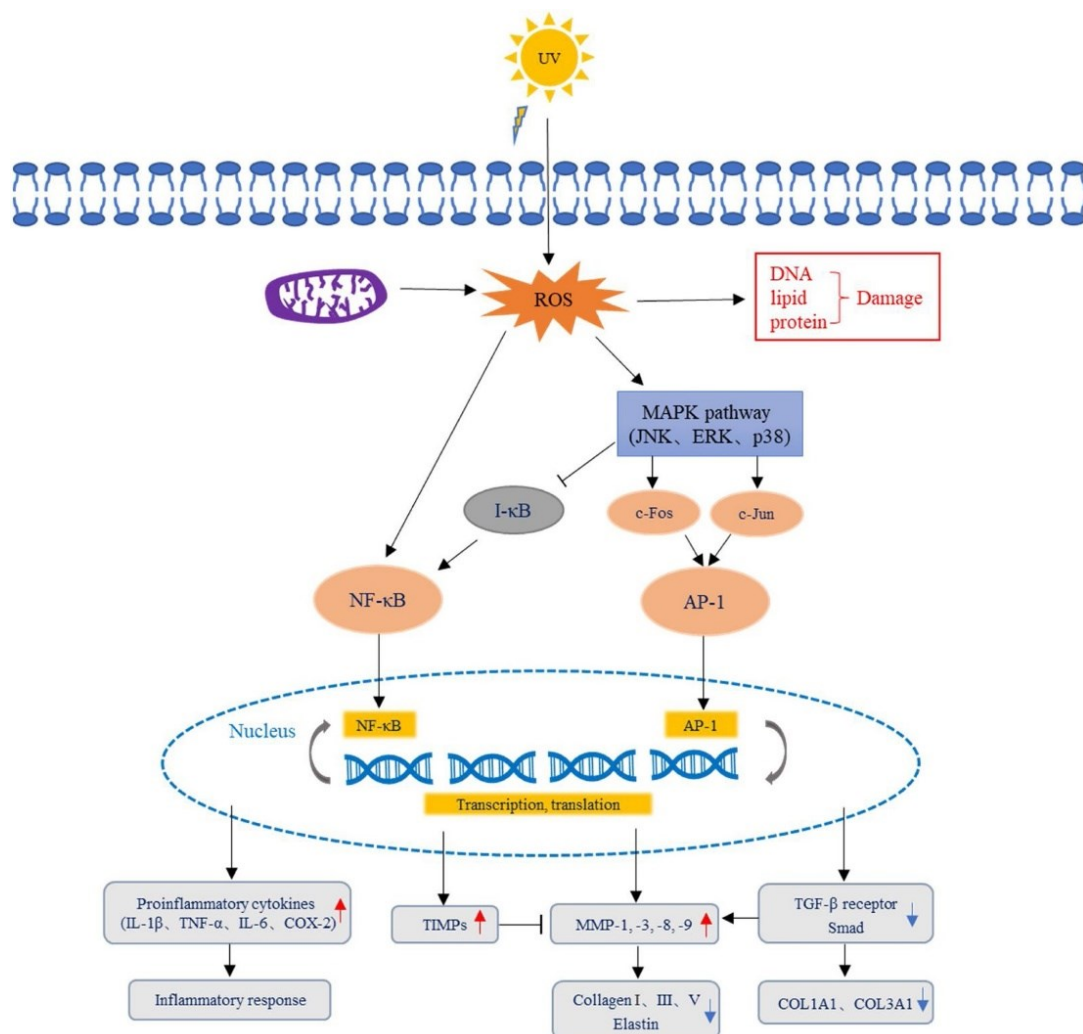
Figure 3. Oxidative stress can promote premature skin aging. Under physiological conditions, reactive oxygen species (ROS) are produced mainly as a byproduct of the mitochondrial electron transport chain. Ultraviolet radiation (UVR) can lead to extensive ROS levels, inducing cellular oxidative stress. This might damage the cells directly and also activates MAPK and NF-κB signaling, resulting in transcriptional and translational changes. Downstream effects of these pathways include inflammatory responses, enriched degradation of extracellular matrix (ECM) by matrix metallopeptidases (MMPs), and reduced synthesis of collagen type I and III. TIMP: Tissue inhibitor of metallopeptidases (Gu *et al.*, 2020).

1.1.3 Epidermal structure and differentiation

The human epidermis is a stratified squamous epithelium with the outermost cornified layer known as stratum corneum, and the subjacent granular, spinous, and basal layers (Moreci and Lechler, 2020; Rognoni and Watt, 2018). During embryogenic development it arises from the non-neural ectoderm, which is highly regulated by different signaling pathways, such as WNT, BMP, and NOTCH (Fuchs, 2007; Moreci and Lechler, 2020).

In total, the epidermis has a high cell density of 9.3 million cells per cm^2, including 7.5 million nucleated keratinocytes, 1.8 million corneocytes (terminally differentiated keratinocytes), 200,000 melanocytes and 140,000 Langerhans cells. Melanocytes are located in the basal layer and are responsible for the skin color and photoprotection, whereas Langerhans cells recognize and present antigens (Arda *et al.*, 2014; Gu *et al.*, 2020). In addition, the epidermis also harbors the endings of sensory dermal nerves, that are coated with Schwann cells and are located close to Merkel cells, transmitting temperature, touch, pain, and itch (Eckhart and Zeeuwen, 2018; Hoath and Leahy, 2003). Cellular adhesion between basal keratinocytes is ensured by adherens junctions and desmosomes, whereas hemidesmosomes and focal adhesions are responsible for adhesion between basal cells and the underlying ECM. Alterations or mutations in these protein complexes can cause severe skin blistering disorders (Moreci and Lechler, 2020).

To maintain the epidermal homeostasis, the whole layer is constantly renewed by a stable balance between basal cell proliferation and suprabasal cell differentiation (Rognoni and Watt, 2018). Therefore, epidermal stem cells in the basal layer start to differentiate, detach from the basement membrane, a process known as delamination, and migrate upward (Figure 4). During this process, distinct differentiated keratinocyte populations develop into the different epidermal layers and the cells constantly adapt to the needs of their respective localization (Kypriotou *et al.*, 2012; Moreci and Lechler, 2020).
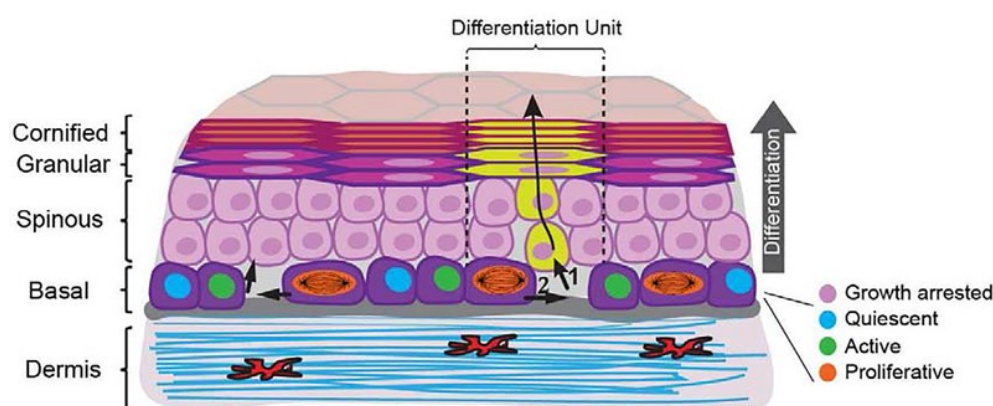
Figure 4. Keratinocyte differentiation during epidermal homeostasis. Schematic model showing human skin structure, including the dermis and four epidermal layers, and displaying keratinocyte differentiation. When basal cells start to differentiate, they detach from the basement membrane and start migrating upward (1), transforming

into spinous, granular and, finally, cornified keratinocytes. Simultaneously, proliferation of neighboring basal cells is induced to compensate for the decreased cell number in the basal layer (2). These mechanisms ensure a constant self-renewal of the whole epidermis (Rice and Rompolas, 2020).

The epidermis is regularly used as a model for stem cell behavior, and the development of live imaging techniques together with inducible fluorescent reporters allowed unbiased tracing of basal keratinocytes *in vivo* (Rompolas *et al.*, 2016; Watt, 2014). Thus, Rompolas *et al.* gained essential insights into epidermal differentiation, such as the observation that neighboring keratinocytes migrate upward independently and not as a whole layer.

Furthermore, recent advances in single-cell RNA sequencing (scRNA-seq) techniques enabled the identification of different subpopulations of epidermal stem cells in the basal layer (Cheng *et al.*, 2018; Haensel *et al.*, 2020; Reynolds *et al.*, 2021; Wang *et al.*, 2020b). In mice, Haensel *et al.* detected four differentiation-related transcriptional profiles in basal keratinocytes, which could be classified into one proliferative and three non-proliferative states (Figure 4). In human basal keratinocytes, these four distinct states have also been identified, and they correlate with distinct locations in the basal layer at the upper and lower parts of the rete ridges, epithelial extensions that project into the dermis. These clusters of different basal cells maintain epidermal communication and suggest a hierarchical differentiation lineage of multiple stem cell subpopulations with distinct proliferation capacities (Wang *et al.*, 2020b).

Basal keratinocytes show high expression of keratin 5/14 (*KRT5/KRT14*) and proliferation-related genes, but differentiation-related genes are actively repressed. Differentiation of basal to spinous cells is facilitated by extensive and mostly irreversible changes in the organization of the cytoplasm and cytoskeleton, as well as changes in gene expression, such as switching from the expression of *KRT5/14* to *KRT1/10*. Furthermore, basal keratinocytes become postmitotic, exit the cell cycle, and migrate upward (Kypriotou *et al.*, 2012; Moreci and Lechler, 2020). To compensate for the loss of keratinocytes in the basal layer, self-renewal responses are induced in neighboring cells (Mesa *et al.*, 2018). These processes are regulated by G1 sizer mechanisms, coupling the growth of basal keratinocytes with cell cycle progression, to induce cell divisions, as soon as a certain cell volume is reached (Xie and Skotheim, 2020).

The further differentiation to granular keratinocytes leads to a decreased expression of *KRT1/10* and the activation of PKC (Koster and Roop, 2007). Moreover, granular cells start expressing the epidermal differentiation complex, a cluster of around 50 genes that are essential for terminal keratinocyte differentiation (Moreci and Lechler, 2020).

With the transition of granular keratinocytes into the stratum corneum, cells lose their cytoplasmic organelles and nuclei, a process known as enucleation. In addition, highly cross-linked proteins replace the plasma membrane, resulting in terminally differentiated keratinocytes with a cornified envelope. This modified cell death program leads to the accumulation of functional cell corpses with a water-resistant lipid bilayer surrounding the corneocytes (Lippens *et al.*, 2005; Moreci and Lechler, 2020; Zijl *et al.*, 2022).

1.1.4 Dermal structure and fibroblast heterogeneity

The human dermis can be divided into two sublayers, which differ in cell density and ECM composition (Rognoni and Watt, 2018). The papillary dermis (300-400µm) is located below the basement membrane and shows a high fibroblast density surrounded by thin and poorly oriented collagen fibers. In contrast, the 1,700µm to 5,600µm thick reticular dermis contains less fibroblasts, but thick and well organized collagen fibers (Sorrell and Caplan, 2004). Moreover, fibroblasts themselves differ in morphology and functions, depending on their dermal localization. Papillary fibroblasts were observed to be small, spindle-shaped, and they showed a high proliferation rate. On the other hand, reticular fibroblasts are large, stellate-shaped, and proliferate less (Janson *et al.*, 2012). In addition, specialized fibroblast subpopulations were identified in the reticular dermis, such as dermal papilla (DP) cells at the hair follicle base and dermal sheath (DS) cells surrounding hair follicles (Rognoni and Watt, 2018) (Figure 5).
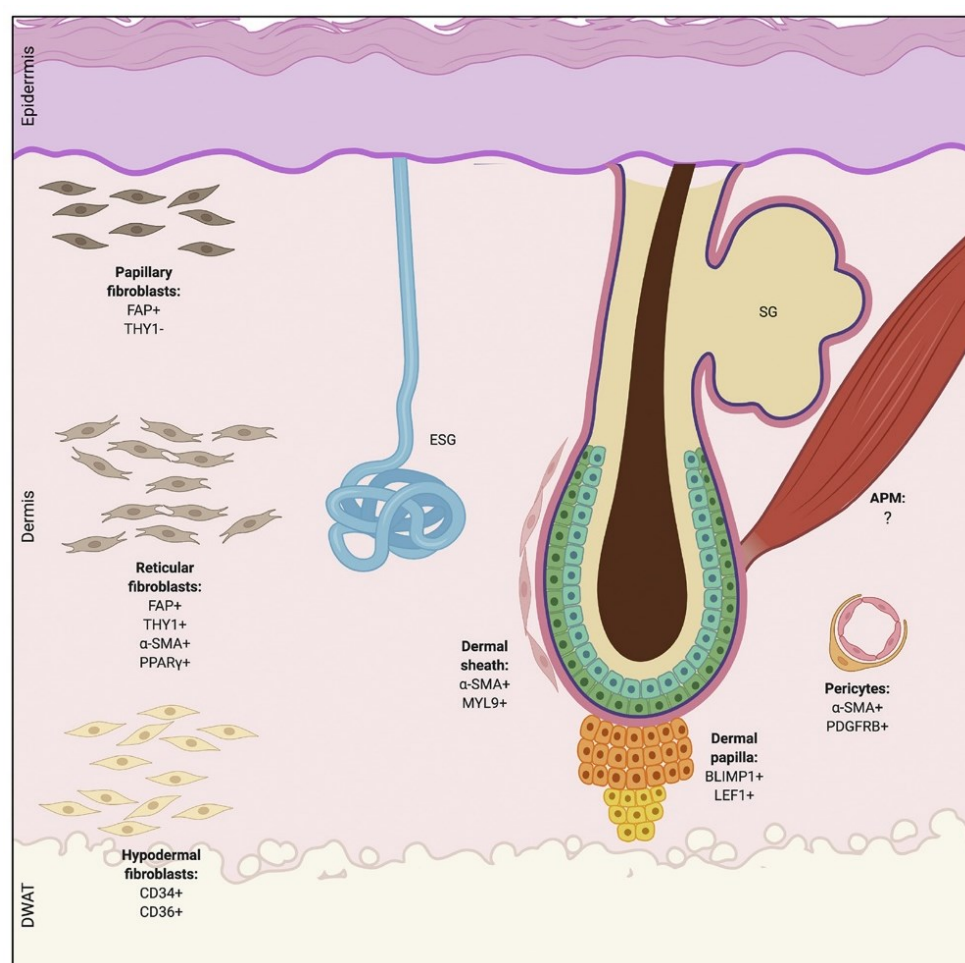
Figure 5. Dermal structure in human skin. Schematic model showing localization-specific fibroblast subpopulations in human papillary and reticular dermis, as well as in the dermal white adipose tissue (DWAT). The dermis also harbors specialized structures, such as eccrine sweat glands (ESGs), sebaceous glands (SGs), arrector pili muscles (APMs), as well as dermal sheath and dermal papilla cells surrounding hair follicles (Modified from Talbott *et al*., 2022).

These differences between the two dermal sublayers are maintained by intrinsic and extrinsic factors. Cell intrinsic features were reinforced by xenograft experiments with fibroblasts from different origins, retaining their transcriptomic profiles and migration behavior at different locations (Rinkevich *et al.*, 2015). Furthermore, fibroblasts show distinct response patterns to paracrine signals from the epidermis. For instance, proliferation and ECM production are influenced by SHH signaling in papillary fibroblasts, and by TGF-β2 signaling in reticular fibroblasts (Lichtenberger *et al.*, 2016). These pathways lead then to differential expression of ECM-related genes, such as upregulation of *DCN* in papillary fibroblasts and *VCAN* in reticular fibroblasts (Sorrell and Caplan, 2004).

Papillary and reticular fibroblasts differ also in their origin. In mice, it was shown that both subpopulations arise from two functionally different cell lineages and develop independently (Driskell *et al.*, 2013). Neonatal mouse papillary fibroblasts show increased WNT signaling and high proliferation, but during the postnatal dermal growth phase these cells stop dividing and start ECM production (Collins *et al.*, 2011). During human embryogenic development, craniofacial dermis develops from neural crest cells, whereas most body skin arise from the mesoderm with migratory and highly proliferative fibroblasts (Thulabandu *et al.*, 2018). During adult homeostasis, cells become quiescent but maintain an active metabolism with constant production and organization of ECM. Therefore, fibroblasts secrete not only ECM proteins but also enzymes to cross-link them (LOX) and to promote (MMPs) or inhibit (tissue inhibitors of metallopeptidases [TIMPs]) their degradation (Kendall and Feghali-Bostwick, 2014; Rognoni *et al.*, 2016; Shaw and Rognoni, 2020).

Dermal fibroblasts are involved in many different processes, such as immune responses and wound healing in skin (Shaw and Rognoni, 2020). In the latter, reticular fibroblasts are recruited early after injury by growth factors and cytokines, such as TGF-β (Stunova and Vistejnova, 2018) (Figure 6). Papillary fibroblasts enter the wound bed later but are important for hair follicle regeneration (Rinkevich *et al.*, 2015). Upon wounding, fibroblasts exit their quiescent condition, can be activated into myofibroblasts, and are able to start proliferation, as well as migration again (Shaw and Rognoni, 2020). In mice, 12 activated fibroblast subpopulations were detected during wound healing, differing in signaling pathway activation, cell cycle state, spatial distribution, and the expression of transcription factors (Guerrero-Juarez *et al.*, 2019). To coordinate these complex interactions between different cell types and activation states, extensive regulative mechanisms are required with selective cell populations responding to certain paracrine signals (Shaw and Rognoni, 2020; Shook *et al.*, 2018). After completed wound healing, activated myofibroblasts typically undergo apoptosis or become senescent, although the exact regulation for these processes still remains unclear (Hiebert *et al.*, 2018). However, specific signals, such as BMP or epidermal SHH signaling could induce the transformation of myofibroblasts into adipocytes or DP cells, respectively (Lim *et al.*, 2018;

Plikus *et al.*, 2017). Interestingly, former injuries are important for future wound healing processes. In epidermal stem cells, an increased chromatin accessibility for specific stress response genes was observed up to 180 days after the first injury (Naik *et al.*, 2017). During a similar study, Gonzales *et al.* showed epigenetic adaptations in epidermal stem cells for wound repair-related genes upon injury. These modifications facilitated an accelerated response to following skin lesions with faster transcription of genes involved in inflammation, cytoskeletal reorganization, and cell migration (Gonzales *et al.*, 2021). Recently, the histone modification ubiquitination of histone H2A at lysine 119 (H2AK119ub) was identified as a key modulator of epigenetic wound memory (Levra Levron *et al.*, 2023). Loss of H2AK119ub in a Lrig1^{+} stem cell subpopulation from murine hair follicles upon injuries, was associated with accelerated healing of future wounds. This "primed" stem cell subpopulation was not only detected closely surrounding the injury but also in undamaged and distal tissue regions, causing the epigenetic wound memory for up to ten months after the initial injury. Interestingly, UVB-induced skin cancer in mice led to similar priming fields with less H2AK119ub and also in human skin tumors lower levels of this histone modification were observed (Levra Levron *et al.*, 2023).
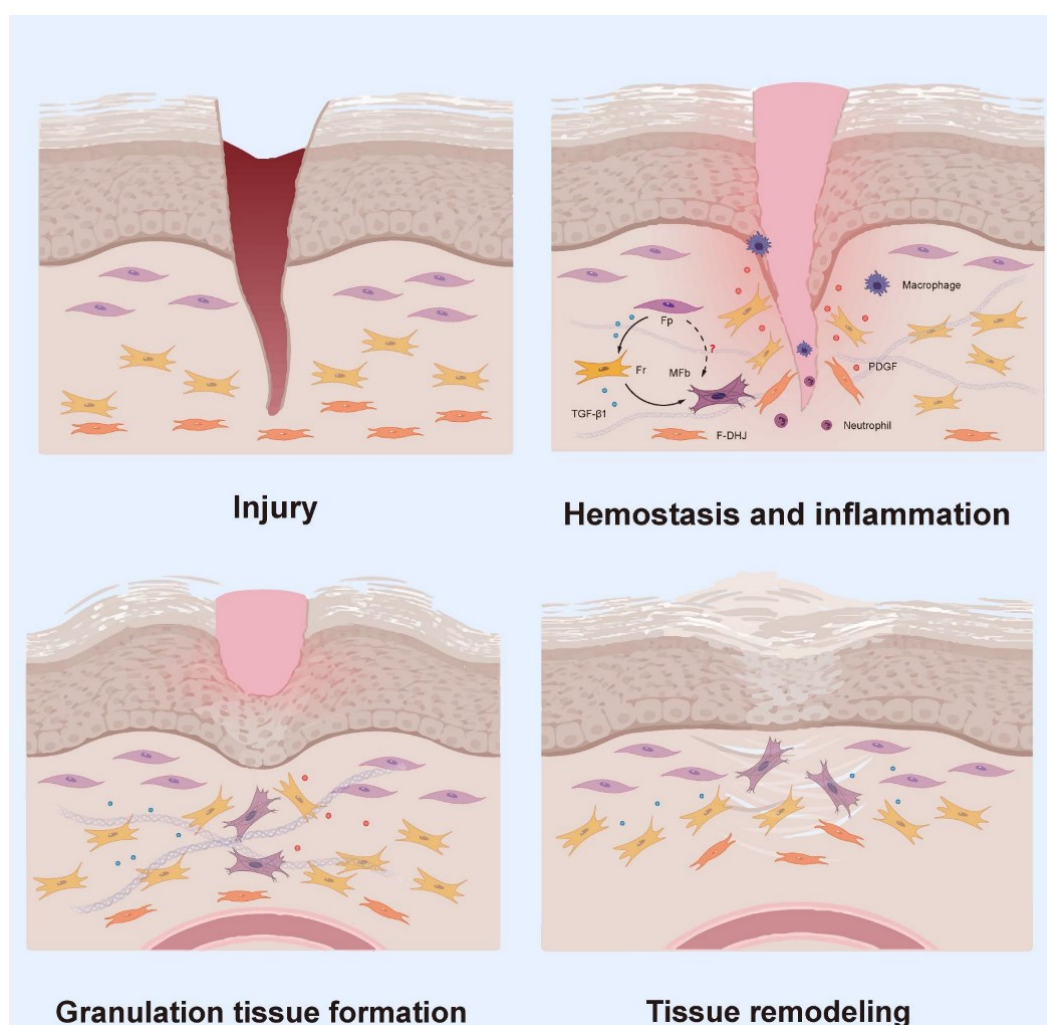
Figure 6. Cutaneous wound healing. Schematic model showing different phases of wound healing in human skin. Upon injury, different signaling cascades are induced, such as TGF-β and PDGF signaling. Reticular fibroblasts

(Fr), dermo-hypodermal junction fibroblasts (F-DHJ), and different immune cell types are recruited to the wound bed. In addition, myofibroblasts (MFb) become activated and contribute to tissue formation and remodeling (Modified from Zou *et al.*, 2021).

Furthermore, dermal fibroblasts are non-terminally differentiated cells with a high degree of plasticity that can be reprogrammed into inducible pluripotent stem cells (Takahashi and Yamanaka, 2006). Their state is influenced by regional and local tissue heterogeneity, as well as tissue condition (Shaw and Rognoni, 2020). Fibroblasts are also able to differentiate into several other cell types, such as adipocytes, DP cells or cartilage-like cells (Barallobre-Barreiro *et al.*, 2019). However, cells from diseased tissues (e.g. chronic wounds, fibrosis, cancer) lose this differentiation capacity and show persistent pathological phenotypes (Shaw and Rognoni, 2020). On the other hand, also epithelial cells can transform into fibroblasts, for instance via epithelial-mesenchymal transition (EMT), which lead to a loss of cell-cell adhesion and apical-basal polarity in epithelial cells (Talbott *et al.*, 2022). During embryogenic development, it was shown that PDGF and TGF-β signaling induce the transformation of epicardial epithelial cells into cardiac fibroblasts (von Gise and Pu, 2012). But also during cutaneous wound healing EMT occurs frequently (Stone *et al.*, 2016).

Detection of dermal fibroblasts and their heterogeneity was challenging for a long time, since no universal marker genes could be identified. Usually, common markers such as *VIM* and *PDGFRA* were used, but they are also expressed in other cell types and not all fibroblasts show an enriched expression for these genes (Guerrero-Juarez *et al.*, 2019; Lynch and Watt, 2018; Talbott *et al.*, 2022). Crucial advances in scRNA-seq techniques during the last years finally allowed the characterization of dermal fibroblast heterogeneity in much more detail, due to greater marker gene panels. For murine skin, different subpopulations were identified with specific cells involved in fibrosis (Rinkevich *et al.*, 2015). In addition, the impact of aging on fibroblast heterogeneity was studied in mice, revealing two subpopulations that become less defined with age, show reduced ECM production, and gain adipogenic traits (Salzer *et al.*, 2018). In human skin, spatial and functional differences between fibroblasts led to the identification of four (Philippeos *et al.*, 2018) or even seven (Tabib *et al.*, 2018) distinct subpopulations. One drawback of these studies is that they were performed with chronically UVR-exposed skin from a heterogeneous group of donors and these factors can confound the data (see Introduction, sections 1.1.1 and 1.1.2).

Therefore, I and other colleagues in our laboratory conducted a scRNA-seq study with more than 15,000 cells from UVR-protected healthy skin of two young (25 and 27 years) and three old (53-70 years) male Caucasian donors (Solé-Boldo *et al.*, 2020). After the identification of all major skin-related cell types, the transcriptomes of nearly 6,000 dermal fibroblasts, distributed among four subpopulations, were analyzed.

Gene expression patterns associated with classical fibroblast-related functions, such as collagen synthesis and ECM organization were observed in three subpopulations (Solé-Boldo

et al., 2020). In one of them, the specific expression of *COL11A1* and *COL24A1*, previously linked to cartilage and bone development, respectively (Li *et al.*, 2018; Wang *et al.*, 2012), suggested mesenchymal functions. Expression patterns for collagen-related genes in the other two ECM-secreting fibroblast subpopulations were associated with specific dermal localizations. One showed high expression of *COL13A1*, *COL18A1*, and *COL23A1*, which are known marker genes for papillary fibroblasts (Haydont *et al.*, 2019; Nauroy *et al.*, 2017; Philippeos *et al.*, 2018; Veit *et al.*, 2011). In the other fibroblast subpopulation, high expression was observed for the collagen-related genes *COL11A1* and *COL14A1* that are common in the reticular dermis (Haydont *et al.*, 2019; Janson *et al.*, 2012; Nauroy *et al.*, 2017; Philippeos *et al.*, 2018). According to these functional and spatial characteristics, the three ECM-related fibroblast subpopulations were labeled mesenchymal, secretory-papillary, and secretory-reticular fibroblasts. In addition, inflammation-related functions (e.g. cell chemotaxis) could be assigned to the fourth subpopulation, allowing their classification as pro-inflammatory fibroblasts (Figure 7A).

In order to validate the presence of these fibroblast subpopulations, RNA fluorescence *in situ* hybridization (FISH) and immunofluorescence (IF) assays were performed with healthy skin from young (28-37 years) and old (54-86 years) donors, which was also part of my Master's Thesis in 2019 (Solé-Boldo *et al.*, 2020). These approaches confirmed the papillary and reticular localization of two secretory subpopulations by the detection of *APCDD1* (RNA FISH) and COL18A1 (IF) or *CTHRC1* (RNA FISH) and TSPAN8 (IF), respectively. The expression patterns of *CCL19* and *APOE* suggested more widespread pro-inflammatory fibroblasts in the human dermis and close proximity to the vasculature. *ASPN*-expressing and POSTN-producing mesenchymal fibroblasts were observed mostly in the reticular dermis, often surrounding hair follicles (Solé-Boldo *et al.*, 2020).

Furthermore, this study revealed that intrinsic aging affects the fibroblast subpopulation composition, and an age-related loss of fibroblast priming in human dermis could be observed (Solé-Boldo *et al.*, 2020). In aged skin, less mesenchymal fibroblasts were detected, as well as an age-dependent loss of functional annotations for each subpopulation (Figure 7B). Immune-related Gene Ontology (GO) terms were also enriched in all old fibroblasts, suggesting the development of a general, chronic, and low-grade inflammatory phenotype (Zhang and Duan, 2018). Another age-dependent change was related to cellular communication between fibroblasts and different cutaneous cell types. Many interactions predicted for young fibroblasts were lost upon intrinsic aging, especially the communication with undifferentiated keratinocytes close to the basement membrane, thus suggesting a dermal contribution to the phenotype of aged skin (Solé-Boldo *et al.*, 2020).
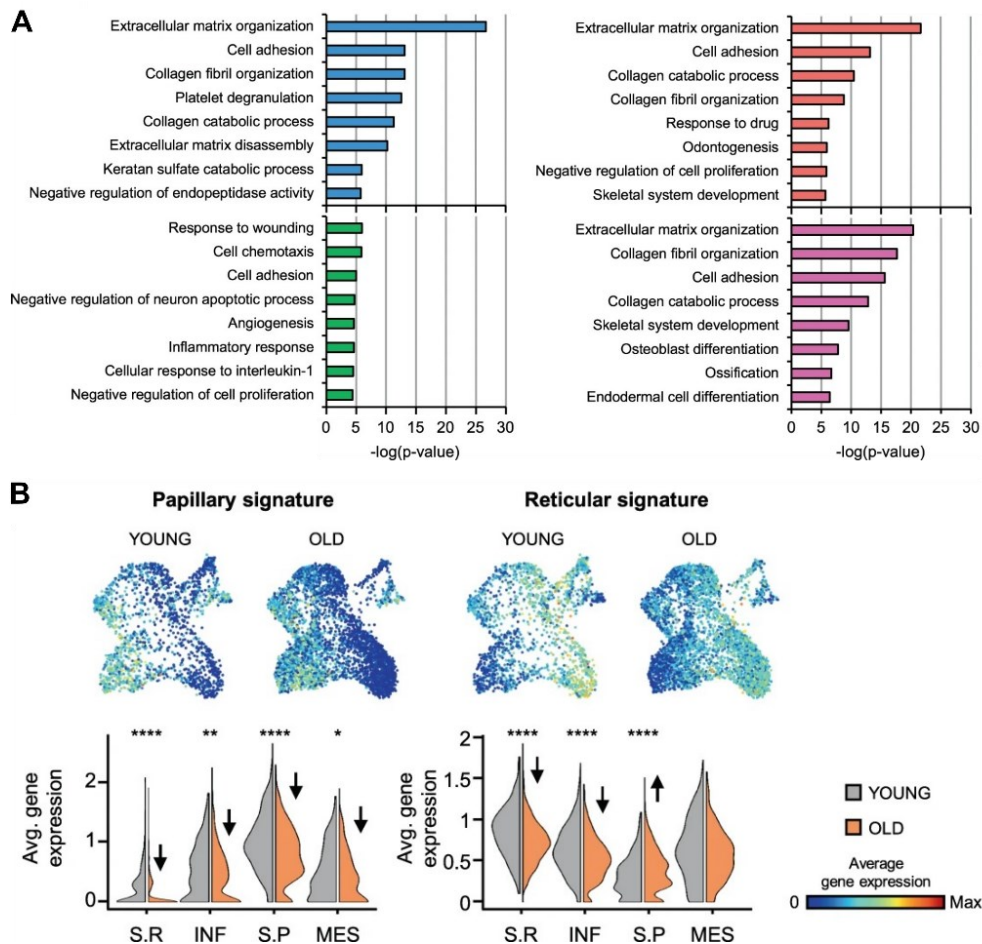
Figure 7. Fibroblast heterogeneity in healthy skin. A single-cell RNA sequencing (scRNA-seq) study with more than 15,000 cells from ultraviolet radiation (UVR)-protected healthy skin of two young (25 and 27 years) and three old (53-70 years) male Caucasian donors identified four fibroblast subpopulations. **(A)** Top enriched Gene Ontology (GO) terms in each subpopulation, sorted by p-value. According to spatial and functional differences between the fibroblast subpopulations, they were labeled as secretory-reticular (S.R; blue), pro-inflammatory (INF; green), secretory-papillary (S.P; red), and mesenchymal (MES; pink). **(B)** Uniform manifold approximation and projection (UMAP) plots and violin plots visualizing the expression of papillary and reticular gene signatures in young and old fibroblasts, suggesting an age-related decrease in expression. For UMAP plots, red indicates maximum expression and blue indicates low or no expression of each particular set of genes. In the violin plots, X-axes depict fibroblast subpopulations and Y-axes represent average expression of each set of genes. Statistical analyses were performed using the Wilcoxon Rank Sum test (*: p-value < 0.05, **: p-value < 0.01, ***: p-value < 0.001, ****: p-value < 0.0001) (Modified from Solé-Boldo *et al*., 2020).

Based on these findings, another study analyzed the impact of aging on the highly specialized DS fibroblast subpopulation, again with my contribution and that of our laboratory (Ahlers *et al.*, 2021). The mesenchyme-derived DS population includes hair follicle dermal stem cells, which show self-renewing capacity and are the progenitors for DP and DS cells (Rahmani *et al.*, 2014; Wang *et al.*, 2020a). What is known about this specialized fibroblast subpopulation and the regulation processes involved, was mostly derived from reporter construct and lineage tracing approaches in mice (Heitman *et al.*, 2020; Rahmani *et al.*, 2014; Shin *et al.*, 2020). Information about human DS cells was more limited although partial overlap of gene expression profiles between both species were detected (Heitman *et al.*, 2020), and *de novo*

hair follicle formation induced by isolated DS cells was observed in human skin (Reynolds *et al.*, 1999; Tsuboi *et al.*, 2020).

Therefore, Ahlers *et al.* performed a scRNA-seq study with 72,000 cells from three young (<30 years) and four old (>60 years) female donors, identifying a specific DS fibroblast subpopulation with stem cell characteristics that decreases upon aging. RNA FISH assays verified the localization of these cells surrounding hair follicles (Figure 8A), and the DS subpopulation showed a substantial overlap in their gene expression pattern with gene signatures determined in mice (Heitman *et al.*, 2020; Shin *et al.*, 2020) (Figure 8B).

Furthermore, my contribution to this study was the validation of DS cells and their loss upon aging in four independent published scRNA-seq datasets for human skin (Rojahn *et al.*, 2020; Solé-Boldo *et al.*, 2020; Tabib *et al.*, 2018; Vorstandlechner *et al.*, 2020) (Figure 8C).

For the identified DS population, also stem cell characteristics were detected via RNA velocity and knockdown experiments with DS marker genes. After the knockdown of *HES1*, *CTNNB1*, *MYL4*, and *COL11A1*, primary human fibroblasts showed less adipogenic differentiation capacity, and a decreased chondrogenic differentiation capacity was observed after *HES1* and *COL11A1* knockdowns. The proliferation capacity of these primary fibroblasts was also reduced upon *HES1* downregulation (Ahlers *et al.*, 2021).

Finally, it was shown that DS-secreted Activin A increased the epidermal thickness and procollagen type I c-peptide production in 3D skin models, which were constructed with aged human fibroblasts (Figures 8D and 8E). This observation suggests the age-dependent contribution of the DS fibroblast subpopulation to a juvenile skin phenotype (Ahlers *et al.*, 2021).
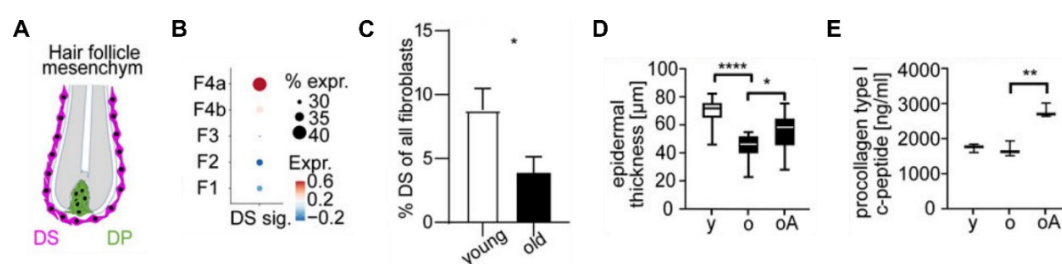
Figure 8. Dermal sheath population in human skin shows stem cell characteristics and undergoes age-related loss. A single-cell RNA sequencing (scRNA-seq) study with 72,000 cells from three young (<30 years) and four old (>60 years) female donors identified a specific dermal sheath (DS) fibroblast subpopulation, showing stem cell characteristics and decreased cell numbers upon aging. **(A)** Schematic model visualizing the localization of DS and dermal papilla (DP) cells surrounding hair follicles. **(B)** Dot plot showing the average expression of ten DS signature genes (DS sig.) (Shin *et al.*, 2020) in all identified fibroblast subpopulations. The highest expression was detected in a subset of mesenchymal cells (F4a), subsequently labeled as DS population. Red indicates maximum expression and blue indicates low or no expression (Expr.). Dot sizes are associated with the percentage of cells expressing the gene signature (% expr.). **(C)** Bar plot depicting the percentages of DS population in young (n = 8) and old (n = 9) skin donors from four integrated scRNA-seq studies (Rojahn *et al.*, 2020; Solé-Boldo *et al.*, 2020; Tabib *et al.*, 2018; Vorstandlechner *et al.*, 2020). **(D) & (E)** Box plots visualizing epidermal thickness **(D)** and procollagen type I c-peptide synthesis **(E)** in 3D skin models constructed with young (y) or old (o) fibroblasts, as well as the effect of Activin A treatment (oA; 100 ng/ml for six weeks). Statistical analyses were performed using unpaired and paired t-tests (*: *p*-value < 0.05, **: *p*-value < 0.01, ****: *p*-value < 0.0001), and error bars show the standard error of the mean (Modified from Ahlers *et al.*, 2021).

1.2 Keratinocyte carcinoma – Initiation and progression

Keratinocyte carcinomas (KCs) in the skin, also known as non-melanoma skin cancers, comprise basal cell carcinomas (BCCs) and cutaneous squamous cell carcinomas (cSCCs), which account for approximately 80% and 20% of all KC cases, respectively (Waldman and Schmults, 2019). KC is the most common cancer entity worldwide in the fair-skinned population (Apalla *et al.*, 2017), with a continuously rising incidence and a 33% increase in cases worldwide between 2007 and 2017 (Fitzmaurice *et al.*, 2019). The global lifetime risk for developing cSCC differs between male and female patients, with 9-14% in males and 4-9% in females (Waldman and Schmults, 2019) (see Introduction, section 1.1.1). Only less than 0.05% of all BCC cases metastasize (Apalla *et al.*, 2017), and also primary cSCC tumors show a relatively low metastatic potential of 3-7%, but frequent recurrence result in an overall metastatic rate of 25-30% for cSCC (Burton *et al.*, 2016; Nagarajan *et al.*, 2019). Moreover, for metastatic cSCCs, poor prognoses were observed with a 5-year survival rate of 50-83% for regional metastases and less than 40% for distant ones (Ahadiat *et al.*, 2017; Sahovaler *et al.*, 2019). Taken together, KCs constitute a serious and increasing burden on public health systems, causing costs of ~4.8 billion dollar in the United States per year (Fitzmaurice *et al.*, 2019; Guy *et al.*, 2015; Mudigonda *et al.*, 2010).

KCs arise from epidermal keratinocytes and there are many unique and shared risk factors known for BCC and cSCC (Nagarajan *et al.*, 2019). The most important one for developing KC is chronic UVR exposure, including UVA (315-400nm) and UVB (280-315nm) (Bosch *et al.*, 2015). This is also indicated by the observation that 90% of all KC tumors develop in UVR-exposed body regions, such as head, neck, and forearms (Boeckmann *et al.*, 2020; Nagarajan *et al.*, 2019). Although the solar spectrum contains only 5% UVB with low skin penetration, this type of radiation is the most potent KC initiator, due to direct energy transfer (Hussein, 2005). It causes pyrimidine dimers, such as cyclobutane pyrimidine dimers (CPDs) and pyrimidine-6,4-pyrimidone dimers (6-4PPs) in the DNA of epidermal keratinocytes (Boeckmann *et al.*, 2020). Since these photoproducts can affect replication and transcription, they are usually repaired in a multistep process by the nucleotide excision repair pathway (Hoeijmakers, 2001). However, accumulation of pyrimidine dimers can lead to DNA damage via C to T base exchanges or CC to TT mutations, one of the main hallmarks of KCs (Brash *et al.*, 1991; Lee *et al.*, 2020; Nagarajan *et al.*, 2019). On the other hand, although UVA comprises less energy, it reaches the dermis and contributes indirectly to tumorigenesis via the induction of oxidative stress. Chronic UVA exposure leads to accumulation of ROS and results, for instance, in ECM degradation and tissue damage (Bachelor and Bowden, 2004) (see Introduction, section 1.1.2). Over time the human skin acquires more and more DNA and cellular damage, potentially resulting in KC initiation (Figure 9).
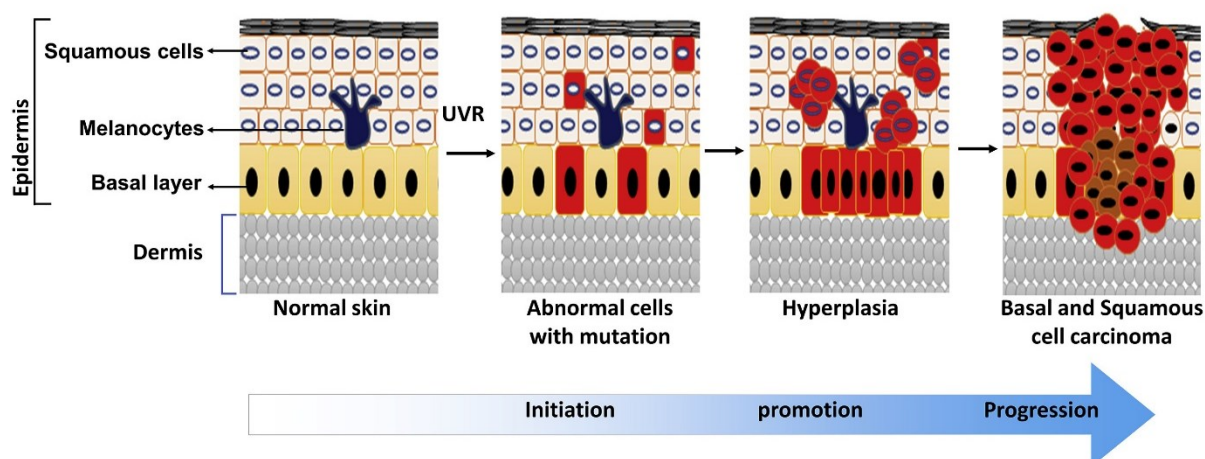
Figure 9. Keratinocyte carcinoma development. Schematic model visualizing the ultraviolet radiation (UVR)-induced initiation and progression of keratinocyte carcinomas, including basal cell carcinoma and cutaneous squamous cell carcinoma (Modified from Prasad *et al.*, 2020).

1.2.1 Characteristics of BCCs

BCC tumors can be subdivided depending on their clinical appearance, with the nodular type as the most common one accounting for 60% of the cases (Boeckmann *et al.*, 2020). Further 25% of all BCCs are diagnosed as multicentric/superficial, and the sclerodermiform/morphea-like type represents 2% but counts as the most problematic one, due to its diffuse tumor margins (Boeckmann *et al.*, 2020; Jacobs *et al.*, 1982).

In BCC, mutations in genes related to the SHH signaling pathway, such as *SHH*, *GLI*, *PTCH1*, *SUFU*, and *SMO*, were observed in 90% of the cases, 50% of which were induced by UVR exposure (Boeckmann *et al.*, 2020; Gailani *et al.*, 1996; Nagarajan *et al.*, 2019). During adult homeostasis, the SHH signaling pathway is mostly inactive, but mutations in its components can induce aberrant activation, which is the driving force of BCC development (Boeckmann *et al.*, 2020; Epstein, 2008). Furthermore, in 50% of all BCC cases, mutations in the tumor suppressor gene *TP53* were detected, again mostly UVR-induced (Auepemkiate *et al.,* 2002; Nagarajan *et al.*, 2019; Pellegrini *et al.*, 2017). Accordingly, BCC tumors from sunscreen users showed a lower mutational level for *TP53* (Rosenstein *et al.*, 1999).

1.2.2 Characteristics of cSCCs

Invasive cSCCs can develop through different intermediate stages. For instance, tumors can progress from the premalignant skin lesion actinic keratosis (AK) with a rate between 0.025% and 16% per year and event (Burton *et al.*, 2016; Ratushny *et al.*, 2012). Interestingly, however, 26% of all AKs regress spontaneously during one year (Boeckmann *et al.*, 2020). Invasive tumors can also develop from a non-invasive carcinoma *in situ*, called Bowen's disease (BD), with a progression rate of 3-5% per year and event (Fania *et al.*, 2021). All these different types

of skin lesions and tumors usually develop in chronically photodamaged regions with keratinocytes harboring the same UVR-induced genetic defects. Therefore, the identification of molecular mechanisms leading to disease progression or regression are largely unknown (Thomson *et al.*, 2021). In addition, cSCC tumors usually have many mutations, which makes it more difficult to detect driver genes (Harwood *et al.*, 2016).

However, some frequently mutated genes were already described for cSCC, such as *TP53*, *CDKN2A*, *TET2*, *TGFBR1/2*, and *NOTCH1/2/3* (Cammareri *et al.*, 2016; South *et al.*, 2012; Yilmaz *et al.*, 2017). Since *TP53* alterations were detected in 60-90% of AK and cSCC cases, and much more often in UVR-exposed skin (74%) than in UVR-protected skin (5%), this mutation is considered UVR-induced, and an early event during the disease progression (Giglia-Mari and Sarasin, 2003; Nakazawa *et al.*, 1994). In addition, aberrant activation of EGFR can lead to further downregulation of *TP53* (Kolev *et al.*, 2008).

Changes in the transcription of non-coding micro RNAs (miRNAs) can also be associated with cSCC progression. These small molecules are involved in the regulation of important processes, such as stem cell maintenance in the epidermis (Zhang *et al.*, 2011). For example, it was shown that upregulation of *MIR21*, which encodes for miRNA 21, and also downregulation of *MIR203* promote tumorigenesis due to the suppression of tumor suppressor genes and stem cell proliferation, respectively (Boeckmann *et al.*, 2020; Dziunycz *et al.*, 2010).

Furthermore, a recent study from our laboratory, combining transcriptomic and methylomic approaches, identified two subtypes for AKs and cSCCs with epidermal stem cell- or keratinocyte-like features (Solé-Boldo *et al.*, 2022). This stratification was based on distinct DNA methylation patterns of regulatory regions in keratinocytes, and was associated with different cells-of-origin for both subclasses. Moreover, it was shown that metastatic and invasive KC tumors were associated with more undifferentiated cells-of-origin and epidermal stem cell-like features (Solé-Boldo *et al.*, 2022).

1.2.3 Therapeutic approaches for KCs

For KCs, different treatment options are available, usually depending on tumor features. Invasive KCs are mostly removed using the Mohs micrographic surgery (MMS) technique, but for superficial lesions also non-surgical options might be sufficient, such as cryosurgery, electrodessication and curettage (EDC), light-based therapies, as well as chemical peels (Nagarajan *et al.*, 2019). In addition, topical treatment compounds can be used for KCs *in situ*, like the chemotherapeutic 5-fluorouracil (Boeckmann *et al.*, 2020). This pyrimidine analog incorporates into DNA and RNA, leading to the inhibition of their synthesis, especially in the more rapidly dividing malignant keratinocytes. However, side effects, such as severe

inflammation, ulceration, scarring, and resistance development, limit its use (Longley *et al.*, 2003).

Unresectable and/or metastatic KC tumors require more potent therapy options, such as systemic chemotherapy, targeted therapy, immunotherapy or checkpoint inhibition therapy (Cranmer *et al.*, 2010; Que *et al.*, 2018). For advanced BCCs, different drugs targeting the SHH signaling showed meaningful response rates, since this pathway is not only important for tumor initiation but also for cancer cell maintenance (Boeckmann *et al.*, 2020; Nagarajan *et al.*, 2019). Cyclopamine, the first SMO inhibitor, leads to decreased *GLI* and *HIP1* expression and reduces BCC tumors by 90% in mice (Athar *et al.*, 2006; Boeckmann *et al.*, 2020). Its topical application was also successful in a human trial, avoiding side effects associated with systemic treatment (Tabs and Avci, 2004). For advanced cSCCs, different therapies aim for targeting EGFR signaling, which previously resulted in apoptosis, cell growth inhibition, and immune stimulation (Boeckmann *et al.*, 2020; Göppner *et al.*, 2010; Wozel *et al.*, 2010).

1.3 Cancer-associated fibroblasts – Important part of the tumor microenvironment

Fibroblasts are the major cell type in connective tissue, which provides elasticity to many organs of the human body, including skin (see Introduction, section 1.1.4). However, fibroblasts are not only important in maintaining homeostasis in these organs, but it was also shown that they are involved in tumorigenesis of almost every solid cancer entity (Comito *et al.*, 2014; Gorchs *et al.*, 2015; Hosein *et al.*, 2015). These so called cancer-associated fibroblasts (CAFs) partially constitute the tumor microenvironment (TME) in variable fractions, together with different other non-malignant cell types, such as endothelial and immune cells (Chhabra and Weeraratna, 2023; Shiga *et al.*, 2015). In contrast to cancer cells, usually no genetic alterations are detected in CAFs (Biffi and Tuveson, 2021).

1.3.1 CAF origin and activation

Although resident fibroblasts are the main progenitors for CAFs, they can also originate from different cell types and sources, such as bone marrow-derived mesenchymal stem cells (BM-MSCs), hematopoietic stem cells, epithelial cells, and endothelial cells, which depends on tissue, cancer type, and activation signals (Figure 10A) (Arina *et al.*, 2016; Öhlund *et al.*, 2017; Orimo and Weinberg, 2007). Furthermore, CAFs develop in response to different and context-dependent stimuli. Cancer cells and immune cells can activate tissue fibroblasts via direct cell-cell contacts or by paracrine signaling via different growth factors, such as TGF-β, PDGF, FGF,

EGF, and inflammatory chemokines, like IL6 or IL1β, as well as miRNAs (Biffi *et al.*, 2019; Chhabra and Weeraratna, 2023; Elenbaas and Weinberg, 2001; Mitra *et al.*, 2012). Interestingly, cancer cells can transform BM-MSCs into CAFs via OPN secretion, inducing TGF-β production in BM-MSCs (Weber *et al.*, 2015), while BM-MSC-derived TGF-β leads to CAF activation of resident fibroblasts (Wen *et al.*, 2015).

In addition, extrinsic factors can promote this transformation, such as ECM stiffness, a high level of ROS, and DNA damage induced by genotoxic therapy or UVR exposure (Figure 10B) (Ke and Wang, 2021; Straub *et al.*, 2015; Sun *et al.*, 2012). The activation process and its kinetics also depend on the body site of CAF development, due to organ-specific transcriptomic profiles of the fibroblasts and other source cell types (Rinn *et al.*, 2006). Activated CAFs show a similar phenotype as myofibroblasts during wound healing, but unlike these temporary activated cells that usually undergo apoptosis after wound closure, CAF transformation seems to be irreversible (Li *et al.*, 2007). However, due to similar cellular processes in the tissue surrounding wounds and in the TME during carcinogenesis, tumors could be considered as "chronic wounds that never heal" (Dvorak, 1986).
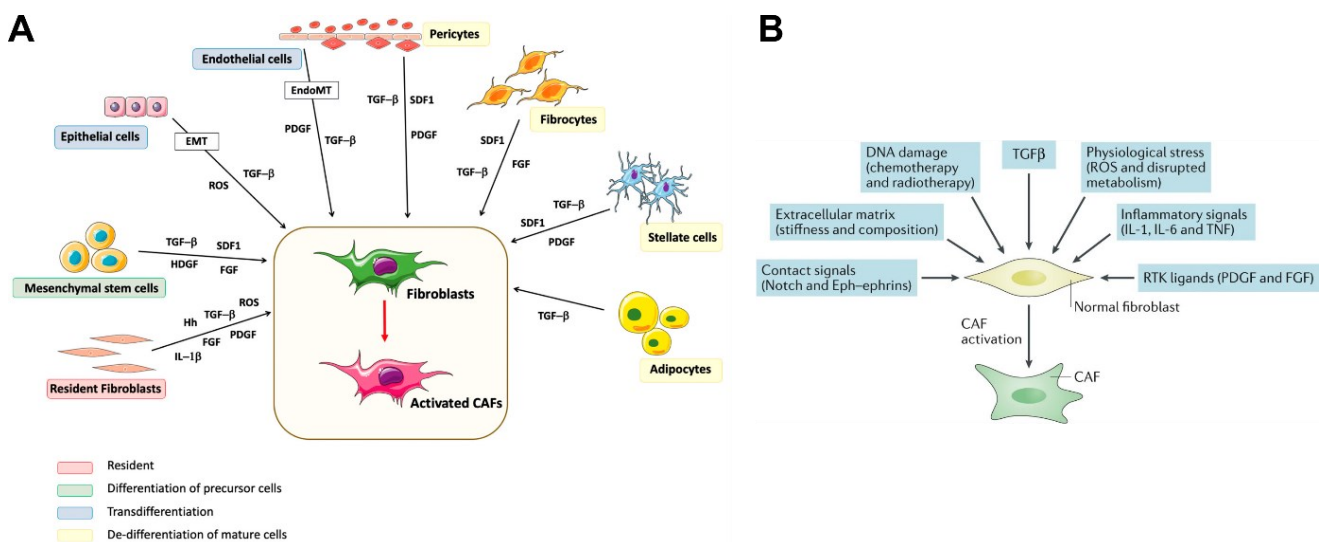
Figure 10. Origin and activation of cancer-associated fibroblasts. (A) Schema visualizing the different cellular sources for cancer-associated fibroblasts (CAFs). Activating signaling pathways for each cell type are also displayed. **(B)** Summary of CAF-activating growth factors, cytokines, and external/tissue-based components (Modified from Louault *et al.*, 2020 and Sahai *et al.*, 2020).

1.3.2 CAF functions during tumorigenesis

CAFs affect tumorigenesis in a stage-dependent manner. During carcinoma initiation, stromal cells exhibiting anti-cancer functions were observed (Chang *et al.*, 2012; Chhabra and Weeraratna, 2023). For instance, in pancreatic ductal adenocarcinoma (PDAC) mouse models, the selective depletion of *ACTA2* (encoding for α-SMA)-expressing CAFs resulted in cancer progression (Özdemir *et al.*, 2015). Similar observations were described in breast,

colon, intestinal, and bladder cancer, suggesting the presence of tumor-restraining CAFs (Gerling *et al.*, 2016; Maris *et al.*, 2015; Pallangyo *et al.*, 2015; Shin *et al.*, 2014). On the other hand, in the TME of advanced tumors, CAFs promote cancer cell proliferation, immune evasion, tumor invasion, and metastasis via the secretion of different growth factors, cytokines, chemokines, extracellular vesicles (EVs), and ECM-degrading enzymes (Biffi and Tuveson, 2021; Chhabra and Weeraratna, 2023; Simon and Salhia, 2022). During this process, CAF-derived ligands induce particular signaling pathways in cancer cells. For instance, POSTN activates integrin/FAK-SRC signaling, HGF and OPN stimulate WNT/β-catenin signaling, CXCL12, HGF and IL22 trigger PI3K/mTOR signaling, and IL6, TGF-β and FGF activate MAPK signaling (Biffi and Tuveson, 2021; Chhabra and Weeraratna, 2023). Furthermore, CAFs secrete angiogenic factors, such as VEGF, CXCL12, and PDGF that facilitate angiogenesis in the tumor and surrounding tissue by the recruitment of endothelial cells and promoting their proliferation (Liu *et al.*, 2015; Shiga *et al.*, 2015; Wang *et al.*, 2019a).

For ECM remodeling processes, MMPs are especially important. In breast cancer, it has been shown that TNF-α and TGF-β secretion of tumor cells induced the expression of *MMP9* in CAFs, resulting in the specific degradation of type IV collagen and laminin in the basement membrane (Stuelten *et al.*, 2005). Furthermore, by regulating the organization of fibronectin, CAFs provide the direction for cancer cell migration (Erdogan *et al.*, 2017). In general, re-organization of the ECM, as the structural scaffold of the tissue, alters physical properties and the biomechanical activity of the TME. Changes in its composition can promote EMT of cancer cells, leading to increased motility and invasion capacity (Aggarwal *et al.*, 2021). CAFs themselves can also migrate to distant metastatic sites, either as individual cells or together with cancer cells, creating a tumor-supporting niche in cooperation with the resident tissue fibroblasts and immune cells in the invaded organ (Duda *et al.*, 2010; Soikkeli *et al.*, 2010).

In addition, CAFs induce a chronic inflammatory but, at the same time, immunosuppressive TME by the secretion of immunomodulatory cytokines, such as TGF-β, IL6, CXCL1, and CXCL12, which promote tumorigenesis and cancer cell survival (Elyada *et al.*, 2019; Hornburg *et al.*, 2021; Mescher, 2017; Wu *et al.*, 2020). It was shown that CAFs can cause a cytotoxic T cell reduction in the TME and an increased infiltration of regulatory T cells (Tregs) (Chakravarthy *et al.*, 2018; Kato *et al.*, 2018; Mariathasan *et al.*, 2018).

Moreover, the TME, including CAFs, is associated with the development of therapeutic drug resistance and tumor reactivation after dormancy (Chhabra and Weeraratna, 2023; Parker and Cox, 2020). In head and neck squamous cell carcinoma (SCC), it was shown that CAF-derived MMP1 protects cancer cells from cetuximab treatment (Johansson *et al.*, 2012). In PDAC, breast cancer, and colorectal carcinoma, it was also observed that CAF-derived IL6, IL17A, PDGF, and IGF induce NF-κB and ERK1/2 signaling in cancer cells, promoting resistance to chemotherapeutic agents, such as doxorubicin, 5-fluorouracil or cisplatin (Lotti *et al.*, 2013;

Louault *et al.*, 2019; Mutgan *et al.*, 2018). In addition, the whole TME can act as a structural barrier, leading to a decreased drug bioavailability, due to adhesion of cancer cells to ECM proteins (Chhabra and Weeraratna, 2023; Paraiso and Smalley, 2013). At metastatic sites, CAFs were associated with cancer cell dormancy, interestingly, causing a more aggressive phenotype after CAF depletion in PDAC (Özdemir *et al.*, 2015; Parker and Cox, 2020).

1.3.3 CAF detection

Similar to dermal fibroblasts, detection of CAFs via the expression of marker genes is complicated, due to their low specificity. Classical and commonly used markers are *ACTA2*, *FAP*, *PDPN*, *PDGFRA/B*, and *S100A4/FSP1* (Bartoschek *et al.*, 2018; Chhabra and Weeraratna, 2023; Li *et al.*, 2017; Öhlund *et al.*, 2017; Simon and Salhia, 2022). However, expression of these genes has been observed not only in CAFs, but also in smooth muscle cells and pericytes for *ACTA2* (Rockey *et al.*, 2013; Rønnov-Jessen *et al.*, 1995), in epithelial cancer cells and macrophages for *FAP* (Arnold *et al.*, 2014; Mentlein *et al.*, 2011), as well as in lymphatic endothelial cells for *PDPN* (Breiteneder-Geleff *et al.*, 1999).

Nevertheless, recent progress in single-cell techniques and transcriptomic analyses of many different carcinomas enabled the characterization of CAF heterogeneity and the identification of distinct CAF subpopulations with specific marker gene panels (Chhabra and Weeraratna, 2023). Furthermore, evolving multiplex imaging techniques provide spatial information about the localization of cancer cells and non-malignant cells in the TME, including CAFs (Jackson *et al.*, 2020). Though, a limiting factor for many of these studies is the lack of long-term sampling from the same human patient at different disease stages, which prevents the detailed characterization of molecular and regulatory processes leading from fibroblasts to activated CAFs (Chhabra and Weeraratna, 2023). Therefore, different *in vitro* assays are used and developed, such as 2D/3D spheroid and organoid models, liquid-air interface models, microfluidics technologies, and bio-printed tissue approaches (Biffi *et al.*, 2019; Franco-Barraza *et al.*, 2016; Langer *et al.*, 2019; Neal *et al.*, 2018; Ootani *et al.*, 2009).

On the other hand, *in vivo* studies with rodents are performed using tissue-restricted cell type labeling techniques that allow cell tracing and following disease initiation and progression. CAF labeling and subsequent live/intravital imaging provide spatial information during tumorigenesis, as well as visualization of CAF interactions with cancer cells and non-malignant cell types (Entenberg *et al.*, 2023; Ewald *et al.*, 2011; Vennin *et al.*, 2019). However, experiments to label distinct CAF subpopulations *in vivo* are limited due to overlapping gene expression patterns for the different groups. Another approach are *ex vivo* cultures with isolated tumor tissue, but depending on culture dish surface, media, and environmental

conditions, culturing-induced changes in morphology and gene expression have been observed in malignant and non-malignant cells (Chhabra and Weeraratna, 2023).

1.3.4 CAF heterogeneity

Although different numbers of CAF subpopulations were described in a tissue- and context-dependent manner, many studies share the detection of immunoregulatory and ECM-remodeling cells (Figure 11) (Chhabra and Weeraratna, 2023). In PDAC, inflammatory CAFs (iCAFs) were detected mostly towards tumor edges, secreting immunomodulatory molecules, such as IL6 and CXCL12. In contrast, ECM-producing myofibroblastic CAFs (myCAFs) were observed close to tumor cells and showed high *ACTA2* expression but low levels of *IL6* (Elyada *et al.*, 2019; Öhlund *et al.*, 2017). Another PDAC study in mice not only confirmed these two CAF subpopulations, but could also identify distinct activation pathways. On the one hand, cancer cell-derived IL1 led to iCAF activation via JAK/STAT signaling and, on the other hand, tumor-secreted TGF-β prevented this process, resulting in myCAF transformation (Biffi *et al.*, 2019). Furthermore, iCAFs and myCAFs were described in different cancer entities, such as breast, lung, ovarian, and colorectal carcinomas (Bhattacharjee *et al.*, 2021; Chhabra and Weeraratna, 2023; Hornburg *et al.*, 2021; Kieffer *et al.*, 2020).
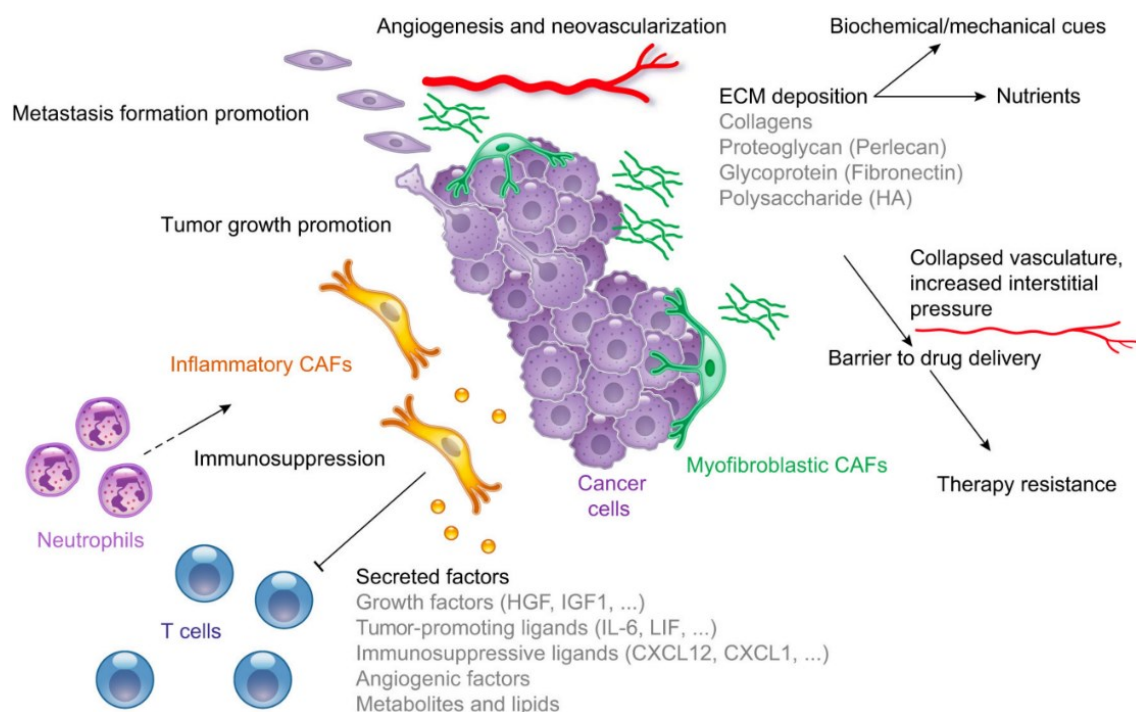
Figure 11. Functions of inflammatory and myofibroblastic cancer-associated fibroblasts. Schema showing distinct tumor-promoting functions of two commonly detected cancer-associated fibroblast (CAF) subpopulations. Inflammatory CAFs (iCAFs) establish an immunosuppressive tumor microenvironment (TME) by secretion of different growth factors and cytokines. Myofibroblastic CAFs (myCAFs) are mostly involved in the re-organization and degradation of extracellular matrix (ECM) components (Modified from Biffi and Tuveson, 2021).

Depending on the study and tissue, several further and more specific CAF subpopulations were identified during the last decade. In late-stage PDAC, CAFs associated with major histocompatibility class II (MHC II) genes were detected. These antigen-presenting CAFs (apCAFs) promoted T cell differentiation into Tregs, resulting in an immunosuppressive TME (Elyada *et al.*, 2019). In another PDAC study with low desmoplastic tumors, CAFs showing a highly activated glycolytic metabolic state (meCAFs) were observed. They caused increased metastasis but, on the other hand, a better response to immunotherapy (Wang *et al.*, 2021b).

For lung and breast cancer, vasculature-associated CAFs (vCAFs) were described with angiogenic functions, resulting in an increased angiogenesis in the TME and promoted vascular development (Bartoschek *et al.*, 2018; Lambrechts *et al.*, 2018). Bartoschek *et al.* also detected development-associated CAFs (dCAFs) and cycling CAFs (cCAFs), which seemed to be involved in the differentiation, development, and morphogenesis of breast tissue, or in cancer cell proliferation, respectively. Interestingly, the authors could determine different cellular sources for the identified CAF subpopulations, such as the perivascular niche for vCAFs and malignant cells undergoing EMT for dCAFs (Bartoschek *et al.*, 2018).

Last year, an extensive scRNA-seq study characterized six CAF subpopulations in ten different solid cancer entities, including thyroid, lung, breast, gastric, pancreatic, colorectal, ovarian, prostate, bladder, and intrahepatic duct carcinoma (Luo *et al.*, 2022). The three main CAF subpopulations were described as cancer-associated myofibroblasts (CAF_{myo}), inflammatory CAFs (CAF_{infla}) and adipogenic CAFs (CAF_{adi}). In addition, minor subpopulations were detected based on their origin, such as endothelial-mesenchymal transition (EndMT) CAFs (CAF_{EndMT}), peripheral nerve-like CAFs (CAF_{PN}), and antigen-presenting CAFs (CAF_{ap}) (Luo *et al.*, 2022).

All these different CAF subpopulations are usually considered as distinct cellular states rather than terminal differentiation endpoints, thus providing a high level of plasticity for these cells (Biffi and Tuveson, 2021; Campbell *et al.*, 2009; Qiu *et al.*, 2008).

1.3.5 Therapeutic approaches targeting CAFs

During the last years, it became more and more clear that understanding tumors with their surrounding TME as a whole is essential to target not only tumor "seeds", like current therapeutic approaches often do, but also the fertilizing "soil", including CAFs and other non-malignant cell types (de Groot *et al.*, 2017). Furthermore, this knowledge will allow better response predictions, as well as stratification of tumor types and patients (Chhabra and Weeraratna, 2023). Since CAFs show a high heterogeneity not only between different cancer entities, but also between patients suffering from the same carcinoma type, in some cases CAFs might also be used as prognostic factors (Chhabra and Weeraratna, 2023).

Current strategies for targeting CAFs alone or in combination with chemo- or immunotherapies include different approaches. Surface markers could be used to eliminate CAFs or specific CAF subpopulations, they could be transformed into a quiescent state, their secretome could be antagonized, or CAF activating pathways could be targeted. So far, clinical studies with CAF-associated molecules provided inconsistent results, thus suggesting a high level of CAF heterogeneity with context- and tissue-dependent tumor-restraining or tumor-promoting functions (Chhabra and Weeraratna, 2023).

1.3.6 The role of CAFs in skin cancer

In skin cancer, CAFs mostly develop from resident fibroblasts (Tirosh *et al.*, 2016). A scRNA-seq study with murine melanoma samples identified three CAF subpopulations (Davidson *et al.*, 2020). CAF-S1 cells resembled iCAFs with functions related to immune crosstalk and the recruitment/regulation of immune cells. In addition, in a myCAF-like population (CAF-S2), upregulation of ECM-associated genes was observed. CAF-S3 cells were found to be involved in the re-organization of actin fibers in the cytoskeleton and were therefore considered a contractile CAF subpopulation (Davidson *et al.*, 2020).

Furthermore, an integrated study of head and neck carcinoma, lung carcinoma, and melanoma identified six CAF subpopulations across all entities, including myCAFs and iCAFs. These groups promoted tumorigenesis via different molecular pathways, and could be associated with particular clinical outcomes and therapy resistance to immune checkpoint blockade (Galbo *et al.*, 2021).

Interestingly, CAF subpopulations are not only shared between different cancer types, but also conserved across species, which was shown by a study of PDAC, BCC, and breast cancer in mice and human patients. The authors identified three superclusters, including steady state-like CAFs, immunomodulatory CAFs, and mechanoresponsive CAFs (Foster *et al.*, 2022).

Also for cSCC, changes in the TME compared to healthy skin were already shown. Extensive stromal reprogramming could be observed via RNA-seq, and further immunohistochemistry assays revealed the overexpression of the tumor-promoting factor *POSTN* in CAFs with increasing levels from BD towards high-risk cSCC (Beebe *et al.*, 2022; Lincoln *et al.*, 2021). Another study examined the effect of 5-aminolevulinic acid-mediated photodynamic therapy (ALA-PDT) on CAFs. This topical treatment option is regularly used for AKs and BDs, inducing ROS production and subsequent death, specifically in cancer cells. Thereby, CAF-derived CXCL13 was shown to be important for immune cell recruitment, resulting in anti-tumoral immune effects (Zhu *et al.*, 2019). In addition, reduced migration and decreased expression of *ACTA2* and *FAP* were detected in CAFs after ALA-PDT *in vitro* (Li *et al.*, 2019a). Interestingly, CAF-secreted TGF-β induced cell cycle arrest in cSCC cells, leading

to a decreased proliferation rate and subsequent resistance to ALA-PDT (Gallego-Rentero *et al.*, 2021).

In 2020, a detailed study characterized ten cSCC tumors with matched normal skin via scRNA-seq, spatial transcriptomic assays, and multiplexed ion beam imaging (Ji *et al.*, 2020). Besides an immunosuppressive TME, the authors described a tumor-specific keratinocyte subpopulation with EMT features localized in a fibrovascular niche at the leading edges of the tumors. These malignant cells showed a very high interaction level with CAFs and seemed to be regulated by CAF-derived TGF-β1/3 (Ji *et al.*, 2020). Another scRNA-seq study investigated differences between primary and recurrent cSCC tumors, including changes in the respective TMEs (Li *et al.*, 2022). In all analyzed tumor samples the authors detected myCAFs, iCAFs, as well as IL7R$^+$-CAFs, with an elevated fraction of myCAFs in primary tumor TME and an enriched amount of IL7R$^+$-CAFs in the recurrent tumor TME. IL7R$^+$-CAFs showed high expression of EMT-related ligands and strong cellular communication with a specific malignant keratinocyte subpopulation (Li *et al.*, 2022).

2. Aims

It is already known that CAFs are an important component of the TME and are involved in tumorigenesis of many different cancer entities (Biffi and Tuveson, 2021). It has also been shown that not only resident fibroblasts but also other cell types, such as BM-MSCs, can be transformed into CAFs by paracrine signaling of various growth factors and inflammatory cytokines (Chhabra and Weeraratna, 2023). Furthermore, CAFs, especially in advanced tumors, appear to be involved in different pro-tumorigenic processes, such as cancer cell proliferation, immune evasion, angiogenesis, ECM remodeling, and even therapeutic drug resistance (Simon and Salhia, 2022). In particular, single-cell techniques enabled the investigation of CAF heterogeneity and interestingly led to the identification of immunoregulatory and ECM-remodeling CAFs in different cancer types, like PDAC, breast, and lung carcinoma (Chhabra and Weeraratna, 2023).

In skin, different studies in murine and human melanoma have also detected iCAF- and myCAF-like subpopulations, among others (Davidson *et al.*, 2020; Galbo *et al.*, 2021). For cSCCs in particular, CAFs overexpressing the tumor-promoting ECM modulator *POSTN* have been associated with disease progression (Beebe *et al.*, 2022; Lincoln *et al.*, 2021). In addition, CAFs have been observed to influence the success and outcome of the cSCC therapeutic approach ALA-PDT. Thus, CAF-derived TGF-β induced cell cycle arrest in malignant keratinocytes, leading to a decreased proliferation rate and subsequent resistance to ALA-PDT (Gallego-Rentero *et al.*, 2021; Zhu *et al.*, 2019). However, details on CAF heterogeneity in cSCC remain unclear. Moreover, it is unknown which normal fibroblast subpopulation is activated and transformed into CAFs, as well as the precise mechanisms of how CAFs affect the TME and cSCC progression.

Therefore, the main aim of this thesis is to provide an extensive characterization of CAFs by scRNA-seq and multiplexed RNA FISH assays at different stages of cSCC tumorigenesis. Potential CAF heterogeneity will be analyzed, as well as tumor-affecting interactions of CAFs with different cell types in the TME. Furthermore, CAF origin/s will be studied taking into account the previous identification of the four distinct fibroblast subpopulations in healthy human skin (Solé-Boldo *et al.*, 2020).

3. Results

3.1 Detection of skin-associated cell types by scRNA-seq

The main aim of this thesis is to detect cSCC progression-related transcriptomic changes in CAFs. Therefore, the following analyses were only performed with skin samples from older (47-93 years) male patients (see Material and Methods, section 6.2.1 and Table 8), in order to avoid possible confounding effects by sex and/or age. It is also known that this group of patients is most affected by KCs (see Introduction, sections 1.1.1, 1.1.2, and 1.2).

Fresh biopsies of three chronically UVR-exposed healthy (EH) skin samples, three BDs, and five invasive cSCCs were kindly provided by the Department of Dermatology, University Hospital of Heidelberg, coordinated by PD Dr. med. Anke Lonsdorf. I then performed the subsequent sample preparation steps and generated the scRNA-seq library using the 10x Genomics platform in the DKFZ single-cell Open Lab (scOpen Lab). Finally, library sequencing was completed in the DKFZ next generation sequencing (NGS) core facility (see Material and Methods, section 6.2.2). After obtaining the raw sequencing reads, the initial processing steps, including demultiplexing and the alignment to the human genome, were performed by Dr. Günter Raddatz.

The total scRNA-seq dataset was further expanded to include data from three UVR-protected healthy (PH) skin samples from Solé-Boldo *et al.* (Solé-Boldo *et al.*, 2020). I then performed the following computational analyses, primarily using the R tool Seurat v4 (Hao *et al.*, 2021) unless otherwise stated.

After several quality control steps, 115,053 single cells were used for data pre-processing and the standard Seurat integration workflow (see Material and Methods, section 6.2.3). Subsequent unsupervised clustering resulted in 30 cell clusters based on distinct gene expression signatures (Figure 12A). Gene expression analyses revealed cluster-specific expression of well-known marker genes (Solé-Boldo *et al.*, 2020) for skin-related cell types (Figure 12B). Cells in the clusters #4, #12, #19, and #23 showed upregulation of genes encoding different types of keratin compared to other clusters, suggesting that these cells represent keratinocytes in distinct differentiation states (14,615 cells). Expression of fibroblast-associated genes, such as *VIM*, *LUM*, and *COL1A2* was enriched in the clusters #1, #3, #6, and #13. Furthermore, marker genes for different immune cell types, like *CD3D* (T cells), *IGLL5* (B cells), *CPA3* (mast cells) or *LYZ* (macrophages) were expressed in distinct clusters. Expression of *SELE*, *CLDN5*, and *RGS5* were observed as well, suggesting the presence of vascular endothelial cells (ECs), lymphatic ECs, and pericytes, respectively. Interestingly, scRNA-seq also allowed the detection of minor cell types, such as erythrocytes, melanocytes, and Schwann cells based on the expression of the corresponding marker genes *HBA1*,

MLANA, and *CRYAB*. These observations, and the identification of the most differentially expressed genes among all clusters, allowed cell type annotations. This demonstrates that scRNA-seq with subsequent data analyses were capable of detecting major and minor cell types in healthy human skin, BDs, and cSCCs.
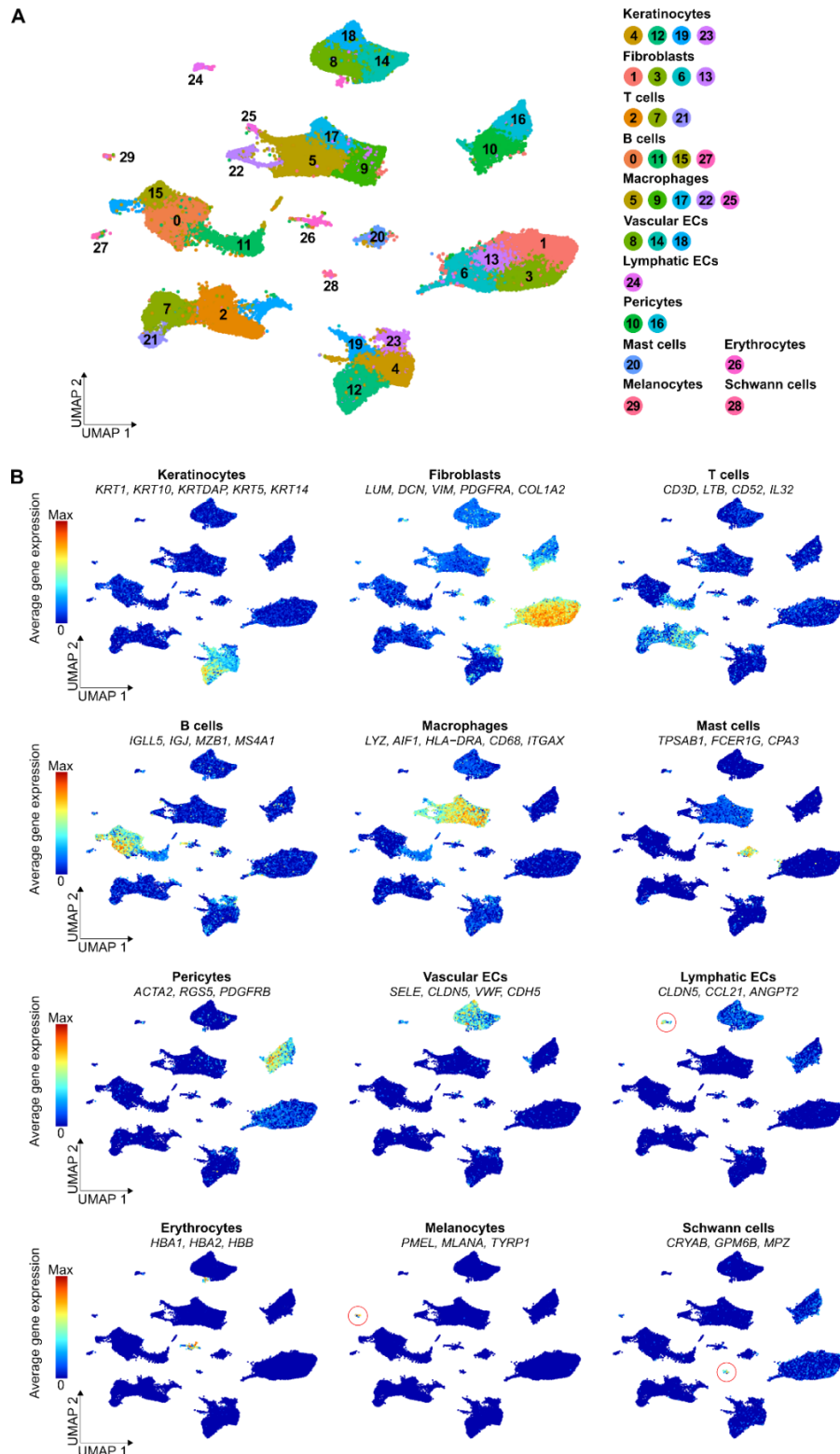
Figure 12. Single-cell RNA sequencing reveals human skin-related cell types. Single-cell RNA sequencing (scRNA-seq) was performed with three healthy but chronically ultraviolet radiation (UVR)-exposed skin samples,

three Bowen's disease (BD) samples, and five invasive cutaneous squamous cell carcinomas (cSCCs) from older (47-93 years) male patients. After processing the raw reads (performed by Dr. Günter Raddatz), data from all samples were integrated together with data of three healthy UVR-protected skin samples from Solé-Boldo *et al*. (Solé-Boldo *et al.*, 2020), following the standard protocol from the R package Seurat v4 (Hao *et al.*, 2021). **(A)** Unsupervised clustering of the integrated dataset revealed 30 cell clusters with distinct gene expression signatures, visualized in an uniform manifold approximation and projection (UMAP) plot. Each dot represents a single cell (n = 115,053). **(B)** UMAP plots depicting the average gene expression levels for cell type-specific marker genes (Solé-Boldo *et al.*, 2020) in the integrated dataset. Red indicates high expression in arbitrary units and blue refers to no or only low expression in arbitrary units. ECs: endothelial cells, Max: maximum.

All 12 identified cell types were detected in each of the four sample entities, illustrating successful data integration and excluding the possibility of sample type-specific cell clusters (Figure 13A). However, when I compared cell type fractions between the samples, entity-related differences could be observed (Figure 13B). On average, a significant (p-value < 0.05, pairwise Holm-Sidak tests) higher amount of T cells were detected in BDs (44% of all cells ± 23% standard deviation [SD]) and cSCCs (13% ± 13% SD) compared to PH (2% ± 0.7% SD) and EH (3% ± 1% SD) skin samples. Also for B cells a similar tendency was shown with on average 14% ± 15% SD of B cells in BDs and 18% ± 20% SD in cSCCs, but only 0.5% ± 0.3% SD in PH and 0.7% ± 0.2% SD in EH samples. These results suggest an increase in immune cell abundance in BDs and cSCCs compared to healthy skin, resulting in an inflammatory TME during tumorigenesis. The observed variability in cell type fractions between different patients of the same entity was caused by patient-specific differences and technical reasons, such as scRNA-seq library generation for the particular patients on different days.

As another data quality control step, I further compared the isolated cell type fractions in the six PH and EH samples with a scRNA-seq study, in which also six healthy skin samples were analyzed in a comparable manner (Tabib *et al.*, 2018). Slight differences in the amount of major cell types are most probably related to diverse sample collection sites in both studies, since skin constitution and its thickness differ according to body region (Figure 13C).

Figure 13. Enriched amount of immune cells in Bowen's disease and cutaneous squamous cell carcinoma. **(A)** Uniform manifold approximation and projection (UMAP) plots depicting the integrated single-cell RNA sequencing (scRNA-seq) dataset after pre-processing and unsupervised clustering, split by sample entity. Ultraviolet radiation (UVR)-protected healthy (PH) skin: n = 3 (Solé-Boldo *et al.*, 2020), UVR-exposed healthy (EH) skin: n = 3, Bowen's disease (BD): n = 3, cutaneous squamous cell carcinoma (cSCC): n = 5. **(B)** Bar plot showing the detected cell type fractions in all scRNA-seq samples. X-axis shows samples and Y-axis shows percentages of all cell types identified in each sample. **(C)** Bar plot visualizing cell type fractions for six healthy skin samples analyzed by scRNA-seq in Tabib *et al.* (Tabib *et al.*, 2018) (black), as well as for the six PH and EH skin samples from this thesis (gray). X-axis shows identified cell types and Y-axis shows average percentages. K: keratinocytes, F: fibroblasts, EC: endothelial cells, P: pericytes, Macro: macrophages, T & B: T cells and B cells, Melano: melanocytes.

3.1.1 Characterization of malignant keratinocytes in BD and cSCC

To ensure high quality of the obtained scRNA-seq data, I used different approaches to confirm that keratinocytes from BDs and cSCCs indeed show malignant characteristics compared to keratinocytes from PH and EH skin samples, which can be considered healthy (although EH-derived keratinocytes were chronically exposed to UVR before sampling).

First, copy number variation (CNV) events were inferred from scRNA-seq data using the R packages InferCNV v1.6 (Patel *et al.*, 2014; Tirosh *et al.*, 2016) and CopyKAT v1.1 (Gao *et al.*, 2021). It has previously been shown, that the accumulation of CNV events results in genome instability, as well as aneuploidy and is associated with cancer initiation and progression (Steele *et al.*, 2022; Tirosh *et al.*, 2016). Keratinocytes from the three PH skin samples were used as control cells and both computational tools detected an increasing number of CNV events in keratinocytes from BDs to cSCCs, confirming their malignant status and reflecting disease progression (Figure 14A). Furthermore, CopyKAT classified significantly (*p*-value < 0.01, t-test) more BD-derived keratinocytes as aneuploid (69% ± 17% SD) than diploid (12% ± 10% SD). Similarly, significantly (*p*-value < 0.0001, t-test) more keratinocytes from cSCC

samples were classified as aneuploid (92% ± 6% SD) than diploid (8% ± 6% SD). This also suggested an accumulation of CNV events during cSCC tumorigenesis (Figure 14B).

In addition, the expression of a previously described cSCC-derived tumor-specific keratinocyte gene signature (Ji *et al.*, 2020) was analyzed in keratinocytes from all sample entities (Figure 14C). Enriched expression was observed for keratinocytes isolated from cSCC tumors, further confirming their identity.

Another characteristic of cancer cells analyzed by scRNA-seq is patient-specific clustering behavior. On the one hand, it has been previously observed that gene expression-based clustering of non-malignant cells in the TME resulted in cell type-specific clusters. On the other hand, malignant cells have formed sample-specific clusters, due to their high transcriptomic variability between different patients (Tirosh *et al.*, 2016). For most of the scRNA-seq analyses in this thesis, data integration of all samples was required (see Material and Methods, section 6.2.3), resulting in keratinocyte clusters comprising cells from healthy samples and tumors (Figures 12A and 13A). This workflow was necessary to ensure biologically meaningful clustering of all cell types and to avoid batch effects that were caused by sequencing library generation on different days. However, less stringent data processing without integration resulted in sample type-specific keratinocyte clusters and was even able to separate keratinocytes of the individual cSCC patients from those of healthy samples (Figure 14D). This further verified their malignant status.
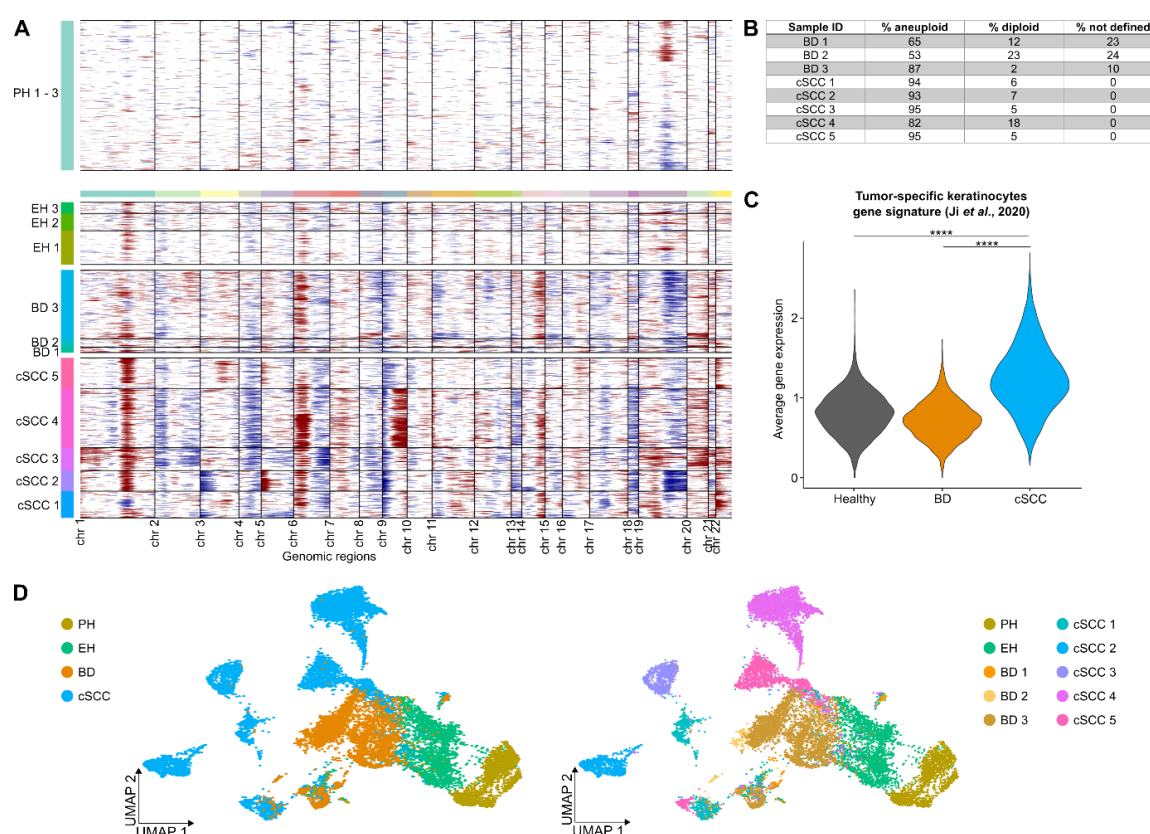
Figure 14. Validation of malignancy status for keratinocytes in Bowen's disease and cutaneous squamous cell carcinoma. (A) Heatmaps showing copy number variation (CNV) events in keratinocytes inferred from single-

cell RNA sequencing (scRNA-seq) data. Cells from three ultraviolet radiation (UVR)-protected healthy (PH) skin samples were used as control. In rows, keratinocytes from different samples are depicted and columns display genomic regions ordered by chromosomes (chr). Blue represents genetic deletions, whereas red indicates gene amplifications. **(B)** Table comprising percentages of keratinocytes in Bowen's disease (BD) samples and cutaneous squamous cell carcinomas (cSCCs) identified as aneuploid or diploid after inferring CNV events from scRNA-seq data. For some cells no clear classification was possible ("% not defined"). **(C)** Violin plot visualizing the average expression of a previously defined cSCC-derived tumor-specific keratinocyte marker gene signature (Ji *et al.*, 2020) in keratinocytes from PH skin, UVR-exposed healthy (EH) skin, BDs, and cSCC samples. Sample types are depicted along the X-axis and the Y-axis shows the average gene expression in arbitrary units. Statistical analyses were performed using Wilcoxon Rank Sum tests (****: *p*-value < 0.0001). **(D)** Uniform manifold approximation and projection (UMAP) plots showing sample type-specific (left) and cSCC patient-specific (right) keratinocyte clusters after scRNA-seq data analysis without integration.

Detailed gene expression analyses were another approach to specify the malignancy status of keratinocytes. Therefore, a GO analysis was performed with the most upregulated genes in BD-derived keratinocytes compared to keratinocytes from PH and EH samples (Figure 15A). Top terms were enriched for tumorigenesis-associated processes, such as angiogenesis, antigen processing, and activation of innate immune response, suggesting the establishment of an inflammatory TME. In addition, gene set enrichment analyses (GSEA) revealed a significant enrichment of signaling pathways involved in cancer progression, such as JAK/STAT and SHH signaling in keratinocytes of BD samples compared to healthy keratinocytes. Genes related to the G2/M cell cycle phase, which is important for cell proliferation, were also enriched in BD-derived keratinocytes (Figure 15B).

Similarly, a GO analysis of the most upregulated genes in cSCC-derived keratinocytes compared to healthy ones showed that these genes seem to be involved in cancer-related metabolic and inflammatory changes, as well as in stress response with top terms, like aerobic respiration, antigen processing, and response to oxidative stress (Figure 15C). Furthermore, GSEA revealed an enrichment of genes associated with processes that are important in cSCC progression, such as oxidative phosphorylation, DNA repair, and cell proliferation (G2/M checkpoint) in keratinocytes from cSCCs (Figure 15D). Taken together, these observations suggest that keratinocytes isolated from BDs and cSCCs were indeed different from healthy keratinocytes and showed cancer-related changes.
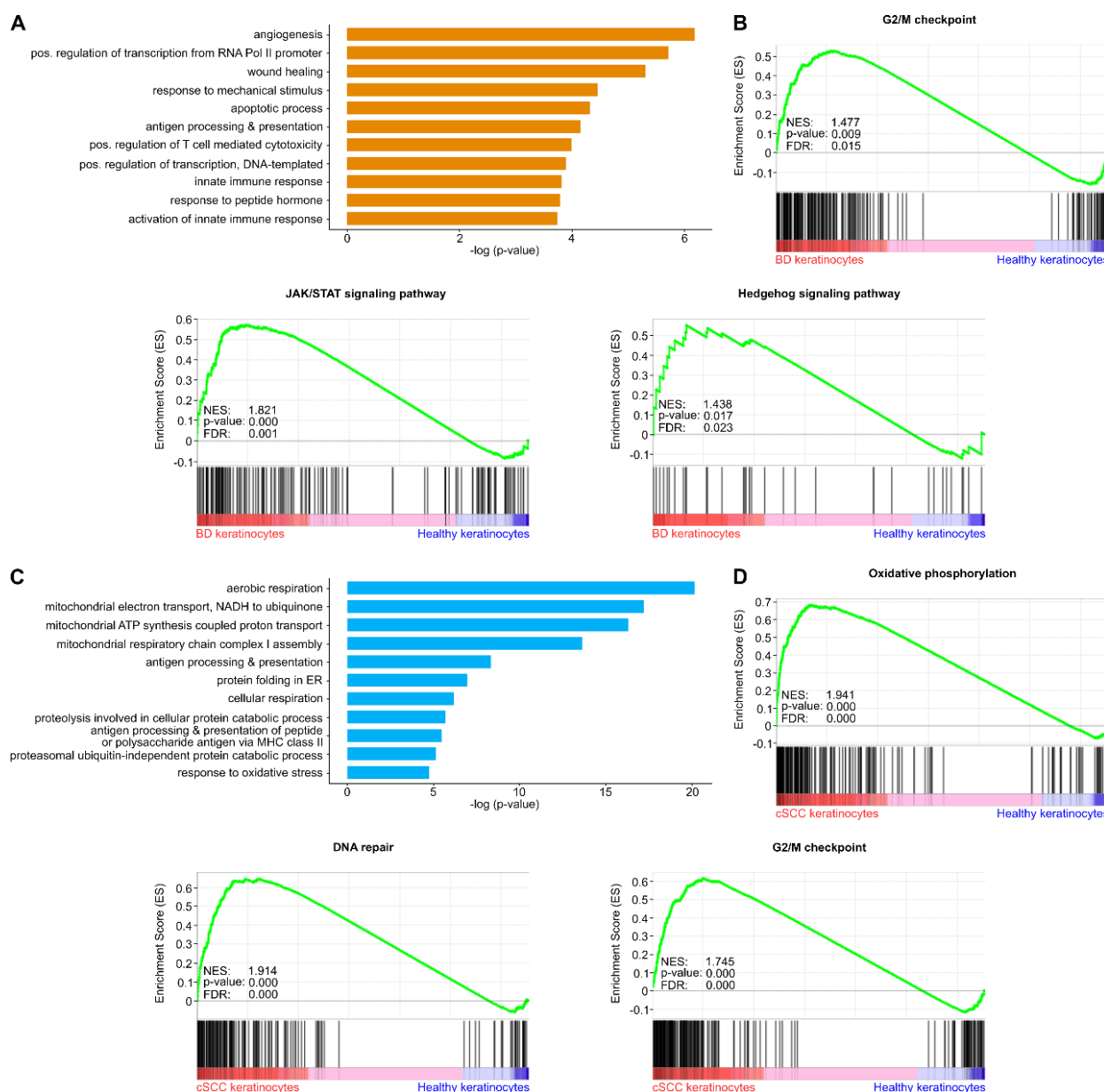
Figure 15. Transcriptomic changes in keratinocytes from healthy skin, Bowen's disease, and cutaneous squamous cell carcinoma. (A) Bar plot showing the top terms from a gene ontology (GO) analysis with the most upregulated genes in Bowen's disease (BD)-derived keratinocytes compared to keratinocytes from ultraviolet radiation (UVR)-protected healthy (PH) skin and UVR-exposed healthy (EH) skin. Terms are ordered according to *p*-value. **(B)** Gene set enrichment analysis (GSEA) plots visualizing the enrichment of pathways related to cancer progression in BD-derived keratinocytes compared to keratinocytes from PH and EH skin samples. **(C)** Bar plot depicting the top terms from a GO analysis with the most upregulated genes in cutaneous squamous cell carcinoma (cSCC)-derived keratinocytes compared to keratinocytes from PH and EH skin samples. Terms are ordered according to *p*-value. **(D)** GSEA plots showing the enrichment of pathways related to cancer progression in cSCC-derived keratinocytes compared to keratinocytes from PH and EH skin samples. For all GSEA plots, normalized enrichment scores (NES), false discovery rates (FDR) and *p*-values are specified. Pol: polymerase, pos.: positive, ER: endoplasmic reticulum.

3.1.2 Fibroblast subpopulations are maintained during cSCC progression

After characterizing the identified keratinocytes in the scRNA-seq dataset and ensuring the malignant status of BD and cSCC samples, fibroblasts were analyzed in greater detail.

Unsupervised clustering of the integrated dataset, including all samples, revealed four distinct fibroblast clusters, which were present in all entities (Figures 12A and 13A). Since our research group, including myself, previously defined four spatially and functionally different fibroblast subpopulations in UVR-protected healthy skin (Solé-Boldo *et al.*, 2020) (see Introduction, section 1.1.4), I checked if these groups were represented by the fibroblast clusters detected during the scRNA-seq analysis for this thesis.

First, fibroblasts (27,382 cells) were isolated from the total dataset and the four clusters were re-arranged for visual reasons (Figure 16A). Then, the average expression levels of the published subpopulation-specific gene signatures (Solé-Boldo *et al.*, 2020) were analyzed. In the uniform manifold approximation and projection (UMAP) plots and in the violin plots cluster-specific expression patterns of the particular marker genes could be observed (Figure 16B). Fibroblasts in cluster #1 showed high expression for the cytokines *CCL19*, *APOE*, *CXCL2*, *CXCL3*, and *EFEMP1*, representing pro-inflammatory fibroblasts. Highest expression of the secretory-reticular gene signature (*CCN5* [also known as *WISP2*], *SLPI*, *CTHRC1*, *MFAP5*, *and TSPAN8*) was detected in the fibroblast cluster #3. The mesenchymal-related genes *ASPN*, *POSTN*, *GPC3*, *TNN*, and *SFRP1* were mostly expressed in the fibroblast cluster #6. Cells in cluster #13 were identified as secretory-papillary fibroblasts, due to enriched expression of the genes *APCDD1*, *ID1*, *WIF1*, *COL18A1*, and *PTGDS*.

Furthermore, these classifications were confirmed by GO analyses with the most differently expressed genes between all fibroblast clusters (Figure 16C). Inflammation-related terms, such as inflammatory response were enriched for pro-inflammatory fibroblasts. Genes involved in mesenchymal-related processes, like osteoblast differentiation and ossification were specifically upregulated in mesenchymal fibroblasts. For the two secretory fibroblast subpopulations, GO terms associated with ECM remodeling and collagen organization were detected.
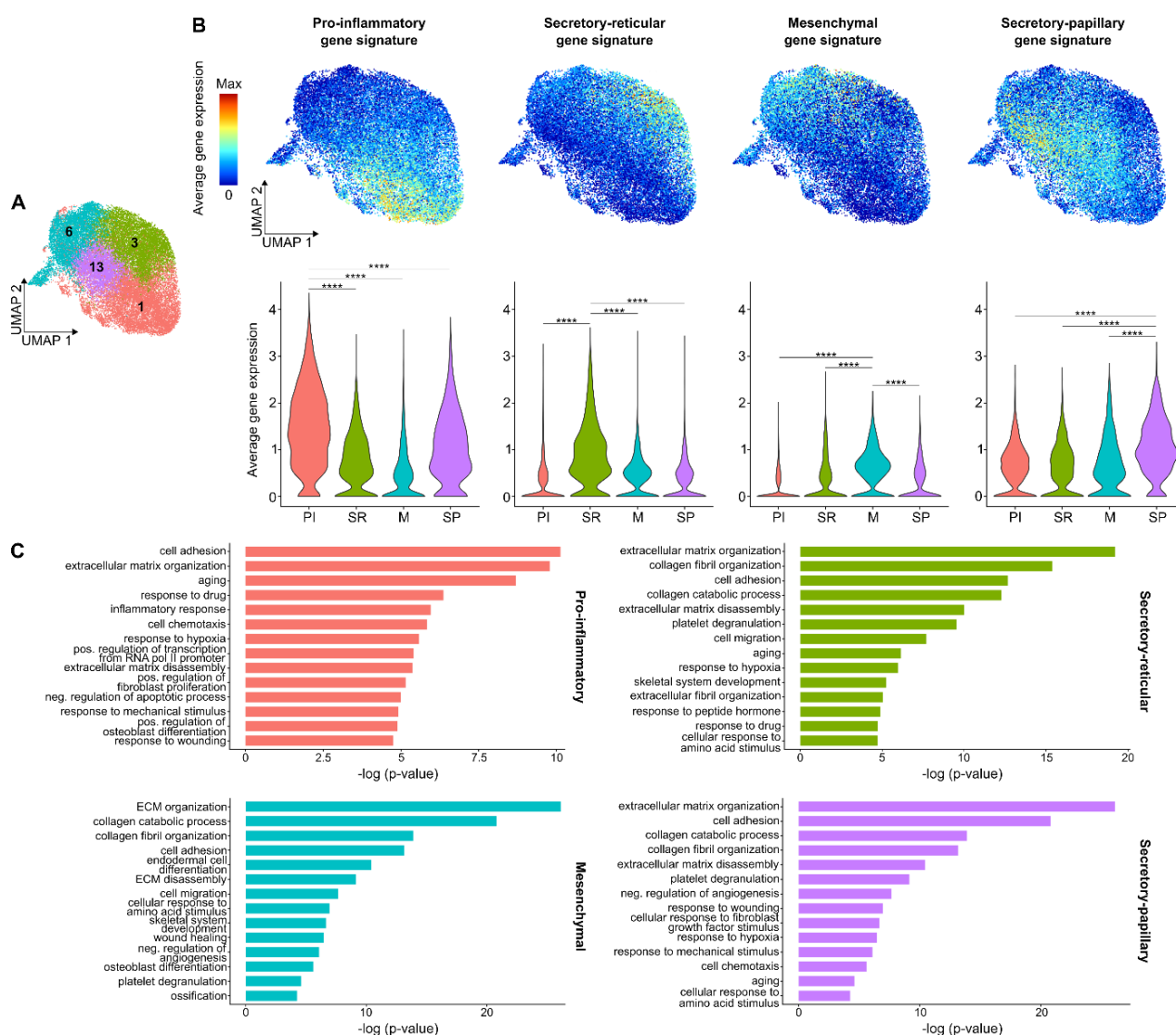
Figure 16. Distinct fibroblast subpopulations are present in healthy skin, Bowen's disease, and cutaneous squamous cell carcinoma. (A) Uniform manifold approximation and projection (UMAP) plot visualizing the four fibroblast clusters after their isolation from the integrated single-cell RNA sequencing (scRNA-seq) dataset, including ultraviolet radiation (UVR)-protected healthy (PH) skin (n = 3) and UVR-exposed healthy (EH) skin (n = 3), Bowen's disease (BD) samples (n = 3), and cutaneous squamous cell carcinomas (cSCCs) (n = 5). For visual reasons, the clusters were re-arranged. **(B)** UMAP and violin plots showing the average expression of previously defined fibroblast subpopulation-specific marker gene signatures (Solé-Boldo *et al.*, 2020). For UMAP plots, red indicates high expression in arbitrary units and blue refers to no or only low expression in arbitrary units. In violin plots, fibroblast clusters are displayed along the X-axes and Y-axes show the average gene expression in arbitrary units. Statistical analyses were performed using Wilcoxon Rank Sum tests (****: *p*-value < 0.0001). **(C)** Bar plots depicting the top terms from gene ontology (GO) analyses with the most differently expressed genes between all four fibroblast subpopulations. Terms are ordered according to *p*-value. Max: maximum, PI: pro-inflammatory, SR: secretory-reticular, M: mesenchymal, SP: secretory-papillary, pos.: positive, Pol: polymerase, ECM: extracellular matrix, neg.: negative.

Interestingly, comparison of fractions for the four fibroblast subpopulations detected in each sample revealed a slight decrease of pro-inflammatory cells and a significant increase of mesenchymal fibroblasts (*p*-value < 0.05, one-way analysis of variance [ANOVA] and pairwise Holm-Sidak test) in cSCCs compared to PH samples (Figure 17A). In order to check if this significant rise was caused by an enriched proliferation of mesenchymal-associated cells in cSCC, cell cycle-related analyses were performed with mesenchymal fibroblasts from all

sample types. Mesenchymal fibroblasts were assigned to the different cell cycle phases (G2/M, S, G1) based on the expression of publicly available cell cycle-related genes (Tirosh *et al.*, 2016). The percentages of mesenchymal fibroblasts in these phases were similar across all sample types, indicating comparable proliferation rates (Figure 17B). Only slight differences were observed in the average expression levels for cell cycle-related genes (Tirosh *et al.*, 2016) in mesenchymal cells from all sample types (Figure 17C). In addition, no increased expression of proliferation-related genes (Whitfield *et al.*, 2006) was detected in cSCC-derived mesenchymal fibroblasts compared to cells from PH samples (Figure 17D). All this suggests, that the detection of an increased fraction of mesenchymal cells in cSCCs was probably not related to cell cycle changes or different proliferation rates during disease progression.

Taken together, the fibroblast subpopulations previously identified in PH samples were also detected in EH skin, BD samples and cSCCs, indicating the maintenance of fibroblast heterogeneity during cSCC progression. However, their proportions seem to change in a cancer-related manner.
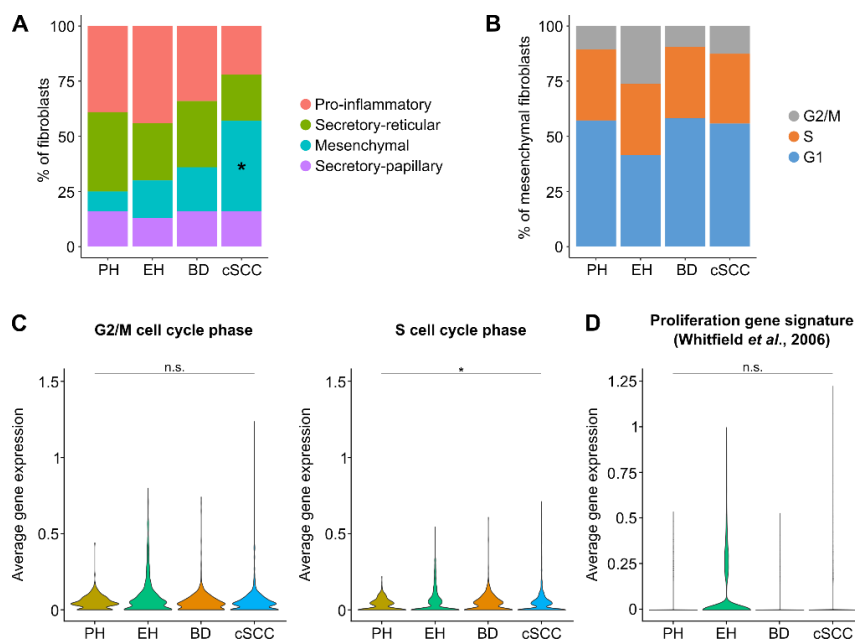
Figure 17. Percentages of fibroblast subpopulations change during cutaneous squamous cell carcinoma progression. (A) Bar plot showing the composition of fibroblasts in ultraviolet radiation (UVR)-protected healthy (PH) skin, UVR-exposed healthy (EH) skin, Bowen's disease (BD) samples, and cutaneous squamous cell carcinomas (cSCCs). The sample types are depicted along the X-axis and the Y-axis displays the percentages for pro-inflammatory, secretory-reticular, mesenchymal, and secretory-papillary fibroblasts with respect to all fibroblasts detected in each sample type. **(B)** Bar plot visualizing the assignment of mesenchymal fibroblasts to the cell cycle phases G2/M, S, and G1 based on the expression of related genes (Tirosh *et al.*, 2016). The X-axis shows the different sample types and the Y-axis depicts the percentages of cells in the three phases with respect to all mesenchymal fibroblasts detected in each sample type. **(C)** Violin plots show the average expression levels for genes related to the G2/M (left) and S (right) cell cycle phases (Tirosh *et al.*, 2016) in mesenchymal fibroblasts from all entities. Sample types are displayed along the X-axes and the Y-axes indicate the average gene expression in arbitrary units. **(D)** Violin plot depicting the average expression of proliferation-related genes (Whitfield *et al.*, 2006) in mesenchymal fibroblasts from all entities. Sample types are displayed along the X-axis and the Y-axis indicates the average gene expression in arbitrary units. For bar plots, statistical analyses were performed using a one-way analysis of variance (ANOVA) with subsequent Holm-Sidak tests for pairwise comparisons and for violin plots, Wilcoxon Rank Sum tests were used (*: p-value < 0.05). n.s.: not significant.

3.2 Characterization of CAFs in BD and cSCC by scRNA-seq

After the general characterization of the two main cell types in human skin, CAF development during cSCC progression should be studied in more detail by scRNA-seq. First, I checked if fibroblasts isolated from BD samples and cSCCs were actually different from healthy fibroblasts and show CAF-related transcriptomic changes. Therefore, the average expression levels of the commonly used CAF marker genes *FAP* and *ACTA2* (Chhabra and Weeraratna, 2023; Simon and Salhia, 2022) were determined in fibroblasts from all sample types. BD- and cSCC-derived fibroblasts showed an upregulation of both genes compared to healthy skin, indicating that they were indeed CAFs (Figure 18A). Furthermore, a trajectory inference approach using the R tool Slingshot v1.8 (Street *et al.*, 2018) showed a progression from PH-derived fibroblasts to CAFs from BD samples and cSCCs (Figure 18B). Based on these observations and the fact, that BD and cSCC biopsies were sampled from the center of the lesions, I considered all BD- and cSCC-derived fibroblasts as CAFs for the following analyses.
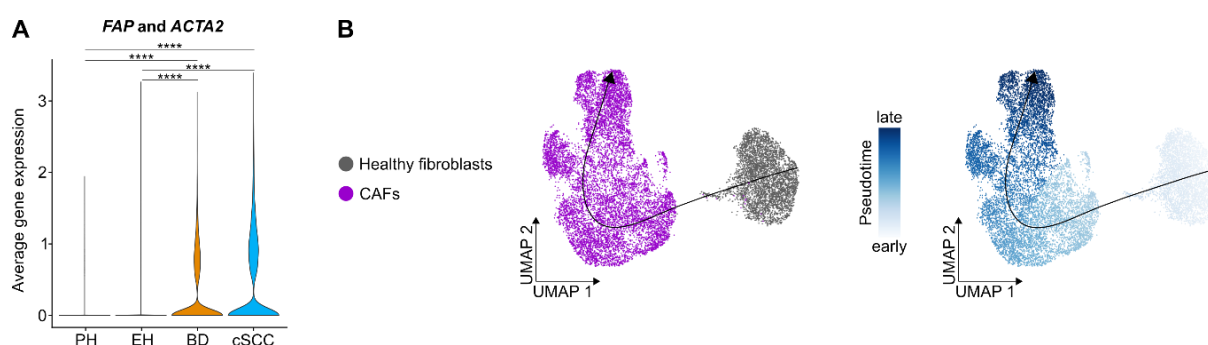
Figure 18. Cancer-associated fibroblasts in Bowen's disease and cutaneous squamous cell carcinoma develop from resident fibroblasts in healthy skin. (A) Violin plot showing the average expression level for commonly used cancer-associated fibroblast (CAF) marker genes *FAP* and *ACTA2* in fibroblasts isolated from ultraviolet radiation (UVR)-protected healthy (PH) skin, UVR-exposed healthy (EH) skin, Bowen's disease (BD) samples, and cutaneous squamous cell carcinomas (cSCCs). Sample types are displayed along the X-axis and the Y-axis indicates the average gene expression in arbitrary units. Statistical analyses were performed using Wilcoxon Rank Sum tests (****: *p*-value < 0.0001). **(B)** Uniform manifold approximation and projection (UMAP) plots visualizing fibroblast trajectory inference from single-cell RNA sequencing (scRNA-seq) data. The progression from PH-derived fibroblasts to CAFs from BD samples and cSCCs is indicated by an arrow. White and light blue represent early time points and dark blue depicts late time points on an arbitrary pseudotime axis.

3.2.1 Detection of two functionally different CAF subpopulations

To focus on CAF characterization, fibroblasts detected in BD samples and cSCCs were isolated (9,763 cells). Unsupervised re-clustering of the cells revealed two clusters comprising 4,937 cells and 4,826 cells, respectively (Figure 19A). Then, GO analyses with the most representative genes of both groups were performed to determine potential functional differences (Figure 19B). For one cluster, terms related to inflammation and stress responses were enriched, such as inflammatory response and response to unfolded proteins, suggesting

upregulation of genes involved in immunoregulatory processes for these CAFs. On the other hand, the second CAF group showed enriched expression of genes associated with ECM remodeling, wound healing, and collagen organization.
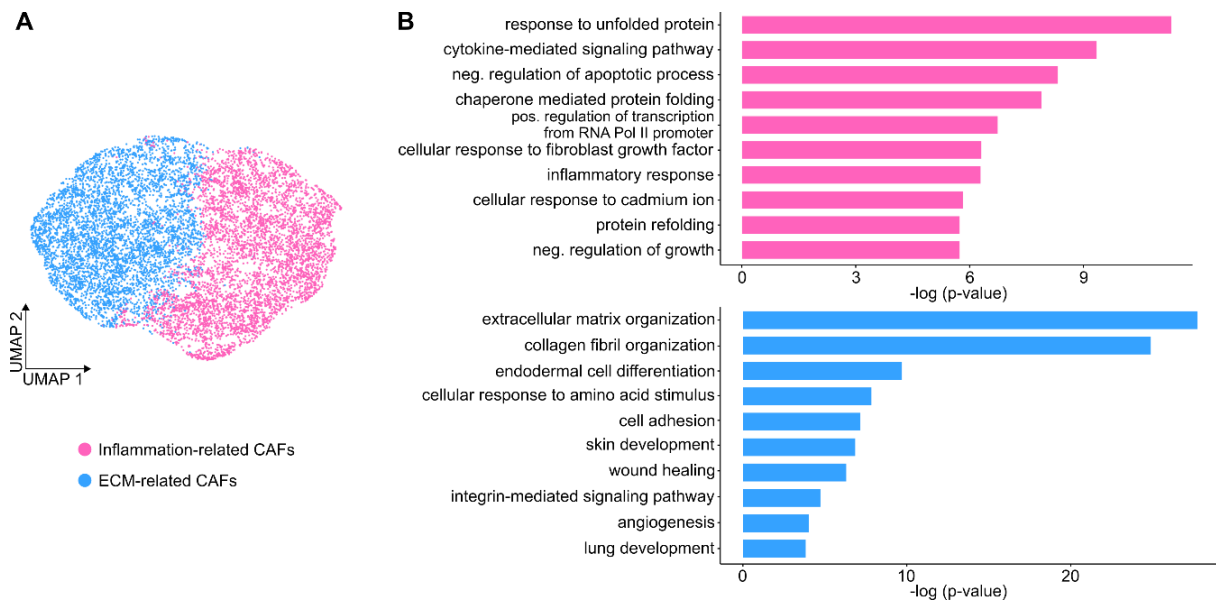
Figure 19. Identification of two cancer-associated fibroblast subpopulations in Bowen's disease and cutaneous squamous cell carcinoma. (A) Uniform manifold approximation and projection (UMAP) plot visualizing two clusters of cancer-associated fibroblasts (CAFs) in Bowen's disease (BD) samples and cutaneous squamous cell carcinomas (cSCCs) analyzed by single-cell RNA sequencing (scRNA-seq). **(B)** Bar plots showing the top terms of gene ontology (GO) analyses performed with the most representative genes of both CAF clusters. Terms are ordered according to *p*-value. ECM: extracellular matrix, neg.: negative, pos.: positive, Pol: polymerase.

In order to check whether these two CAF groups represent iCAFs and myCAFs, previously described in different cancer types (Bhattacharjee *et al.*, 2021; Chhabra and Weeraratna, 2023; Kieffer *et al.*, 2020; Öhlund *et al.*, 2017), I then performed several analyses. In PDAC studies, specific iCAF and myCAF marker gene signatures were identified, including *CXCL2*, *C3*, *IL6* or *MMP11*, *TAGLN*, *ACTA2*, respectively (Elyada *et al.*, 2019; Öhlund *et al.*, 2017). Expression analyses with these signatures revealed a differential expression pattern in the BD- and cSCC-derived CAFs (Figure 20A). High expression of iCAF marker genes were detected in the CAF group, that was associated with inflammation-related GO terms, whereas CAFs associated with ECM-related GO terms showed high expression of the myCAF marker genes. This was also supported by higher similarity scores for the iCAF signature in inflammation-related CAFs and for the myCAF signature in ECM-related CAFs.

Furthermore, the same PDAC-derived CAF signatures were used to perform GSEA with CAFs isolated from BD samples and cSCCs, separately. Inflammation-related CAFs from both entities showed significant enrichment for the iCAF marker gene signature compared to ECM-related CAFs (Figure 20B). In contrast, the myCAF marker gene signature was significantly enriched in BD- and cSCC-derived ECM-related CAFs compared to inflammation-related

CAFs (Figure 20C). Therefore, the nomenclature of iCAFs and myCAFs was transferred to CAFs from BDs and cSCCs.
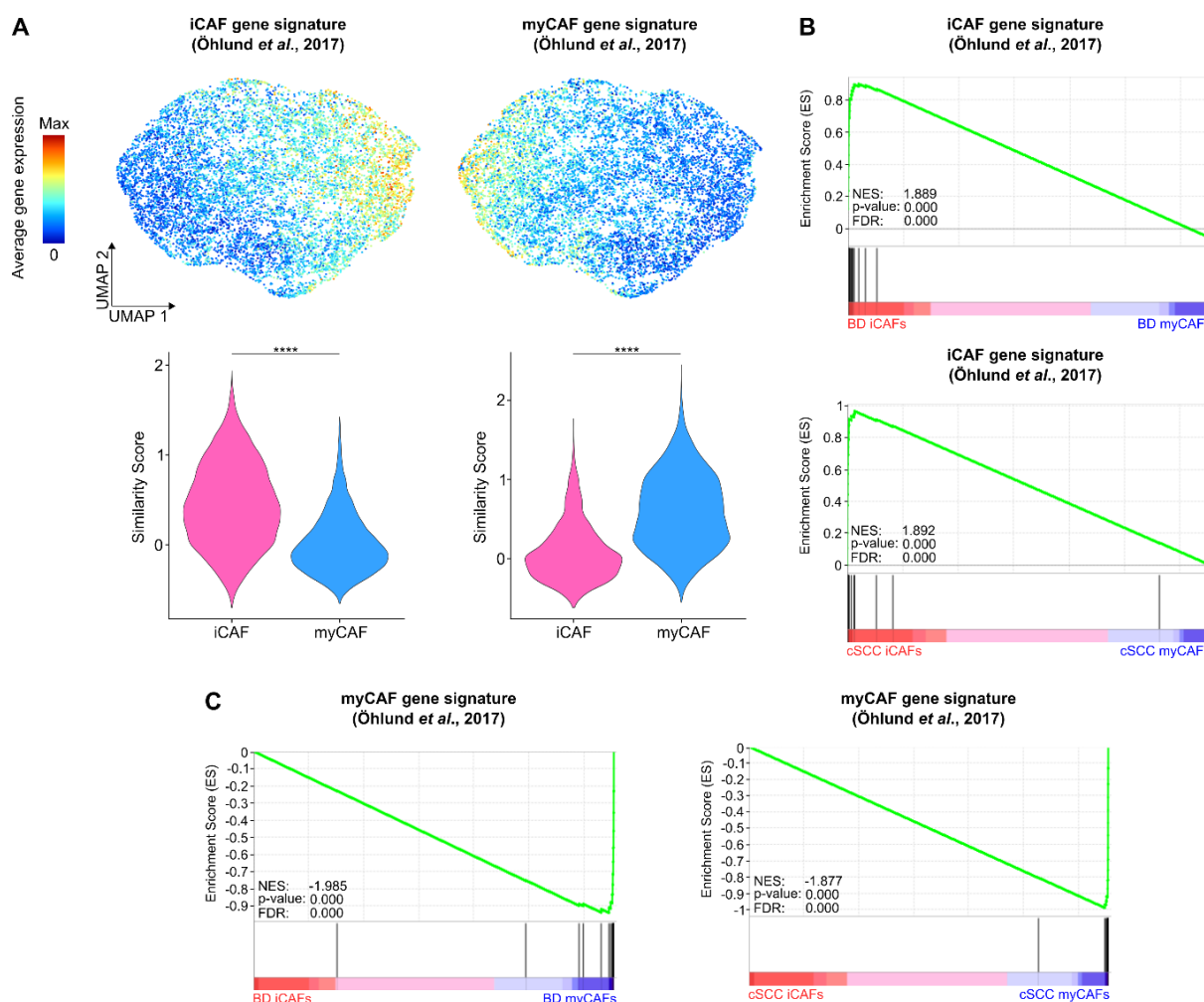
Figure 20. Inflammatory and myofibroblastic cancer-associated fibroblasts are present in Bowen's disease and cutaneous squamous cell carcinoma. (A) Uniform manifold approximation and projection (UMAP) plots and violin plots showing the average expression of pancreatic inflammatory cancer-associated fibroblast (iCAF) and myofibroblastic CAF (myCAF) gene signatures (Elyada *et al.*, 2019; Öhlund *et al.*, 2017) (up) and their similarity scores (down) with CAFs derived from Bowen's disease (BD) and cutaneous squamous cell carcinoma (cSCC) samples. For UMAP plots, red indicates high expression in arbitrary units and blue refers to no or only low expression in arbitrary units. In violin plots, CAF clusters are displayed along the X-axes and Y-axes show the average gene expression in arbitrary units. Statistical analyses were performed using Wilcoxon Rank Sum tests (****: *p*-value < 0.0001). **(B)** Gene set enrichment analysis (GSEA) plots visualizing the enrichment of the pancreatic iCAF gene signature (Elyada *et al.*, 2019; Öhlund *et al.*, 2017) in iCAFs isolated from BD samples (up) and cSCCs (down) compared to myCAFs. **(C)** GSEA plots visualizing the enrichment of the pancreatic myCAF gene signature (Elyada *et al.*, 2019; Öhlund *et al.*, 2017) in myCAFs isolated from BD samples (left) and cSCCs (right) compared to iCAFs. For all GSEA plots, the normalized enrichment score (NES), false discovery rate (FDR) and *p*-value are given. Max: maximum.

In order to analyze potential differences regarding CAFs from BD samples and cSCCs, I determined the proportions of iCAFs and myCAFs in each sample. In BDs, on average 61% ± 9% SD of all CAFs were classified as iCAFs, whereas only 40% ± 20% SD in cSCCs (Figure 21A). In contrast, 39% ± 9% SD myCAFs were detected in BD samples and 60% ± 20% SD in cSCCs.

To check whether these differences were caused by changes in the proliferation rate of CAFs during cSCC progression, the expression levels of proliferation-related genes (Whitfield *et al.*, 2006) were determined in the sample type-specific CAF subpopulations (Figure 21B). None of them showed significant expression, excluding the possibility of more proliferating iCAFs and myCAFs in BDs and cSCCs, respectively. For cell cycle-related genes (Tirosh *et al.*, 2016) differential expression was detected between both CAF subpopulations in BD samples and cSCCs (Figure 21C). However, the effect size for these differences was quite small, and when CAFs were assigned to the different cell cycle phases (G2/M, S, G1) based on the gene expression levels, similar proportions of CAFs were observed in the respective phases for all groups (Figure 21D). These observations suggest that the different percentages of iCAFs and myCAFs in BD samples and cSCCs were probably not related to changes in cell cycle or proliferation rate during the disease progression, but might reflect cancer stage-dependent conditions.
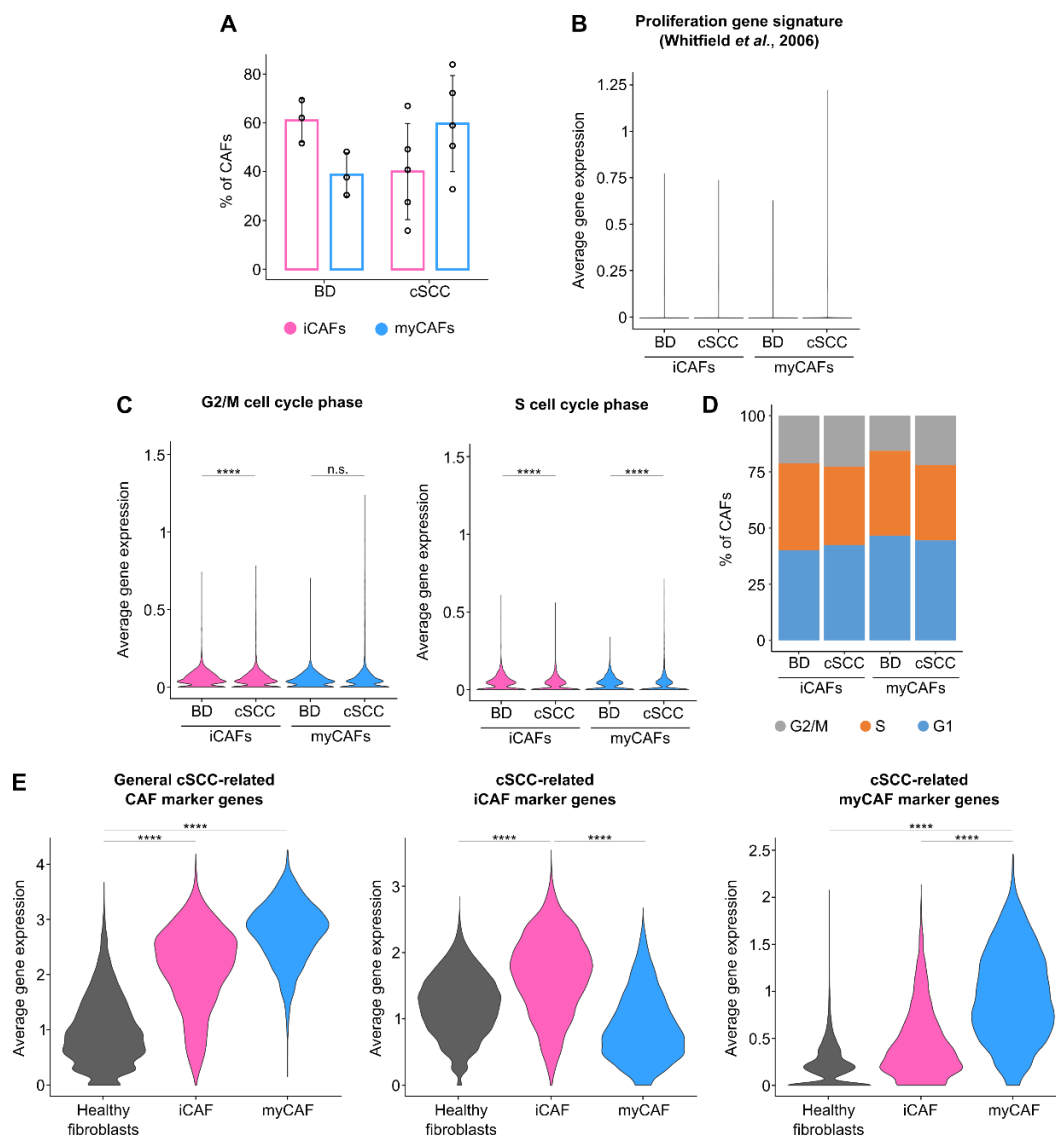
Figure 21. Different proportions of inflammatory and myofibroblastic cancer-associated fibroblasts in Bowen's disease and cutaneous squamous cell carcinoma. (A) Bar plot showing the proportions of

inflammatory cancer-associated fibroblasts (iCAFs) and myofibroblastic CAFs (myCAFs) in Bowen's disease (BD) and cutaneous squamous cell carcinoma (cSCC). CAF subpopulations from both entities are displayed along the X-axis and the Y-axis indicates the percentages of detected iCAFs and myCAFs related to the total amount of CAFs in each sample type. Each dot represents one single-cell RNA sequencing (scRNA-seq) sample and error bars indicate the standard deviation. **(B)** Violin plot visualizing the average expression of proliferation-related genes (Whitfield *et al.*, 2006) in iCAFs and myCAFs from BD samples and cSCCs. **(C)** Violin plots depicting the average expression levels for genes related to the G2/M (left) and S (right) cell cycle phases (Tirosh *et al.*, 2016) in iCAFs and myCAFs from BD samples and cSCCs. **(D)** Bar plot showing the assignment of iCAFs and myCAFs from BD samples and cSCCs to the cell cycle phases G2/M, S, and G1 based on the expression of related genes (Tirosh *et al.*, 2016). The X-axis shows the different sample types and the Y-axis depicts the percentages of cells in the three phases with respect to all iCAFs or myCAFs detected in each sample type. **(E)** Violin plots visualizing the average expression levels for general cSCC-related CAF marker genes (left), as well as for iCAF- (middle) and myCAF-specific (right) gene signatures in fibroblasts and CAFs from all sample types (Table 1). For all violin plots, CAF subpopulations in the particular sample entities are displayed along the X-axes and the Y-axes indicate the average gene expression in arbitrary units. Statistical analyses were performed using Wilcoxon Rank Sum tests and t-tests (****: *p*-value < 0.0001). n.s.: not significant.

All these scRNA-seq analyses indicate the presence of two functionally distinct CAF subpopulations that have important roles in inflammatory processes and ECM organization, respectively. Based on their gene expression patterns, representative marker gene signatures were generated for both, including *CXCL12* and *IGF1* for iCAFs or *MMP11* and *WNT5A* for myCAFs (Table 1). However, although the two subpopulations show significant differences in their transcriptome, common upregulated genes were also detected compared to healthy fibroblasts, such as *IGLL5* and *COL3A1* (Table 1), indicating general cancer-related transcriptomic changes caused by cSCC-related CAF activation. As expected, these different CAF signatures were enriched in iCAFs and/or myCAFs from BD samples and cSCCs, compared to PH- and EH-derived fibroblasts (Figure 21E).

	Gene	Fold change	% CAFs	% healthy	Adjusted *p*-value
General cSCC-related CAF marker genes	IGLL5	15	47	6	0
	COL1A1	5.7	97	73	0
	COL3A1	4.9	95	63	0
	POSTN	4.5	61	20	0
	COL5A1	4.1	64	14	0
	COL6A1	3.8	93	60	0
	COL1A2	3.8	98	81	0
	S100A9	3.5	43	11	0
	S100A7	3.4	36	6	0
	COL5A2	3.4	72	25	0
cSCC-related iCAF marker genes	IGF1	2.2	39	15	0
	JUND	2.2	68	43	0
	MGP	1.9	69	55	2.5E-126

	JUN	1.9	78	57	1.9E-246
	HSP90AA1	1.9	83	67	1.6E-162
	XBP1	1.9	37	27	1.1E-53
	HSPA1A	1.7	83	70	1E-127
	GPC3	1.7	27	10	6E-228
	CCDC80	1.7	80	75	2.4E-46
	CXCL12	1.7	70	54	1.4E-111
	C3	1.6	52	33	5E-133
	TSC22D3	1.5	38	23	4.1E-95
	MMP11	5.2	35	4	0
	TAGLN	3.7	43	13	0
	TDO2	3.3	26	3	0
	COL11A1	3	35	5	0
	SULF1	2.8	30	4	0
	BGN	2.8	80	39	0
cSCC-related myCAF marker genes	*WNT5A*	2.7	28	3	0
	ASPN	2.7	28	7	0
	IFI6	2.5	47	22	0
	PTK7	2.4	40	9	0
	NREP	2.3	32	7	0
	TPM1	2.3	59	29	0
	MYL9	2.2	57	28	0

Table 1. Most representative marker genes of cancer-associated fibroblasts in Bowen's disease and cutaneous squamous cell carcinoma. Marker gene signatures for cutaneous squamous cell carcinoma (cSCC)-related cancer-associated fibroblasts (CAFs) in general, as well as for specialized inflammatory CAFs (iCAFs) and myofibroblastic CAFs (myCAFs). The expression characteristics, such as fold change, percentage of cells expressing the particular gene (% CAFs, % healthy), and *p*-value are based on single-cell RNA sequencing (scRNA-seq) analyses. Statistical analyses were performed using Wilcoxon Rank Sum tests and adjusted *p*-values were Bonferroni-corrected.

3.2.2 iCAFs and myCAFs potentially originate from distinct healthy fibroblast subpopulations

After functional characterization of iCAFs and myCAFs in BD and cSCC, I studied their origin with respect to the four healthy fibroblast subpopulations. Expression analyses of the particular healthy fibroblast gene signatures (Solé-Boldo *et al.*, 2020) in both CAF subtypes revealed an upregulation of pro-inflammatory-related genes in iCAFs, whereas myCAFs showed enriched expression of mesenchymal-related genes (Figure 22A).

Furthermore, the overlap of the most representative genes of the four healthy fibroblast subpopulations with both CAF subtypes was determined (Figure 22B). Among all pairwise comparisons, the highest number of intersecting genes was detected between iCAFs and pro-inflammatory fibroblasts, as well as between myCAFs and mesenchymal fibroblasts. In contrast, iCAFs and mesenchymal fibroblasts or myCAFs and pro-inflammatory fibroblasts had no marker genes in common.

Since CAFs from BD samples and cSCCs showed co-expression of fibroblast subpopulation-related genes and CAF subtype-specific genes, it could be observed that iCAFs and myCAFs cluster mostly with pro-inflammatory and mesenchymal fibroblasts, respectively (Figure 22C). Accordingly, the significant majority of iCAFs was also classified as pro-inflammatory cells (p-value < 0.0001, paired t-test) and most myCAFs could also be classified as mesenchymal fibroblasts (p-value < 0.0001, paired t-test) (Figure 22D).

Taken together, the predicted inflammation-related functions of iCAFs and their similarity to pro-inflammatory fibroblasts suggest that this healthy fibroblast subpopulation is potentially the source of iCAFs. In contrast, the involvement of myCAFs in ECM remodeling and their correlation with mesenchymal fibroblasts may indicate cSCC-related activation of mesenchymal healthy fibroblasts to myCAFs.
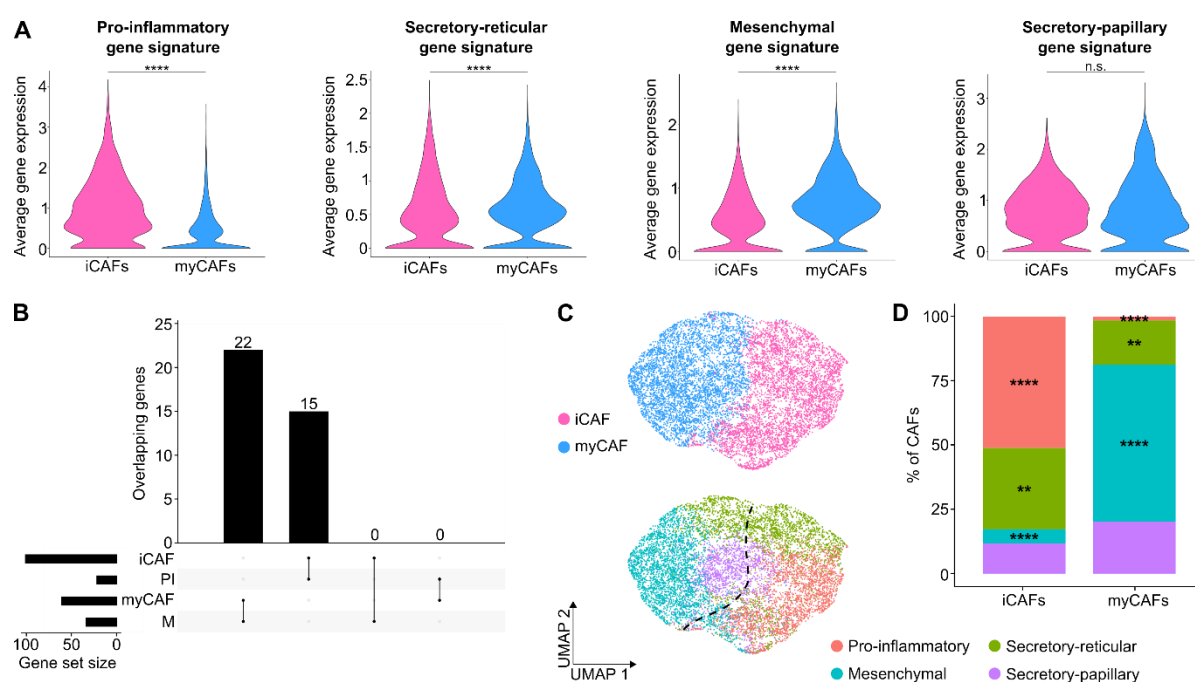
Figure 22. Cancer-associated fibroblasts in Bowen's disease and cutaneous squamous cell carcinoma may originate from different healthy fibroblast subpopulations. (A) Violin plots showing the average expression of gene signatures from healthy fibroblast subpopulations (Solé-Boldo *et al*., 2020) in Bowen's disease (BD)- and cutaneous squamous cell carcinoma (cSCC)-derived inflammatory cancer-associated fibroblasts (iCAFs) and myofibroblastic CAFs (myCAFs). The CAF subtypes are displayed along the X-axes and Y-axes indictae the average gene expression in arbitrary units. **(B)** Bar plot visualizing the overlapping genes between the most representative markers of iCAFs, myCAFs, mesenchymal (M) healthy fibroblasts, and pro-inflammatory (PI) healthy fibroblasts. **(C)** Uniform manifold approximation and projection (UMAP) plots showing CAFs from BD samples and cSCCs. The upper plot displays iCAF and myCAF classifications and the lower plot visualizes CAF assignment to the four fibroblast subpopulations. **(D)** Bar plot depicting the fractions of iCAFs and myCAFs classified as pro-

inflammatory, secretory-reticular, mesenchymal or secretory-papillary fibroblasts. Both CAF subtypes are displayed on the X-axis and the Y-axis shows the percentages of CAFs detected in each group. Statistical analyses were performed using Wilcoxon Rank Sum tests and paired t-tests (**: p-value < 0.01, ****: p-value < 0.0001). n.s.: not significant.

3.2.3 CAFs communicate with malignant keratinocytes via collagen and fibronectin 1 signaling networks

After a general CAF characterization in cSCC, I wanted to further study how these cells influence tumorigenesis in terms of cellular communication within the TME. Therefore, I performed interaction analyses with the R tools CellChat (Jin *et al.*, 2021) and LIANA (Dimitrov *et al.*, 2022), which are based on the comparison of scRNA-seq data with databases, including well-known ligand-receptor pairs. Overall, both CAF subpopulations were identified as the most important cell type with outgoing interactions (sender cells) in the TME of BDs and cSCCs (Figure 23A). Interestingly, in BDs, iCAFs showed an even higher outgoing interaction strength than myCAFs, whereas the opposite was the case for cSCCs. This might further support the cancer stage-dependent relevance of iCAFs and myCAFs, respectively. The highest incoming interaction strength was observed for T cells in BD samples and for keratinocytes in cSCCs (receiver cells).

It was then studied in more detail how CAFs affect malignant cells in cSCC. Thus, collagen and FN1 signaling pathways were determined as interaction networks with CAFs as the most important sender cells and malignant keratinocytes as the most important receiver cells (Figure 23B). Further analyses showed that many ligand-receptor pairs contributed to both interaction networks, but mostly collagen type I and VI, as well as FN1 were secreted by CAFs. Both computational tools predicted that these ligands preferentially bind to CD44 and SDC1/4, produced by malignant keratinocytes in cSCC (Figures 23C and 23D). Interestingly, several pathways activated by CD44 are already known to be involved in the proliferation and invasion of cancer cells (Chen *et al.*, 2018).
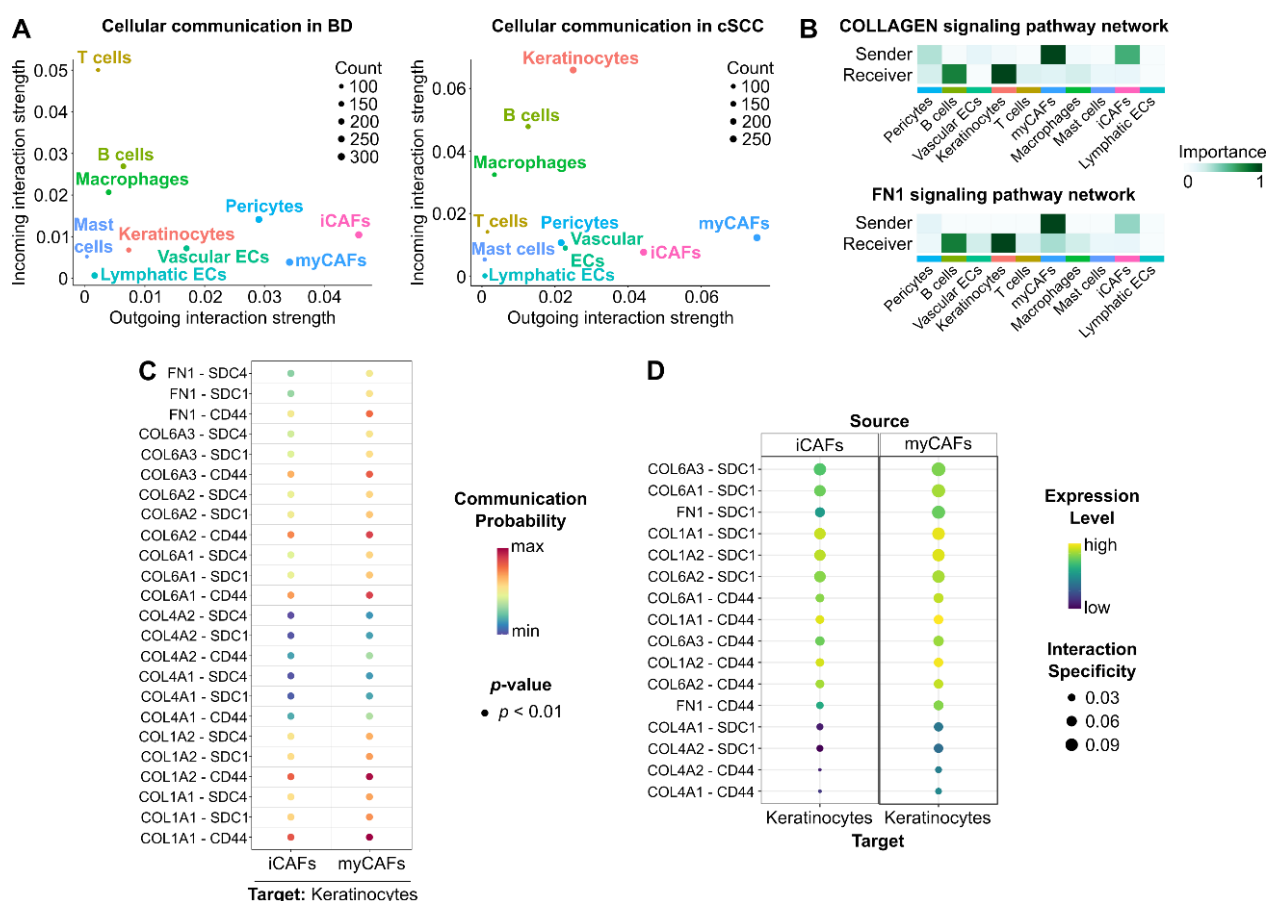
Figure 23. Cancer-associated fibroblasts influence cutaneous squamous cell carcinoma-derived keratinocytes by collagen and fibronectin 1 signaling. (A) Scatter plots showing the incoming (Y-axis) and outgoing (X-axis) interaction strength for the main cell types in the tumor microenvironment (TME) of Bowen's disease (BD; left) samples and cutaneous squamous cell carcinomas (cSCCs; right). **(B)** Heatmaps visualizing the importance of different cell types as sender and receiver cells in cSCC for the collagen (up) and fibronectin 1 (FN1; down) signaling pathway networks. **(C)** Dot plot depicting significant collagen- and FN1-related interaction pairs involved in the cellular communication between cancer-associated fibroblasts (CAFs) and cSCC-derived malignant keratinocytes. Red means high communication probability, whereas blue indicates low probability. Dot sizes correlate with the *p*-values of the particular interactions. The plot was generated using the R tool CellChat (Jin *et al.*, 2021). **(D)** Dot plot showing significant collagen- and FN1-related interaction pairs involved in the cellular communication between CAFs and cSCC-derived malignant keratinocytes. Yellow implies high expression of the ligand-receptor pair in both cell types, whereas purple depicts low expression. Here the dot sizes indicate the interaction specificity. The plot was generated using the R tool LIANA (Dimitrov *et al.*, 2022). iCAFs: inflammatory CAFs, myCAFs: myofibroblastic CAFs, ECs: endothelial cells, max: maximum, min: minimum.

3.2.4 Both CAF subpopulations establish a pro-tumorigenic TME via different cellular interactions with non-malignant cell types

After analyzing the common interactions between both CAF subpopulations and malignant keratinocytes, potential differences in their cellular communication were studied in more detail. For iCAFs, the CALCR and CXCL signaling networks were detected to be particular active. Both computational interaction tools inferred that the ligands ADM and CXCL12 were mostly secreted by iCAFs and bind to the receptors CALCRL, produced by vascular ECs, and CXCR4 on the surface of T cells and macrophages, respectively (Figures 24A and 24B). In addition, independent gene expression analyses for the two ligands revealed an upregulation for both

of them in cSCC-derived iCAFs compared to myCAFs (Figure 24C). Interestingly, for ADM, paracrine pro-tumorigenic functions were already observed by regulating angiogenesis and immune cell chemotaxis in the TME (Benyahia *et al.*, 2017; Zudaire *et al.*, 2006). Furthermore, signaling pathways initiated by the interaction pair CXCL12-CXCR4 are known to be involved in immunosuppression and T cell modulation (Sarchio *et al.*, 2014). GO analysis also showed, that genes that were upregulated in cSCC-derived T cells compared to T cells isolated from EH skin, are important for antigen procession, immune responses, and T cell activation (Figure 24D). This suggests cancer-related transcriptomic changes in T cells that might be caused by their interaction with iCAFs, creating an immunosuppressive TME.
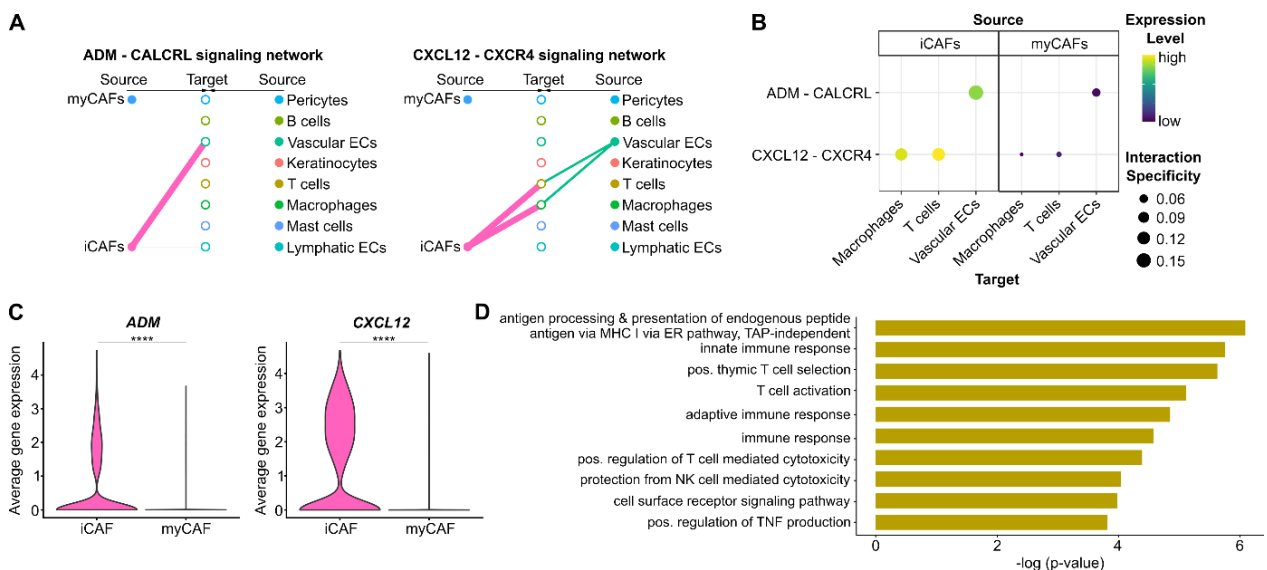
Figure 24. Inflammatory cancer-associated fibroblasts establish a pro-tumorigenic microenvironment by influencing vascular endothelial cells, macrophages, and T cells. (A) Plots showing sender and receiver cell types involved in the ADM-CALCRL (left) and CXCL12-CXCR4 (right) signaling networks in the tumor microenvironment (TME) of cutaneous squamous cell carcinoma (cSCC). Line thickness indicates the strength of the interaction, i.e. thicker lines mean stronger signals. **(B)** Dot plot visualizing the two interaction pairs ADM-CALCRL and CXCL12-CXCR4, that are involved in the cellular communication between inflammatory cancer-associated fibroblasts (iCAFs) and macrophages, T cells or vascular endothelial cells (ECs). Yellow indicates high expression of the ligand-receptor pair in both cell types, whereas purple means low expression. The dot sizes imply the interaction specificity. **(C)** Violin plots depicting the average expression levels of *ADM* (left) and *CXCL12* (right) in cSCC-derived iCAFs and myofibroblastic CAFs (myCAFs). The CAF subpopulations are displayed along the X-axes and Y-axes indictae the average gene expression in arbitrary units. Statistical analyses were performed using Wilcoxon Rank Sum tests (****: *p*-value < 0.0001). **(D)** Bar plots showing the top terms of a gene ontology (GO) analysis, performed with the most upregulated genes in cSCC-derived T cells compared to T cells from ultraviolet radiation (UVR)-exposed healthy (EH) skin samples. Terms are ordered according to *p*-value. ER: endoplasmic reticulum, TAP: transporter associated with antigen processing, pos.: positive, NK cell: natural killer cell.

In contrast, myCAFs were observed to interact with vascular ECs and pericytes rather than immune cells. Both computational interaction tools predicted that in the cSCC-related TME, myCAF-derived ANGPTL2 and WNT5A bind to integrin α5β1 (ITGA5/ITGB1) and MCAM, respectively (Figures 25A and 25B). The two interaction pairs are known to promote ECM remodeling, angiogenesis, and cell motility (Kadomatsu *et al.*, 2014; Richardson *et al.*, 2014; Ye *et al.*, 2013), similar to myCAF-related functions. Ligand specificity was further

demonstrated by expression analyses of *ANGPTL2* and *WNT5A*, which showed upregulation in cSCC-derived myCAFs compared to iCAFs (Figure 25C). Interestingly, a GO analysis of the most upregulated genes in vascular ECs from cSCCs compared to EH skin-derived ECs revealed that these cancer-related transcriptomic changes are predominantly involved in angiogenesis, vasculogenesis, and cell migration (Figure 25D).

Taken together, these results suggest that iCAFs and myCAFs not only influence malignant cSCC-derived keratinocytes to promote tumorigenesis, but also interact with different non-malignant cell types. Both subpopulations contribute to the establishment of a pro-tumorigenic TME by the secretion of specific ligands, that activate different signaling pathways, resulting in enriched angiogenesis, immunosuppression, ECM remodeling, and cell motility. In addition to the common cellular communication between all CAFs and vascular ECs, the specific interactions of iCAFs with immune cells and myCAFs with pericytes support their predicted functions, as revealed by previous gene expression analyses.
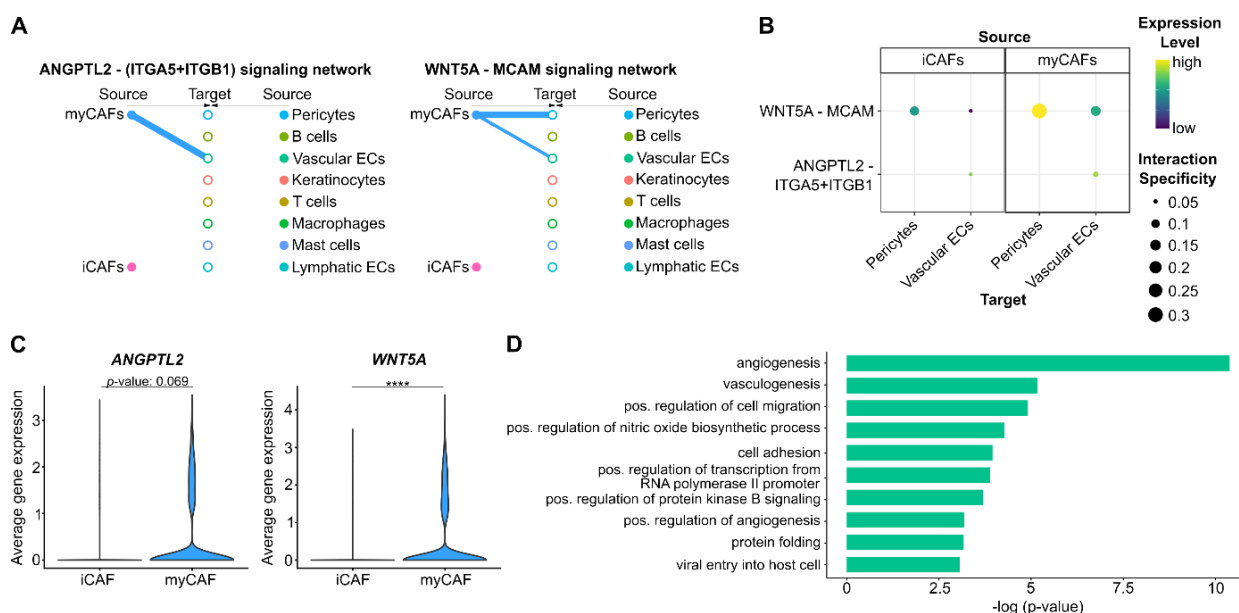
Figure 25. Myofibroblastic cancer-associated fibroblasts establish a pro-tumorigenic microenvironment by influencing vascular endothelial cells and pericytes. (A) Plots showing sender and receiver cell types involved in the ANGPTL2-(ITGA5+ITGB1) (left) and WNT5A-MCAM (right) signaling networks in the tumor microenvironment (TME) of cutaneous squamous cell carcinoma (cSCC). Line thickness indicates the strength of the interaction, i.e. thicker lines mean stronger signals. **(B)** Dot plot visualizing the two interaction pairs ANGPTL2-(ITGA5+ITGB1) and WNT5A-MCAM involved in the cellular communication between myofibroblastic cancer-associated fibroblasts (myCAFs) and pericytes or vascular endothelial cells (ECs). Yellow indicates high expression of the ligand-receptor pair in both cell types, whereas purple means low expression. The dot sizes imply the interaction specificity. **(C)** Violin plots depicting the average expression levels of *ANGPTL2* (left) and *WNT5A* (right) in cSCC-derived inflammatory CAFs (iCAFs) and myCAFs. The CAF subpopulations are displayed along the X-axes and Y-axes indictae the average gene expression in arbitrary units. Statistical analyses were performed using Wilcoxon Rank Sum tests (****: *p*-value < 0.0001). **(D)** Bar plots showing the top terms of a gene ontology (GO) analysis, performed with the most upregulated genes in cSCC-derived vascular ECs compared to ECs from ultraviolet radiation (UVR)-exposed healthy (EH) skin samples. Terms are ordered according to *p*-value. pos.: positive.

3.3 Detection of CAFs during cSCC progression by multiplexed RNA FISH assays

After this functional CAF characterization via scRNA-seq, the next aim was to detect CAFs *in situ* during cSCC progression, and to validate previous findings. Therefore, multiplexed RNA FISH assays were performed using specific fluorescent probes that hybridize with mRNA molecules of selected marker genes (see Material and Methods, section 6.2.5). For these experiments, three formalin-fixed paraffin-embedded (FFPE) sections of EH skin were used, as well as three from AK samples, three BD sections, and five from cSCC tumors. As for scRNA-seq, only samples from older (65-88 years) male donors and patients were selected for the multiplexed RNA FISH assays (Table 7).

FFPE sections of AK, BD, and cSCC samples were kindly provided by the tissue bank of the National Center for Tumor Diseases (NCT) in Heidelberg, coordinated by PD Dr. med. Anke Lonsdorf. Moreover, diseased skin sections were reviewed by PD Dr. med. Anke Lonsdorf and Prof. Dr. med. Jochen Hoffmann, to define regions of non-tumoral skin, AK, BD, and cSCC. In contrast, fresh biopsies of EH skin were kindly provided by the Department of Dermatology, University Hospital of Heidelberg, coordinated by PD Dr. med. Anke Lonsdorf and then processed by me (see Material and Methods, section 6.2.4). Multiplexed RNA FISH assays with subsequent image analyses and signal quantifications were then also performed by me (see Material and Methods, section 6.2.5).

3.3.1 Two CAF subpopulations are present in BD and cSCC but not in chronically UVR-exposed human skin

In order to visualize cSCC-related iCAFs and myCAFs with multiplexed RNA FISH, several marker genes were selected, according to their specificity and expression levels determined by scRNA-seq (Table 1). As a general cSCC-related CAF marker *COL3A1* was used and probes binding to *C3* and *IGF1* transcripts or *MMP11* and *WNT5A* transcripts were applied to detect iCAFs or myCAFs, respectively. In addition, *KRT14* expression was used to display the localization of non-malignant and malignant keratinocytes in the skin sections.

With this marker combination, microscopy image analyses showed high expression of *COL3A1* in BDs and cSCCs, but not in EH skin samples, localizing CAFs only in diseased skin. Furthermore, specific iCAFs and myCAFs could also be detected in BDs and cSCCs by the co-expression of *COL3A1* and their respective subpopulation-specific marker genes (Figure 26).
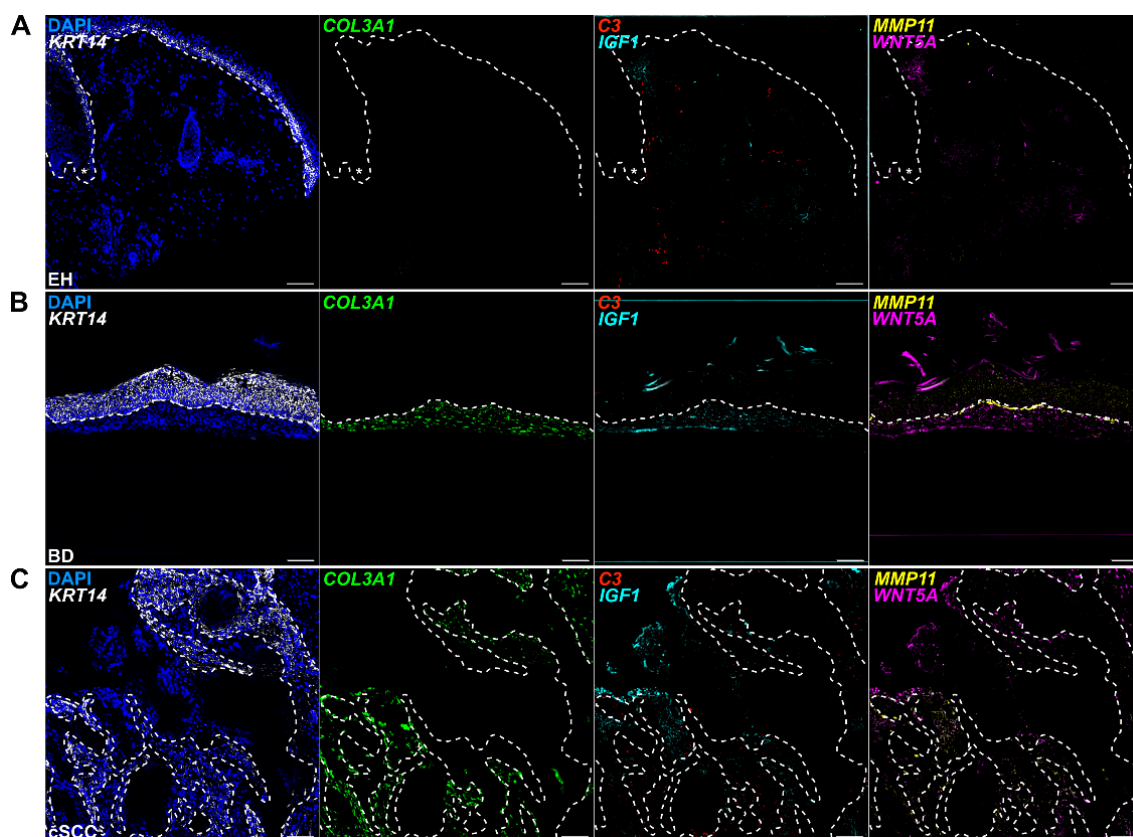
Figure 26. Detection of two cancer-associated fibroblast subpopulations in Bowen's disease and cutaneous squamous cell carcinoma by multiplexed RNA fluorescence *in situ* hybridization. Exemplary microscopy images of multiplexed RNA fluorescence *in situ* hybridization (FISH) assays performed with formalin-fixed paraffin-embedded (FFPE) sections of human ultraviolet radiation (UVR)-exposed healthy (EH) skin **(A)**, Bowen's disease (BD) samples **(B)**, and cutaneous squamous cell carcinomas (cSCCs) **(C)**. Fluorescent probes were hybridized with mRNA transcripts of *KRT14* (white), indicating keratinocytes, *COL3A1*-binding probes (green) were used as general cancer-associated fibroblast (CAF) marker, probes for *C3* (red) and *IGF1* (cyan) visualized inflammatory CAFs (iCAFs), and *MMP11* (yellow) and *WNT5A* (magenta) were marker genes for myofibroblastic CAFs (myCAFs). Nuclei were counterstained with DAPI. Dashed lines separate epidermal keratinocytes from dermal cells and asterisks mark hair follicles. Scale bar: 100µm.

Interestingly, the absence of *COL3A1* expression and therefore the lack of CAFs was not only observed in sections from EH skin, but also for peripheral non-tumoral and chronically UVR-exposed skin regions in cSCC sections (Figure 27). This further confirmed, that the selected marker genes were indeed capable of distinguishing dermal fibroblasts and activated cSCC-related CAFs.

Regarding CAF localization, no spatial pattern with respect to malignant keratinocytes was detected for iCAFs or myCAFs. Both subpopulations were identified throughout the TME (Figures 26B, 26C, and 27).
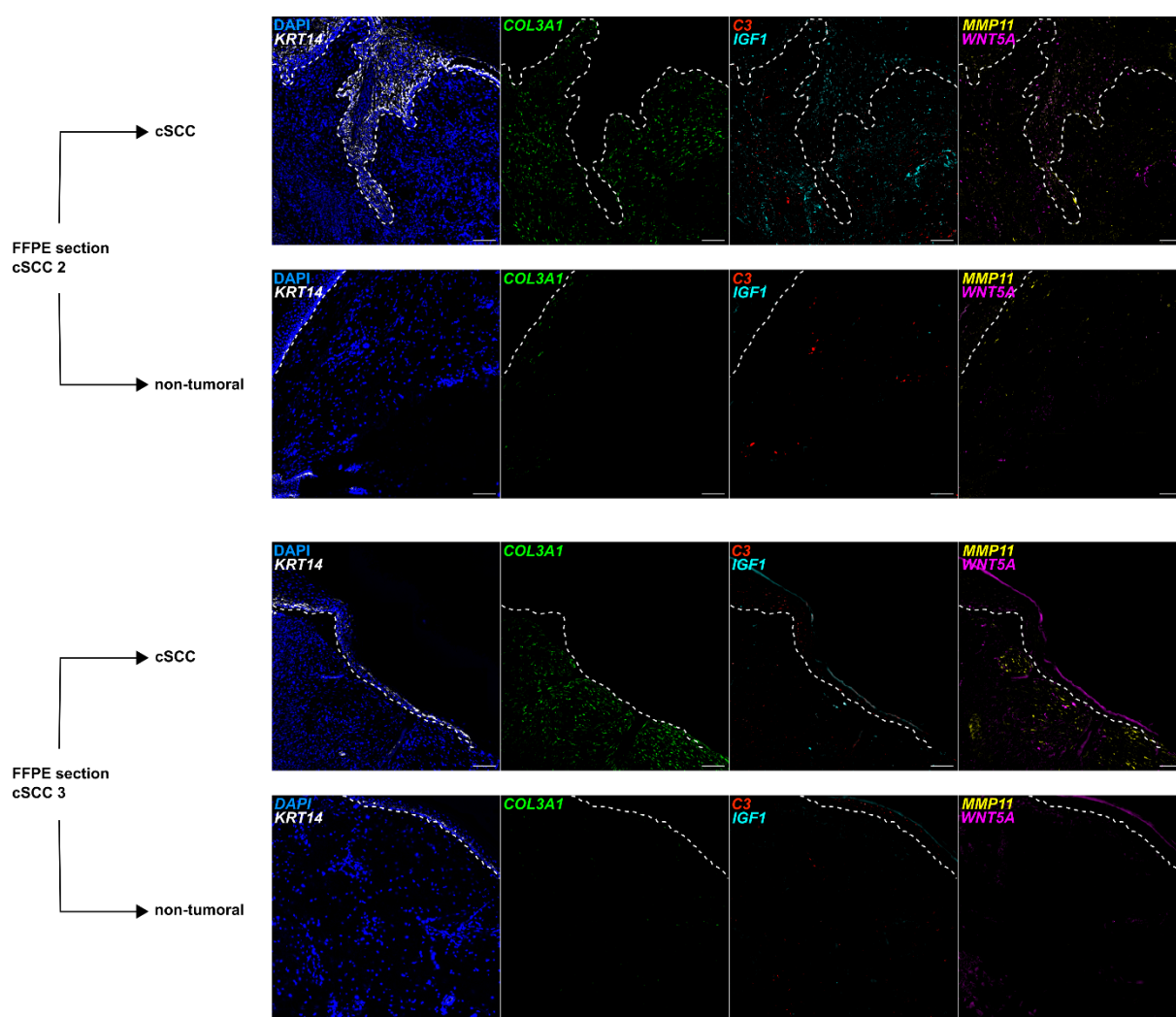
Figure 27. Cancer-associated fibroblasts are not present in non-tumoral skin adjacent to cutaneous squamous cell carcinomas. Representative microscopy images of multiplexed RNA fluorescence *in situ* hybridization (FISH) assays showing the direct comparison of tumor areas and non-tumoral, but chronically ultraviolet radiation (UVR)-exposed skin regions of the same cutaneous squamous cell carcinoma (cSCC) formalin-fixed paraffin-embedded (FFPE) sections. Fluorescent probes were hybridized with mRNA transcripts of *KRT14* (white), indicating keratinocytes, *COL3A1*-binding probes (green) were used as general cancer-associated fibroblast (CAF) marker, probes for *C3* (red) and *IGF1* (cyan) visualized inflammatory CAFs (iCAFs), and *MMP11* (yellow) and *WNT5A* (magenta) were marker genes for myofibroblastic CAFs (myCAFs). Nuclei were counterstained with DAPI. Dashed lines separate epidermal keratinocytes from dermal cells. Scale bar: 100µm.

In order to determine the amount of iCAFs and myCAFs in BD and cSCC skin sections, the two subpopulations were quantified according to co-expression of *COL3A1* and *C3*/*IGF1* (iCAFs) or *COL3A1* together with *MMP11*/*WNT5A* (myCAFs) (Figure 28A). In BD and cSCC samples, on average 49% ± 15% SD and 56% ± 18% SD of all detected CAFs (*COL3A1*$^+$) were classified as myCAFs, respectively. In contrast, significantly (*p*-value < 0.001, paired t-tests) less CAFs (*COL3A1*$^+$) were identified as iCAFs in BD (13% ± 7% SD) and cSCC (15% ± 16% SD) sections (Figure 28B).

For this quantification, only CAFs that showed a positive signal for marker genes of just one of the two subpopulations were considered, which was the case for 72% ± 12% SD of all CAFs detected in cSCC samples. On the other hand, the significant (*p*-value < 0.0001, t-tests)

smaller fractions of CAFs with mixed marker combinations (18% ± 11% SD) or no expression of specific iCAF or myCAF marker genes at all (10% ± 12% SD), were neglected during quantitative analyses (Figure 28C).

Moreover, co-expression of *COL3A1*, as general cSCC-related CAF marker, and just one of the subpopulation-specific genes was sufficient to classify cells as iCAFs or myCAFs. Therefore, not only triple-positive iCAFs (*COL3A1⁺*, *C3⁺*, *IGF1⁺*) and myCAFs (*COL3A1⁺*, *MMP11⁺*, *WNT5A⁺*) were quantified, but also double-positive cells. In fact, on average, significantly more double-positive iCAFs (67% ± 20% SD, *p*-value < 0.001, t-test) and myCAFs (59% ± 14% SD, *p*-value < 0.01, t-test) than triple-positive CAFs could be detected in cSCC samples (Figure 28D).

Taken together, it was shown that multiplexed RNA FISH assays, performed with specific marker genes, can localize CAFs in BDs and cSCCs, and is capable to distinguish between iCAFs and myCAFs. Furthermore, more myCAFs than iCAFs were detected in both disease stages.
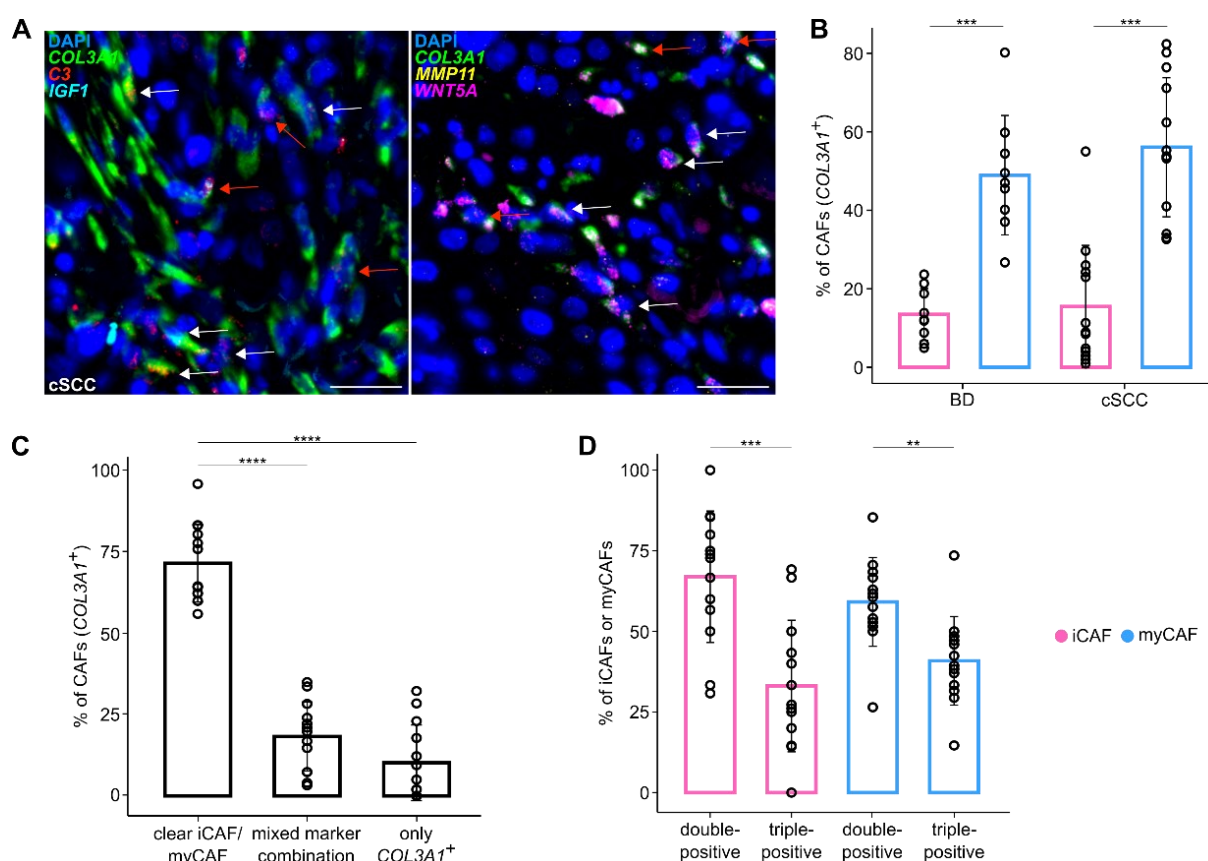
Figure 28. Multiplexed RNA fluorescence *in situ* hybridization detects more myofibroblastic than inflammatory cancer-associated fibroblasts in Bowen's disease and cutaneous squamous cell carcinoma. **(A)** Exemplary microscopy images of multiplexed RNA fluorescence *in situ* hybridization (FISH) assays, performed with formalin-fixed paraffin-embedded (FFPE) sections of cutaneous squamous cell carcinomas (cSCCs). Fluorescent probes were hybridized with mRNA transcripts of *COL3A1* (green), as general cancer-associated fibroblast (CAF) marker, probes for *C3* (red) and *IGF1* (cyan) visualized inflammatory CAFs (iCAFs), and *MMP11* (yellow) and *WNT5A* (magenta) were marker genes for myofibroblastic CAFs (myCAFs). Nuclei were counterstained with DAPI. White arrows indicate double-positive iCAFs (*COL3A1⁺*, *C3⁺* or *IGF1⁺*) (left) and myCAFs (*COL3A1⁺*, *MMP11⁺* or *WNT5A⁺*) (right), whereas red arrows indicate triple-positive iCAFs (*COL3A1⁺*, *C3⁺*, *IGF1⁺*)

(left) and myCAFs (*COL3A1*+, *MMP11*+, *WNT5A*+) (right). Scale bar: 25µm. **(B)** Bar plot showing the proportions of iCAFs and myCAFs detected in Bowen's disease (BD) samples and cSCCs by multiplexed RNA FISH. CAF subpopulations from both entities are displayed along the X-axis and the Y-axis indicates the percentages of detected iCAFs and myCAFs, related to the analyzed CAFs in each sample type. **(C)** Bar plot visualizing the proportions of CAFs that show additional expression of specific marker genes of either iCAFs (*C3* and/or *IGF1*) or myCAFs (*MMP11* and/or *WNT5A*), mixed marker combinations, and CAFs without subpopulation-specific marker expression in multiplexed RNA FISH assays with cSCC sections. The X-axis shows different marker combinations and the Y-axis indicates the percentages of detected CAFs in each group, related to the analyzed CAFs in cSCC samples. **(D)** Bar plot depicting the fractions of double-positive (*COL3A1*+, *C3*+ or *IGF1*+) or triple-positive (*COL3A1*+, *C3*+, *IGF1*+) iCAFs and double-positive (*COL3A1*+, *MMP11*+ or *WNT5A*+) or triple-positive (*COL3A1*+, *MMP11*+, *WNT5A*+) myCAFs in cSCC detected by multiplexed RNA FISH. The X-axis shows different marker combinations and the Y-axis indicates the percentages of detected CAFs in each group, related to the analyzed iCAFs or myCAFs in cSCC samples. For all bar plots, statistical analyses were performed using paired and unpaired t-tests (**: *p*-value < 0.01, ***: *p*-value < 0.001, ****: *p*-value < 0.0001) and error bars show the standard deviation. Each dot represents a dermal region with around 100 CAFs (*COL3A1*+).

3.3.2 CAFs are not yet activated in AK

Unfortunately, it was not possible to perform scRNA-seq with premalignant AK samples, but they could at least be analyzed by multiplexed RNA FISH. In contrast to BD and cSCC sections and similar to EH skin, in two third of the AK sections only very low levels of *COL3A1* expression were detectable (Figure 29A). Interestingly, in the only AK section showing enriched *COL3A1* expression, no signal for CAF subpopulation-specific markers could be observed (Figure 29B). Similar results were obtained when I compared *COL3A1* expression levels in tumoral regions and AK areas of the same cSCC sections. The detected *COL3A1* signals in these AK parts were also much lower than in the TME directly surrounding cancer cells (Figure 29C).

This indicates, that fibroblasts are not yet fully activated and transformed into iCAFs and myCAFs in the disease stage of premalignant AKs.
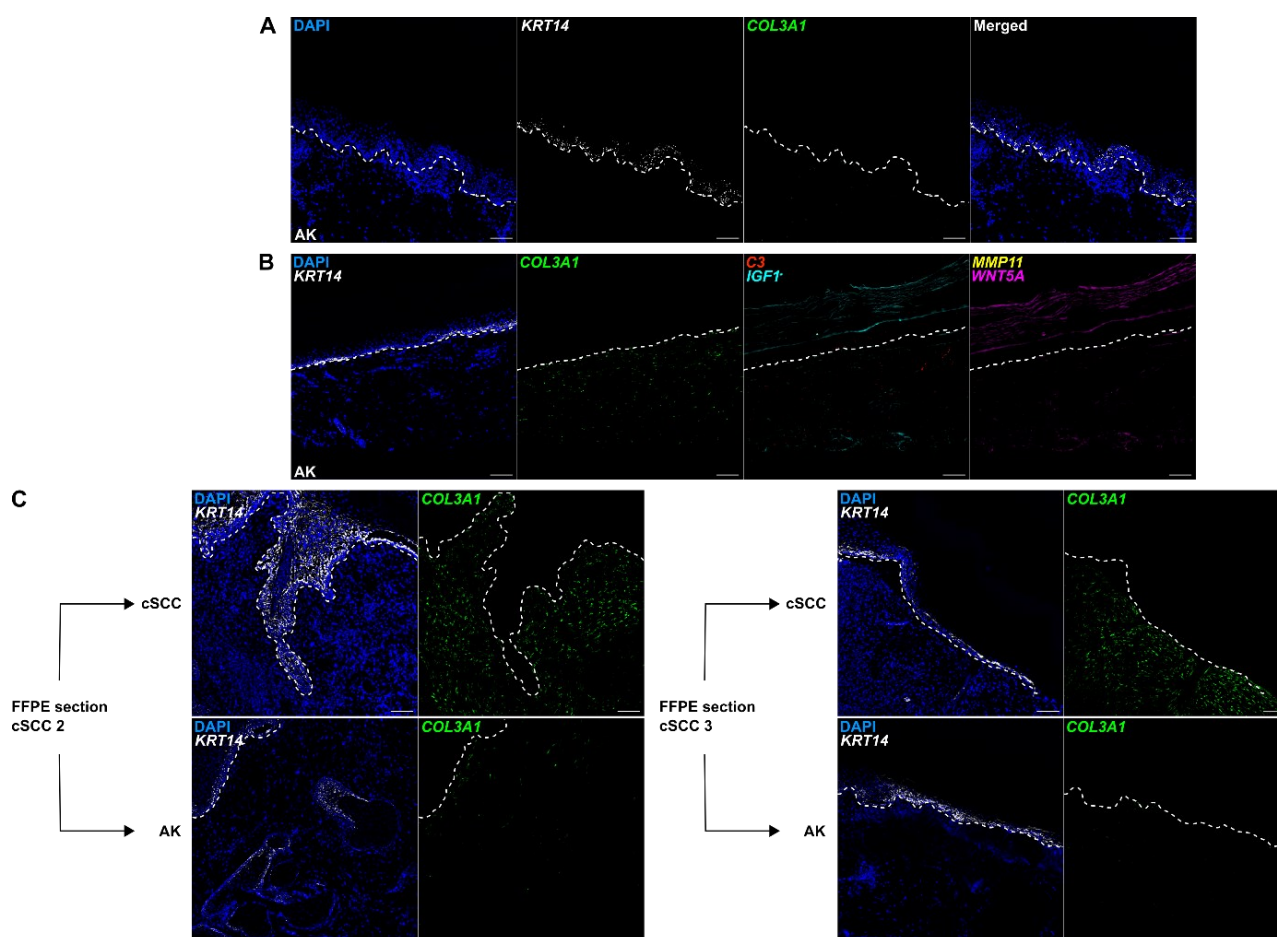
Figure 29. Cancer-associated fibroblasts are not detectable in actinic keratosis by multiplexed RNA fluorescence *in situ* hybridization. (A) & (B) Exemplary microscopy images of multiplexed RNA fluorescence *in situ* hybridization (FISH) assays, performed with formalin-fixed paraffin-embedded (FFPE) sections of human actinic keratosis (AK). **(C)** Representative microscopy images showing the direct comparison of tumoral regions and AK areas for RNA FISH assays, performed in the same cutaneous squamous cell carcinoma (cSCC) samples. Fluorescent probes were hybridized with mRNA transcripts of *KRT14* (white), indicating keratinocytes, *COL3A1*-binding probes (green) were used as general cancer-associated fibroblast (CAF) marker, probes for *C3* (red) and *IGF1* (cyan) visualized inflammatory CAFs (iCAFs), and *MMP11* (yellow) and *WNT5A* (magenta) were marker genes for myofibroblastic CAFs (myCAFs). Nuclei were counterstained with DAPI. Dashed lines separate epidermal keratinocytes from dermal cells. Scale bar: 100µm.

3.3.3 Detection of pro-inflammatory and mesenchymal gene expression in iCAFs and myCAFs, respectively

After confirming that multiplexed RNA FISH is capable of CAF detection in human BD and cSCC samples, I also wanted to verify the potential distinct origins of iCAFs and myCAFs, indicated by previous scRNA-seq analyses. The aim was to analyze, whether an enriched expression of pro-inflammatory-related and mesenchymal-related genes could be observed in iCAFs and myCAFs, respectively. Therefore, the probe panel for all multiplexed RNA FISH assays not only contained specific CAF markers, but also genes related to secretory-papillary (*APCDD1*, *DIO2*), secretory-reticular (*CCN5* [also known as *WISP2*]), pro-inflammatory

(*APOE*), and mesenchymal (*POSTN*) fibroblasts (Solé-Boldo *et al.*, 2020). Dermal signals for all these genes were detected in BD and cSCC sections (Figure 30).
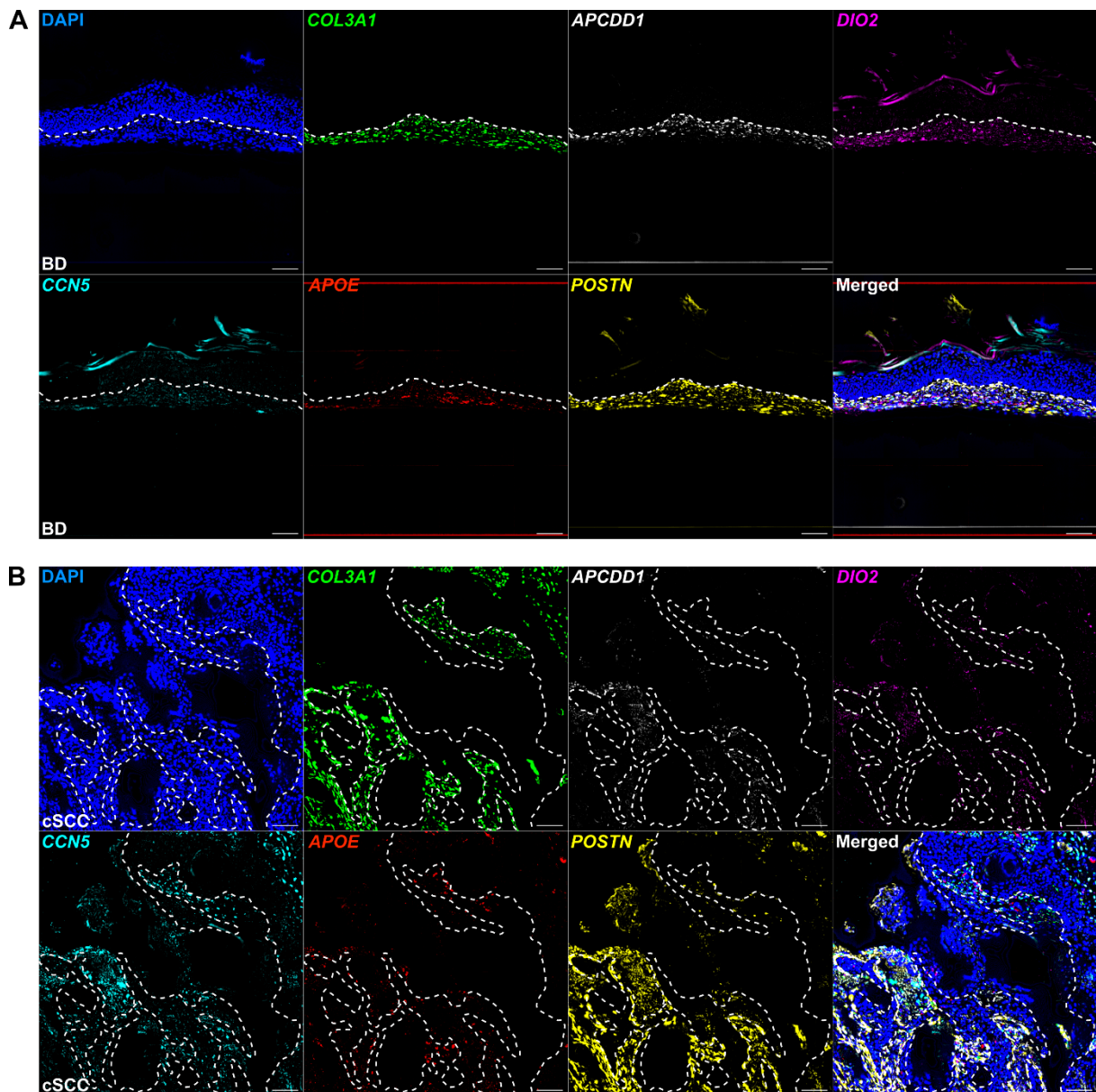
Figure 30. Detection of fibroblast subpopulation-specific marker genes by RNA fluorescence *in situ* hybridization. Representative microscopy images of multiplexed RNA fluorescence *in situ* hybridization (FISH) assays, performed with formalin-fixed paraffin-embedded (FFPE) sections of human Bowen's disease (BD) samples **(A)**, and cutaneous squamous cell carcinomas (cSCCs) **(B)**. Fluorescent probes were hybridized with mRNA transcripts of *COL3A1* (green) to indicate all cancer-associated fibroblasts (CAFs), *APCDD1* (white) and *DIO2* (magenta) as secretory-papillary fibroblast marker genes, *CCN5* (also known as *WISP2*; cyan) as secretory-reticular fibroblast-related gene, *APOE* (red) to visualize pro-inflammatory fibroblast-related gene expression and *POSTN* (yellow) as mesenchymal fibroblast marker gene. Nuclei were counterstained with DAPI. Dashed lines separate epidermal keratinocytes from dermal cells. Scale bar: 100µm.

In order to validate the scRNA-seq finding that cSCC-related iCAFs and myCAFs originate from resident pro-inflammatory and mesenchymal fibroblasts, respectively, the expression of *APOE* (pro-inflammatory marker gene) and *POSTN* (mesenchymal marker gene) was analyzed in more detail (Figure 31A). Quantifications of *APOE* signals in CAFs revealed that

significantly (*p*-value < 0.05, paired t-test and Wilcoxon Rank Sum test) more iCAFs in BD and cSCC samples expressed it than myCAFs (Figure 31B). On the other hand, in BD sections, significantly (*p*-value < 0.001, paired t-test) more myCAFs expressed the mesenchymal-related gene *POSTN* than iCAFs, and also for cSCC samples the same tendency (*p*-value = 0.056, paired t-test) could be observed (Figure 31C).

These results further support that iCAFs and myCAFs develop from two distinct resident and healthy fibroblast subpopulations with inflammatory- and mesenchymal-related functions, respectively.
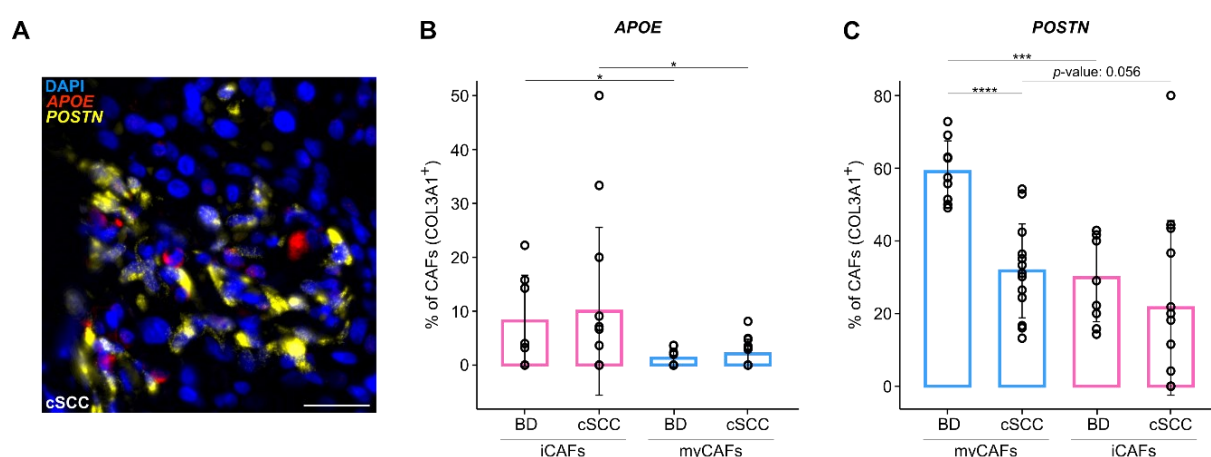
Figure 31. Cancer-associated fibroblast subpopulations show differential inflammatory- and mesenchymal-related gene expression in RNA fluorescent *in situ* hybridization. (A) Exemplary microscopy image of multiplexed RNA fluorescence *in situ* hybridization (FISH) assay, performed with formalin-fixed paraffin-embedded (FFPE) sections of human cutaneous squamous cell carcinomas (cSCCs). Fluorescent probes were hybridized with mRNA transcripts of *APOE* (red) to visualize pro-inflammatory fibroblast-related gene expression and *POSTN* (yellow) as mesenchymal fibroblast marker gene. Nuclei were counterstained with DAPI. Scale bar: 25µm. **(B) & (C)** Bar plots showing the proportions of inflammatory cancer-associated fibroblasts (iCAFs) (*COL3A1*[+], *C3*[+]/*IGF1*^{+}) and myofibroblastic CAFs (myCAFs) (*COL3A1*[+], *MMP11*^{+}/*WNT5A*^{+}) in Bowen's disease (BD) and cSCC sections, expressing the inflammatory-related gene *APOE* **(B)** or the mesenchymal-related gene *POSTN* **(C)** detected by multiplexed RNA FISH. For the two bar plots, CAF subpopulations from both entities are displayed along the X-axes and the Y-axes indicate the percentages of detected iCAFs and myCAFs related to the analyzed CAFs in each sample type. Statistical analyses were performed using paired t-tests and Wilcoxon Rank Sum tests (*: *p*-value < 0.05, ***: *p*-value < 0.001, ****: *p*-value < 0.0001) and error bars show the standard deviation. Each dot represents a dermal region with around 100 CAFs (*COL3A1*[+]).

3.3.4 Detection of specific interactions between iCAFs and T cells or myCAFs and vascular ECs

Further scRNA-seq findings that I wanted to verify *in situ*, were the CAF subpopulation-specific cellular interactions with non-malignant cell types. Computational analyses indicated that iCAFs and myCAFs actively communicate via different interaction pairs with T cells and vascular ECs, respectively. To further investigate this, additional multiplexed RNA FISH assays with two independent cSCC samples (Table 7) were performed, using fluorescent probes hybridizing with mRNA molecules of *COL3A1* (general cSCC-related CAF marker), *C3*

(iCAF marker), *CXCL12* (iCAF interaction ligand), *WNT5A* (myCAF marker and interaction ligand), *CD3D* (T cell marker), *CXCR4* (T cell interaction receptor), *VWF* (vascular EC marker), and *MCAM* (vascular EC interaction receptor).

Image analyses showed iCAFs (*COL3A1$^+$*, *C3$^+$*), expressing the interaction ligand *CXCL12*, in close proximity to T cells (*CD3D$^+$*), which expressed the interaction receptor *CXCR4* (Figure 32A). Moreover, *CXCR4* expression could be detected in the significant majority of T cells (67% ± 2% SD, *p*-value < 0.0001, t-test) (Figure 32B). Further signal quantifications revealed that, on average, more *CXCR4*-positive T cells had iCAFs in their direct neighborhood (14% ± 3% SD) than myCAFs (9% ± 7% SD). For *CXCR4*-negative T cells, overall slightly less CAF neighbors were observed but with the same tendency of more neighboring iCAFs (13% ± 12% SD) than myCAFs (8% ± 6% SD) (Figure 32C). Interestingly, almost all iCAFs surrounding T cells showed expression for the interaction ligand *CXCL12* (94% ± 11% SD, *p*-value < 0.001, t-test) (Figure 32D).
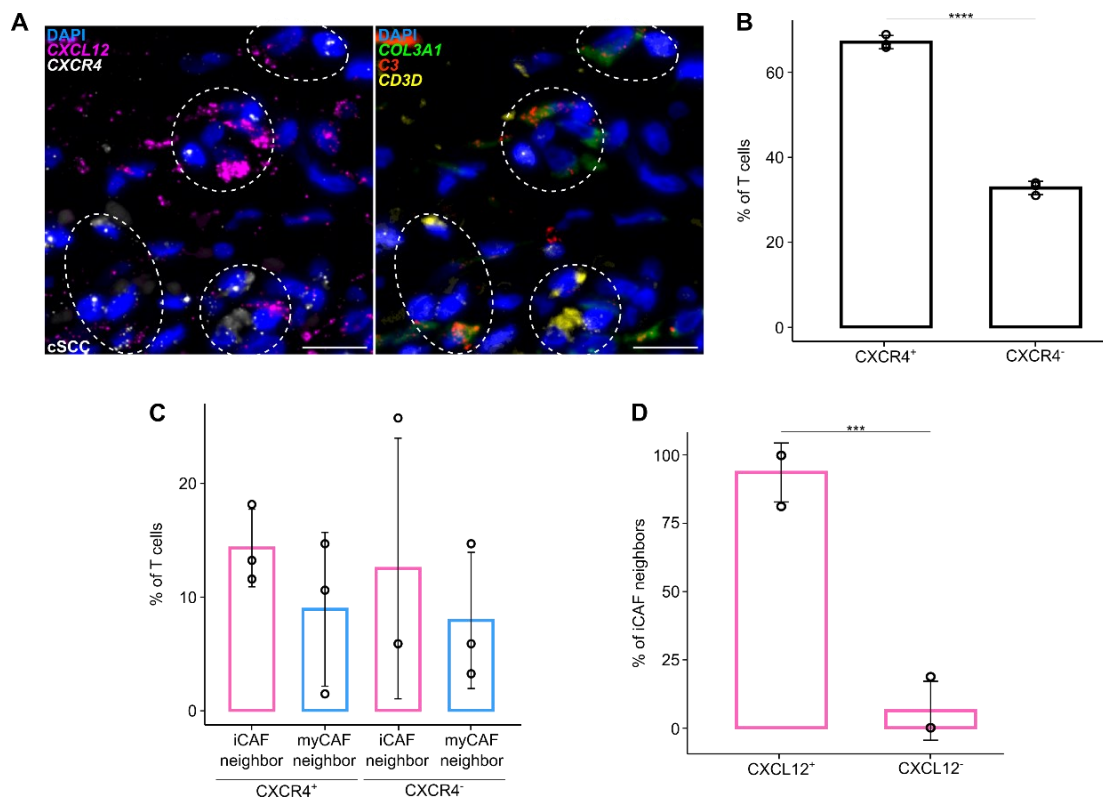
Figure 32. Multiplexed RNA fluorescence *in situ* hybridization detects cellular interaction between inflammatory cancer-associated fibroblasts and T cells. (A) Representative microscopy images of multiplexed RNA fluorescence *in situ* hybridization (FISH) assays, performed with formalin-fixed paraffin-embedded (FFPE) sections of human cutaneous squamous cell carcinomas (cSCCs). To visualize cellular interaction, fluorescent probes were hybridized with mRNA transcripts of *CXCL12* (magenta) and *CXCR4* (white), to detect ligand and receptor expression in inflammatory cancer-associated fibroblasts (iCAFs) and T cells, respectively. *COL3A1* (green) was used as general cSCC-related CAF marker, *C3* (red) as iCAF marker gene, and *CD3D* expression (yellow) identified T cells. Nuclei were counterstained with DAPI. Dashed lines indicate interaction areas. Scale bar: 25µm. **(B)** Bar plot showing the proportions of T cells expressing the receptor *CXCR4* detected by multiplexed RNA FISH. **(C)** Bar plot visualizing the ratios of *CXCR4*-positive and *CXCR4*-negative T cells with iCAFs or myofibroblastic CAFs (myCAFs) in their direct neighborhood detected by multiplexed RNA FISH. **(D)** Bar plot depicting the percentages of iCAFs surrounding T cells that express the ligand *CXCL12* detected by multiplexed

RNA FISH. For all bar plots, the X-axes depict the *CXCR4* expression status of T cells and/or their CAF-related neighborhood, whereas the Y-axes indicate the percentages of analyzed T cells or neighboring iCAFs. Statistical analyses were performed using t-tests (***: *p*-value < 0.001, ****: *p*-value < 0.0001) and error bars show the standard deviation. Each dot represents a dermal region with around 100 T cells (*CD3D*⁺).

In addition, the computationally predicted interaction between myCAFs (*COL3A1*⁺, *WNT5A*⁺) and vascular ECs (*VWF*⁺) via WNT5A-MCAM could also be detected by multiplexed RNA FISH. *WNT5A* expression was used here not only to detect myCAFs, but the gene also encodes for the secreted ligand that binds to the receptor MCAM (Figure 33A). Further quantitative analyses showed that most of the vascular ECs express the receptor *MCAM* (84% ± 15% SD, p-value < 0.01, t-test) (Figure 33B). Importantly, more *MCAM*-positive vascular ECs were detected in cSCC with myCAFs (22% ± 11% SD) in their direct surrounding compared to iCAFs (4% ± 4% SD). A similar trend could be observed for *MCAM*-negative vascular ECs (9% ± 9% SD for myCAF neighbors and 1% ± 1% SD for iCAF neighbors), but with overall less CAFs nearby (Figure 33C).

Taken together, these multiplexed RNA FISH results support the scRNA-seq findings that iCAFs and myCAFs establish a pro-tumorigenic TME via distinct interactions with non-malignant cell types, such as T cells and vascular ECs, respectively.
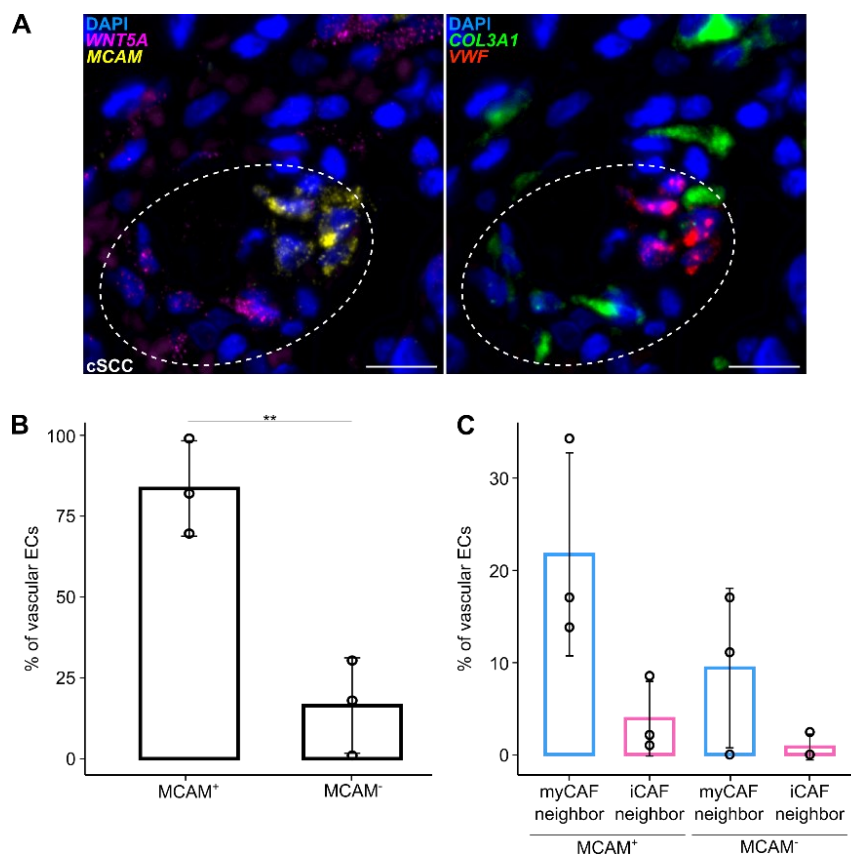
Figure 33. Multiplexed RNA fluorescence *in situ* hybridization detects cellular interaction between myofibroblastic cancer-associated fibroblasts and vascular endothelial cells. (A) Exemplary microscopy images of multiplexed RNA fluorescence *in situ* hybridization (FISH) assays, performed with formalin-fixed paraffin-embedded (FFPE) sections of human cutaneous squamous cell carcinomas (cSCCs). To visualize cellular interaction, fluorescent probes were hybridized with mRNA transcripts of *WNT5A* (magenta) and *MCAM* (yellow) to

detect ligand and receptor expression in myofibroblastic cancer-associated fibroblasts (myCAFs) and vascular endothelial cells (ECs), respectively. *COL3A1* (green) was used as general cSCC-related CAF marker, *WNT5A* (magenta) also as myCAF marker gene, and *VWF* expression (red) identified vascular ECs. Nuclei were counterstained with DAPI. Dashed lines indicate interaction areas. Scale bar: 25µm. **(B)** Bar plot showing the proportions of vascular ECs expressing the receptor *MCAM* detected by multiplexed RNA FISH. **(C)** Bar plot visualizing the ratios of *MCAM*-positive and *MCAM*-negative vascular ECs with myCAFs or inflammatory CAFs (iCAFs) in their direct neighborhood detected by multiplexed RNA FISH. For all bar plots, the X-axes depict the *MCAM* expression status of vascular ECs and/or their CAF-related neighborhood, whereas the Y-axes indicate the percentages of analyzed vascular ECs. Statistical analyses were performed using t-tests (**: *p*-value < 0.01) and error bars show the standard deviation. Each dot represents a dermal region with around 100 vascular ECs (*VWF*[+]).

3.4 CAFs in cSCC and BCC differ

After this detailed characterization of CAFs in the cSCC disease continuum, the remaining question was, whether these observations are valid in all KCs. Therefore, I studied CAFs in BCC, the other main KC type, by analyzing publicly available scRNA-seq datasets (Guerrero-Juarez *et al.*, 2022; Yerly *et al.*, 2022). Together, these studies comprised nine BCC samples and the integration of all single datasets with subsequent unsupervised clustering resulted in 17 clusters with 31,205 cells overall (Figure 34A). Expression analyses with well-known fibroblast marker genes (Solé-Boldo *et al.*, 2020), such as *LUM*, *VIM*, and *PDGFRA*, identified cluster #3 as fibroblasts (Figure 34B). These 3,998 cells were then isolated and used for multiple gene expression analyses, comparing BCC- and cSCC-derived fibroblasts and CAFs. Fibroblasts from BCCs showed lower expression, not only for pancreatic-related CAF genes (Elyada *et al.*, 2019; Öhlund *et al.*, 2017), but also for general cSCC-derived CAF markers identified in this thesis (Figure 34C and Table 1). Additionally, much lower expression levels for cSCC-related specific iCAF and myCAF genes (Table 1) were detected in BCC-derived fibroblasts compared to cSCC (Figure 34D).
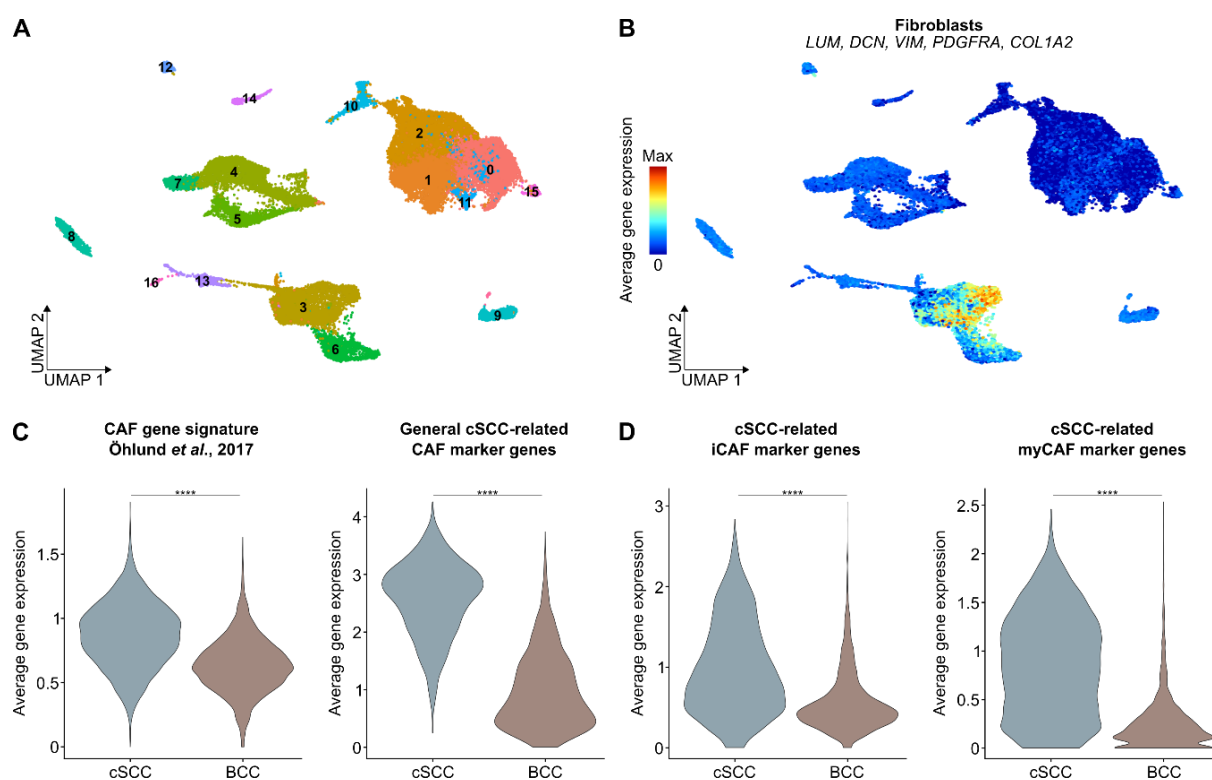
Figure 34. Fibroblasts from basal cell carcinomas show low expression of cutaneous squamous cell carcinoma-related cancer-associated fibroblast gene signatures. (A) Uniform manifold approximation and projection (UMAP) plot showing the integrated and clustered dataset of nine basal cell carcinoma (BCC) samples from two publicly available single-cell RNA sequencing (scRNA-seq) studies (Guerrero-Juarez *et al.*, 2022; Yerly *et al.*, 2022). Each dot represents a single cell (n = 31,205). **(B)** UMAP plot visualizing the average expression of well-known fibroblast marker genes (Solé-Boldo *et al.*, 2020) in all clusters of the BCC scRNA-seq dataset. Red indicates high expression in arbitrary units and blue refers to no or only low expression in arbitrary units. **(C)** Violin plots depicting the average expression levels of cancer-associated fibroblast (CAF) marker genes in CAFs from cutaneous squamous cell carcinoma (cSCC) and fibroblasts from BCC. Left: Pancreatic ductal adenocarcinoma (PDAC)-derived CAF gene signature (Elyada *et al.*, 2019; Öhlund *et al.*, 2017). Right: General cSCC-derived CAF gene signature (Table 1). **(D)** Violin plots showing the average expression of cSCC-related specific inflammatory CAF (iCAF; left) and myofibroblastic CAF (myCAF; right) marker genes (Table 1) in cSCC- and BCC-derived CAFs and fibroblasts, respectively. For all violin plots, cancer types are displayed along the X-axes and Y-axes indictae the average gene expression in arbitrary units. Statistical analyses were performed using Wilcoxon Rank Sum tests (****: *p*-value < 0.0001). Max: maximum.

To further characterize BCC-derived fibroblasts, the cells were re-clustered into four distinct groups (Figure 35A). Expression analysis with the commonly used CAF marker genes *FAP* and *ACTA2* (Chhabra and Weeraratna, 2023; Simon and Salhia, 2022) revealed varying expression with the highest values in the fibroblast (FB) clusters #1 and #2 (Figure 35B). Similarly, the expression of cSCC-related general CAF genes and specific iCAF/myCAF marker gene signatures (Table 1) was also enriched in FB 1 and FB 2 (Figures 35C and 35D). However, it was not possible to clearly identify one of the two subpopulations as iCAFs or myCAFs. These results indicate that the analyzed BCCs might not only contain CAFs, but a mixture of fibroblasts (FB 0 and FB 3) and CAFs (FB 1 and FB 2).
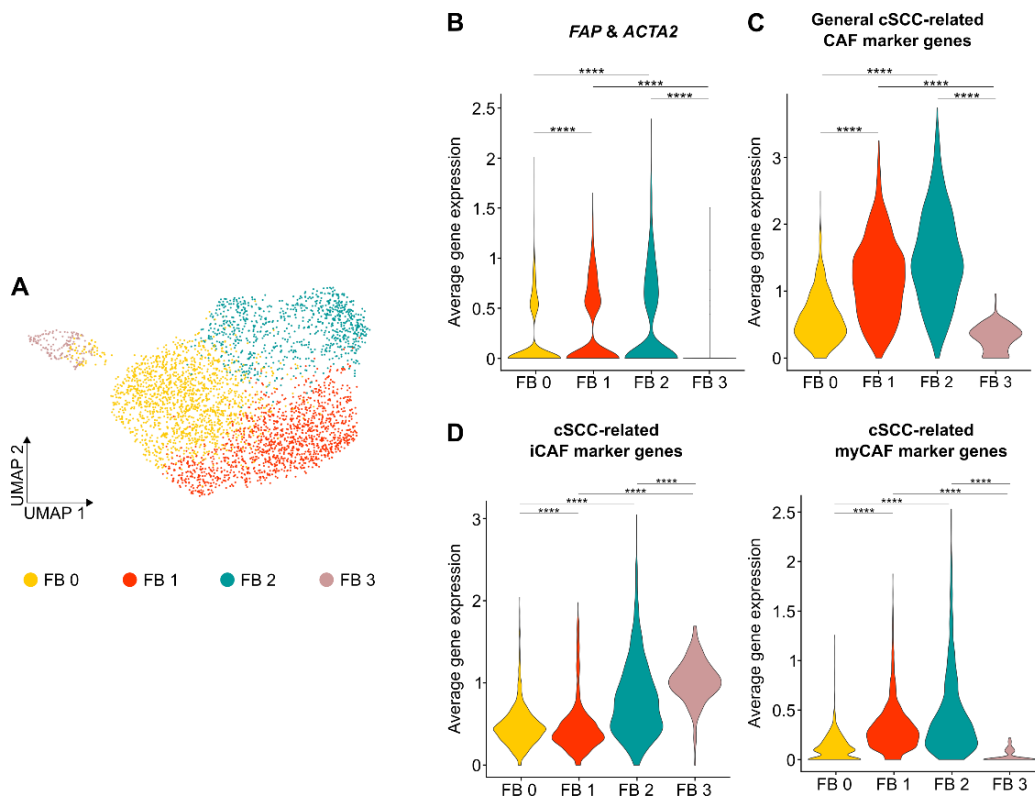
Figure 35. Analyzed basal cell carcinoma samples might contain fibroblasts and cancer-associated fibroblasts. (A) Uniform manifold approximation and projection (UMAP) plot showing the isolated and re-clustered fibroblasts (FB) of nine basal cell carcinoma (BCC) samples from two publicly available single-cell RNA sequencing (scRNA-seq) studies (Guerrero-Juarez *et al.*, 2022; Yerly *et al.*, 2022). Each dot represents a single cell (n = 3,998). **(B)** Violin plot visualizing the average expression of the commonly used cancer-associated fibroblast (CAF) marker genes *FAP* and *ACTA2* (Chhabra and Weeraratna, 2023; Simon and Salhia, 2022) in the four BCC-derived FB clusters. **(C)** Violin plot depicting the average expression of cutaneous squamous cell carcinoma (cSCC)-related general CAF marker genes (Table 1) in the four BCC-derived FB clusters. **(D)** Violin plots showing the average expression levels of specific cSCC-related inflammatory CAF (iCAF; left) and myofibroblastic CAF (myCAF; right) marker gene signatures (Table 1) in the four BCC-derived FB clusters. For all violin plots, BCC-derived fibroblast clusters are displayed along the X-axes and Y-axes indictae the average gene expression in arbitrary units. Statistical analyses were performed using Wilcoxon Rank Sum tests (****: *p*-value < 0.0001).

According to the previous results, the 2,223 cells from the clusters FB 1 and FB 2 were isolated, in order to obtain only "real" CAFs. They were again divided into four subpopulations by unsupervised re-clustering (Figure 36A). Interestingly, also for these putative CAF groups varying expression levels for general cSCC-related CAF marker genes (Table 1) were detected with the highest expression in cluster CAF 2 (Figure 36B). Furthermore, expression analyses with specific cSCC-related gene signatures (Table 1) could not identify iCAFs and myCAFs as distinct clusters, but the expression for both signatures was enriched in cluster CAF 2. These differences between the BCC CAF clusters became even more obvious, by analyzing the expression levels for single iCAF- or myCAF-related genes. For the marker genes *CXCL12*, *JUND*, and *TSC22D3* (Table 1) of cSCC-related iCAFs, expression was only observed in CAF 2 (Figure 36C). This was also the case for the cSCC-related myCAF markers *MMP11*, *TAGLN*, and *COL11A1* (Table 1 and Figure 36D).
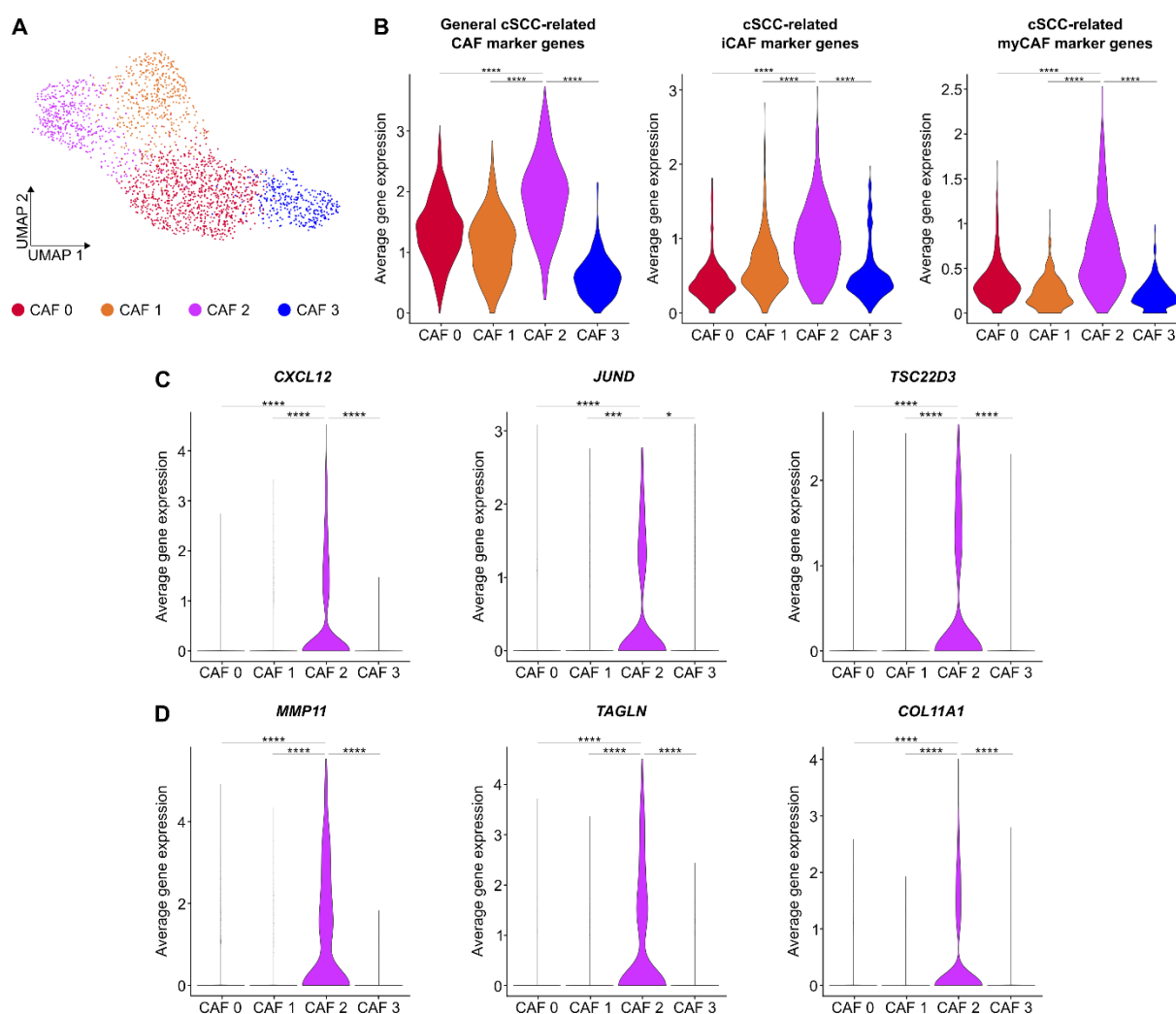
Figure 36. Cancer-associated fibroblasts in cutaneous squamous cell carcinoma and basal cell carcinoma differ. (A) Uniform manifold approximation and projection (UMAP) plot showing the isolated and re-clustered cancer-associated fibroblasts (CAFs) of nine basal cell carcinoma (BCC) samples from two publicly available single-cell RNA sequencing (scRNA-seq) studies (Guerrero-Juarez *et al.*, 2022; Yerly *et al.*, 2022). Each dot represents a single cell (n = 2,223). **(B)** Violin plots visualizing the average expression of cutaneous squamous cell carcinoma (cSCC)-related general CAF marker genes (left), as well as specific cSCC-related inflammatory CAF (iCAF; middle) and myofibroblastic CAF (myCAF; right) marker gene signatures (Table 1) in BCC-derived CAFs. **(C)** Violin plots depicting the average expression levels for the cSCC iCAF-related genes *CXCL12* (left), *JUND* (middle), and *TSC22D3* (right) in BCC-derived CAFs. **(D)** Violin plots depicting the average expression levels for the cSCC myCAF-related genes *MMP11* (left), *TAGLN* (middle), and *COL11A1* (right) in BCC-derived CAFs. For all violin plots, BCC-derived CAF clusters are displayed along the X-axes and Y-axes indictae the average gene expression in arbitrary units. Statistical analyses were performed using Wilcoxon Rank Sum tests (*: *p*-value < 0.05, ***: *p*-value < 0.001, ****: *p*-value < 0.0001).

Since BCC CAFs did not show clear separation into iCAFs and myCAFs, like in cSCC, GO analyses were performed with the most representative genes of each CAF cluster, in order to determine their functions in the TME (Figure 37). For the group CAF 0, the analysis predicted functions in the metal ion metabolism with enriched terms, like detoxification of copper ion and cellular zinc ion homeostasis. Upregulated genes in CAF 1 seemed to be involved in different cellular processes, such as transcription, angiogenesis, proliferation, and apoptosis. The CAF 2 subpopulation, with the highest expression levels for cSCC-related CAF genes, showed enriched GO terms associated with translation, ECM organization, and cell adhesion, which is

partially overlapping with the myCAF functions detected in cSCC. However, the predicted functions for cells in CAF 3 are the most skin-related ones, including cellular response to UVA, wound healing, ECM organization, and collagen synthesis.

Similar to the previous gene expression analyses, also GO analyses were not able to identify two clear CAF subpopulations with functions in inflammatory and matrix-related processes in BCC. Rather two CAF groups showed similar functions to myCAFs (CAF 2 and CAF 3) and additionally, cells involved in ion metabolism (CAF 0) and proliferation (CAF 1) were detected.

Taken together, these results indicate transcriptomic differences between CAFs from cSCC and BCC. The clear distinguishable iCAFs and myCAFs, which were identified in several cancer types, including cSCC, could not be detected in BCC, although one BCC-derived CAF group showed mixed iCAF- and myCAF-related gene expression. However, GO analyses suggested that also CAFs in BCC affect tumorigenesis, but further studies comprising more samples are necessary to characterize them in more detail.
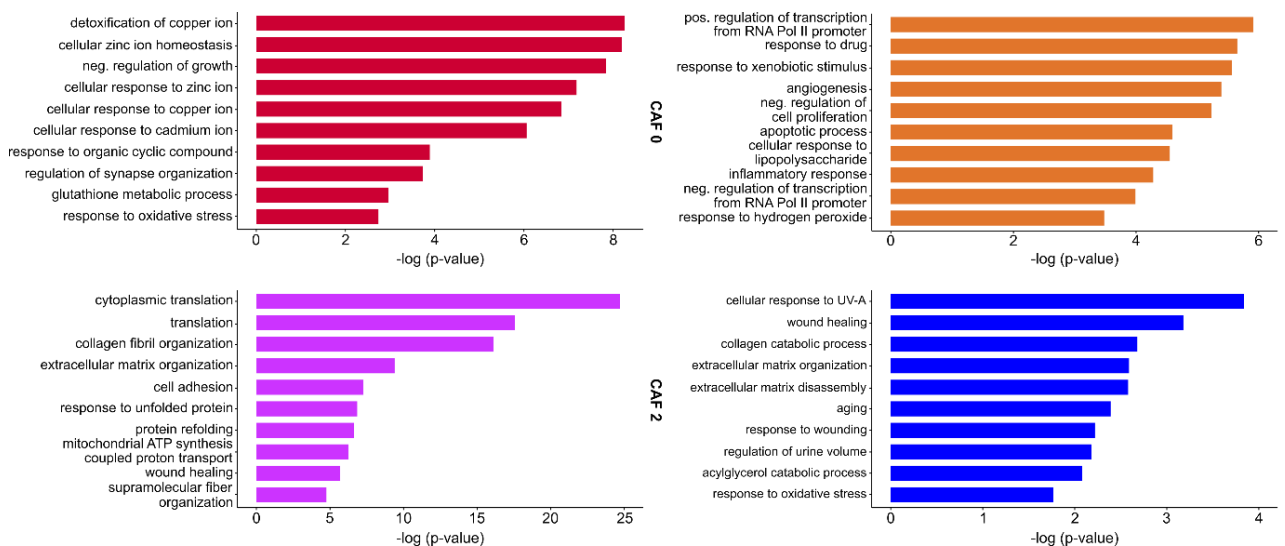
Figure 37. Cancer-associated fibroblasts in basal cell carcinoma show matrix-related functions. Gene ontology (GO) analyses were performed with the most representative genes of each cancer-associated fibroblast (CAF) cluster detected in nine basal cell carcinoma (BCC) samples from two publicly available single-cell RNA sequencing (scRNA-seq) studies (Guerrero-Juarez et al., 2022; Yerly et al., 2022). Top GO terms are shown and ordered according to *p*-value.

4. Discussion

During the last years it became more and more clear that tumor characteristics, such as growth and invasion, are heavily influenced by non-malignant cell types in the surrounding TME. Especially for CAFs, important pro-tumorigenic functions were already observed for almost all solid cancer entities (Comito *et al.*, 2014; Gorchs *et al.*, 2015; Hosein *et al.*, 2015). Therefore, many of the newly developed cancer therapies not only focus on malignant cells, but also try to target CAFs. However, to date, different studies and clinical trials obtained contradictory results, thus suggesting strong CAF heterogeneity (Chhabra and Weeraratna, 2023). A better and more detailed understanding of these cells, as well as their impact on tumor initiation and progression, will be essential for future therapeutic approaches.

In this thesis, scRNA-seq was performed with samples from healthy skin and different cSCC stages in order to investigate cancer-driven transcriptomic changes between chronically UVR-exposed unremarkable fibroblasts and CAFs. Furthermore, CAF heterogeneity and origin were investigated, as well as their direct and indirect influence on tumorigenesis via cellular communication. Importantly, this thesis was not only restricted to computational analyses but CAFs were also studied by multiplexed RNA FISH assays. Like this, scRNA-seq findings were backed up *in situ* and the time window for CAF activation could also be narrowed down.

4.1 Strict patient selection ensures data compatibility

In order to follow CAF development in cSCC initiation and progression, three PH skin samples (Solé-Boldo *et al.*, 2020), three EH skin samples, three BDs, and five cSCCs were analyzed by scRNA-seq. All samples were taken from fair-skinned male patients older than 45 years (Table 8). This group was selected because of their increased skin cancer risk. In general, KC is the most common cancer type in the fair-skinned population (Apalla *et al.*, 2017). Furthermore, it is known that enriched urinary cortisol levels in males increase the probability for skin cancer development, due to higher UVR sensitivity than in female skin (Damian *et al.*, 2008; Lasithiotakis *et al.*, 2008). Especially head and neck regions of bald males are extensively UVR-exposed. Early diagnosis of KC may also be less likely in males, since it is known that they seek less often medical attention, and data from the United Kingdom even showed that males between 21 and 58 years old are half as likely as females to see a general practitioner (Schlichthorst *et al.*, 2016; Wang *et al.*, 2013).

Regarding patient's age, it is well accepted that aging is one of the most important risk factors for tumor initiation, and cancer incidence is known to increase with age (López-Otín *et al.*, 2023b). In contrast to internal organs, skin is affected not only by endogenous aging but also by exogenous aging, due to its high environmental exposure (Gu *et al.*, 2020; Tobin,

2017). It has been shown that external factors, like air pollution, cigarette smoke, and especially chronic UVR-exposure accelerate skin aging (Bocheva *et al.*, 2019). This then leads to premalignant skin lesions, and invasive KCs developing first in chronically UVR-exposed areas rather than in protected skin, which is affected only by intrinsic aging (Boeckmann *et al.*, 2020; Nagarajan *et al.*, 2019). Therefore, it was important to include not only PH skin samples into the study, but also biopsies from chronically UVR-exposed body regions. This ensured that the transcriptomic changes detected in BD- or cSCC-derived malignant keratinocytes and CAFs, compared to EH skin, could be clearly considered cancer-driven. In contrast, gene expression differences between PH skin samples and tumor tissue are simultaneously influenced by UVR exposure and tumorigenesis, which would have complicated cancer-related CAF characterization.

4.2 cSCC-related keratinocytes show cancer-associated changes

To ensure that the obtained BD and cSCC punch biopsies mainly consisted of tumor tissue, sampling was performed from the center of each lesion. Furthermore, the malignant status of the keratinocytes from these sample types was verified by several approaches. One method was to check the presence of cancer-specific transcriptomic patterns in cSCC-derived keratinocytes. In 2020, Ji *et al.* analyzed ten cSCC samples with matched normal skin by scRNA-seq, spatial transcriptomics, and multiplexed ion beam imaging. Detailed characterization of malignant keratinocytes revealed four transcriptomic states, three of which represented the specific subpopulations (basal, cycling, and differentiating) also found in healthy skin (Ji *et al.*, 2020). The fourth keratinocyte subpopulation detected in cSCCs did not correlate with the corresponding normal skin samples and showed upregulation for genes involved in cell motility and ECM disassembly. In addition, an enriched expression of EMT marker genes, such as *VIM* and *ITGA5*, could be observed in this specific subpopulation, and the included cells were found to accumulate at the tumor leading edges, indicating invasive behavior (Ji *et al.*, 2020). Interestingly, expression analyses with the most representative genes of these specialized keratinocytes revealed upregulation in the malignant cells of the cSCCs, studied in this thesis, compared to healthy and BD-derived keratinocytes. This suggested the presence of invading cancer cells and confirmed their malignant status.

To further verify this for keratinocytes in BDs and cSCCs, and to show that scRNA-seq is capable of distinguishing tumor tissue from healthy skin, CNV inference from transcriptomic data was performed. It has been previously shown that cSCCs have a high mutational burden with 50 mutations per megabase (South *et al.*, 2014). The majority of these mutations contain a "UV signature", such as characteristic C to T base exchanges or CC to TT mutations, which again identifies UVR-exposure as a major KC risk factor (Inman *et al.*, 2018; Lee *et al.*, 2020;

Nagarajan *et al.*, 2019). Computational inference tools indeed revealed a continuous increase in CNV events from baseline PH-derived keratinocytes through EH skin and BDs to cSCCs. Interestingly, some of the CNV events that were detected in keratinocytes from several cSCC patients, such as the gain of chromosome (chr) 1q or the loss of chr5q and chr9p, were already described in different single nucleotide polymorphism (SNP) or whole exome sequencing studies in cSCC (Hameetman *et al.*, 2013; Inman *et al.*, 2018; Salgado *et al.*, 2010), indicating common cancer-related genomic changes in cSCC.

However, genomic alterations appear to be influenced by the immune status of the patients and the therapy they received. For example, Inman *et al.* identified a novel mutational signature associated with the exposure to the immunosuppressive drug azathioprine (Inman *et al.*, 2018). Therefore, further studies with cSCCs from immunosuppressed patients will be required to investigate, if not only mutational signatures are influenced by the immune status, but also the transcriptomes of malignant keratinocytes and CAFs.

4.3 CAF subpopulations show distinct functions and origins

The detailed scRNA-seq study of multiple BD and cSCC samples revealed two major CAF subpopulations that could also be detected *in situ*. Further gene expression analyses indicated the presence of myCAFs involved in ECM organization and iCAFs associated with inflammatory responses. Interestingly, many studies investigating different cancer entities detected CAFs with similar functions, independent of the final number of identified subpopulations (Bhattacharjee *et al.*, 2021; Chhabra and Weeraratna, 2023; Hornburg *et al.*, 2021; Kieffer *et al.*, 2020). Additionally, highly specialized CAF subpopulations were observed in different tissues, such as apCAFs, which promote the establishment of an immunosuppressive TME in late-stage murine PDAC. For human PDAC, however, it turned out that apCAFs are only a very minor fraction in the main group of iCAFs (Elyada *et al.*, 2019). In murine breast cancer, CAFs associated with cell differentiation and tissue morphogenesis were identified (Bartoschek *et al.*, 2018). These so called dCAFs expressed not only ECM-related genes, but also genes correlated with different kinds of stem cells, such as *SCRG1* and *SOX9*. Moreover, overlapping gene expression with malignant cells was detected, suggesting that dCAFs originate from cancer cells undergoing EMT (Bartoschek *et al.*, 2018). However, a similar CAF subpopulation could not be identified in BD or cSCC samples analyzed in this thesis. This might be due to species- and cancer entity-specific differences, as well as distinct invasion rates, since it is known that EMT-related processes are especially important for tumor migration and metastasis formation (Dongre and Weinberg, 2019). In general, primary cSCCs show a relatively low metastatic potential of 3-7% (Burton *et al.*, 2016; Nagarajan *et al.*, 2019). Furthermore, dCAFs were found to be only a minor CAF subpopulation containing not even

enough cells for determining a marker gene signature (Bartoschek *et al.*, 2018). They may have been found only because the more sensitive plate-based Smart-seq2 method was used, which detects more genes per cell and especially low abundance transcripts, rather than the droplet-based 10x Genomics platform that I used for this thesis (Bartoschek *et al.*, 2018; Wang *et al.*, 2021a).

Spatial information about cSCC-related CAFs were obtained by multiplexed RNA FISH assays. Both subpopulations were detected throughout the dermis, and no specific spatial patterns with respect to any malignant and non-malignant cell types were observed. In contrast, PDAC-derived myCAFs were specifically identified in close proximity to cancer cells (Öhlund *et al.*, 2017), and a murine breast cancer study detected a CAF subpopulation with roles in vascular development and angiogenesis only closely surrounding blood vessels (Bartoschek *et al.*, 2018). These differences might be cancer type- and/or tissue-specific. However, it is also known that CAF activation depends on organ-related transcriptomic profiles of fibroblasts and other source cell types (Rinn *et al.*, 2006). Therefore, the spatial localization of pancreatic myCAFs and breast vascular CAFs could also be influenced by their origin. Thus, myCAFs in PDAC develop from pancreatic stellate cells, and breast cancer-associated vascular CAFs are believed to originate from specific perivascular cells (Bartoschek *et al.*, 2018; Öhlund *et al.*, 2017). In contrast, it has been shown that skin-related CAFs mainly arise from resident dermal fibroblasts (Tirosh *et al.*, 2016), and that, for example, bone marrow-derived stromal cells have only a negligible influence on CAF development in skin (Davidson *et al.*, 2020).

Although multiplexed RNA FISH assays visualized iCAFs and myCAFs in the whole TME of both analyzed cancer entities, differences regarding the CAF subpopulation proportions could be observed. Contrary to scRNA-seq, which identified relatively more iCAFs than myCAFs in BDs, quantitative analyses of multiplexed RNA FISH assays revealed significantly more myCAFs in BDs and cSCCs. This discrepancy might be caused by the fact that, in the *in situ* approach, both CAF subpopulations were only identified by the expression of one common marker gene and two specific genes, respectively. In contrast, scRNA-seq-related iCAF/myCAF classifications are based on the expression of many more genes, allowing a much more precise CAF stratification. However, further studies will be required to confirm potential enrichments of specific CAF subpopulations in the different stages of cSCC progression.

With scRNA-seq and multiplexed RNA FISH, this thesis was also able to characterize the origin of CAFs in a subpopulation-specific manner, and with respect to the four functionally and spatially different fibroblast groups identified in PH skin (Solé-Boldo *et al.*, 2020). Different computational and *in situ* approaches revealed a high similarity between pro-inflammatory healthy fibroblasts and iCAFs, as well as between mesenchymal healthy fibroblasts and

myCAFs, indicating these two functionally related fibroblast subpopulations as the main sources of cSCC-associated CAFs. To my knowledge, no other cSCC scRNA-seq study characterized the origin of CAFs in such a detail and separately for different subpopulations, so far. A functional correlation between normal cells and a particular CAF subtype was not only observed in this thesis for cSCC, but also, for example, in the case of vascular CAFs in breast carcinoma, which might develop from perivascular cells (Bartoschek *et al.*, 2018). Further cSCC studies, especially including *in vivo* lineage tracing approaches, will be required to further confirm these findings.

The identification of different sources for cSCC-related CAFs might also imply diverse activation pathways. It has been shown that cancer cells, and also immune cells, are able to activate CAFs via direct cell-cell contacts, or by paracrine signaling through the secretion of growth factors, chemokines, and miRNAs (Biffi *et al.*, 2019; Chhabra and Weeraratna, 2023; Elenbaas and Weinberg, 2001; Mitra *et al.*, 2012). In murine PDAC, it was observed that cancer cells secrete IL1, as well as TGF-β, leading to iCAF and myCAF transformation, respectively (Biffi *et al.*, 2019), which indeed suggests CAF subpopulation-specific activation signaling. For the cSCC-related samples analyzed in this thesis, scRNA-seq and multiplexed RNA FISH assays detected CAFs already in BD, a carcinoma *in situ*, indicating paracrine activation in the case of malignant cells due to their spatial separation by the basement membrane between epidermis and dermis. However, computational analyses also revealed an increase of T cells and B cells already in BD tissue, suggesting an inflammatory TME at this disease stage, that might facilitate additional immune cell-related CAF activation. Further studies will be required to investigate the complex activation processes during cSCC initiation and progression, as well as potential CAF subpopulation-specific stimuli from different malignant and non-malignant cell types. This knowledge might be beneficial to prevent CAF formation in the future.

4.4 CAF activation does not yet occur in the premalignant skin lesion AK

Another important aim of this thesis was to study the CAF activation timing. For this purpose, the analysis of AK samples would be particularly interesting, since this condition is classified as a premalignant skin lesion. Unfortunately, the availability of AKs for scRNA-seq is limited. Due to their small size, all shaved material from patients is usually used for pathology and diagnosis. However, FFPE AK sections could be provided by the NCT tissue bank in Heidelberg and were included into the multiplexed RNA FISH assays. This way, the time window for CAF activation could be narrowed down to later tumor stages, since no iCAFs or myCAFs were detected in the precancerous tissue lesions. Furthermore, even in AK regions

in the periphery of cSCC tumors, no CAF signal was observed, indicating that their activation is restricted to the TME in close proximity to malignant BD or cSCC keratinocytes. This is especially interesting because the deficiency of CAFs might contribute to the spontaneous regression that 26% of all AKs show during one year (Boeckmann *et al.*, 2020; Fania *et al.*, 2021). Further analyses will be required to determine the exact time frame and mechanisms of CAF activation in more detail.

Interestingly, similar to cSCC, also for esophageal SCCs (ESCCs), CAF-related differences were observed between tumor and paratumor tissue with an enrichment of immunosuppressive CAFs close to malignant cells compared to adjacent tissue. Moreover, in early ESCC stages, less CAF-associated cellular communication was detected than in later stages, further indicating an increasing importance for CAFs during cancer progression (Liu *et al.*, 2023). In PDAC, CAF activation was also studied by scRNA-seq, observing an increase of myCAFs from non-invasive low-grade intraductal papillary mucinous neoplasms (LGD-IPMNs), to high-grade IPMNs (HGD-IPMNs), to invasive tumors, suggesting myCAF transformation as an early event in PDAC progression. In contrast, iCAFs were only detected in later PDAC stages (Bernard *et al.*, 2019).

Moreover, CAFs were also previously detected in the TME of hepatocellular carcinomas (HCCs), originating from hepatic stellate cells (Kaps and Schuppan, 2020). It was shown, that strong CAF infiltration and high expression levels of *ACTA2* in the TME increased the risk for recurrence after HCC removal (Affo *et al.*, 2017; Ju *et al.*, 2009). The majority of HCCs develop in cirrhotic livers, which is an advanced stage of tissue fibrosis, and interestingly, already during this premalignant disease stage, activated myofibroblasts were observed (Kaps and Schuppan, 2020). Also in fibrotic skin diseases, myofibroblasts play an important role. These diseases are characterized by dermal fibroblast hyperproliferation, accumulation of ECM components, as well as inflamed tissue, and comprise, for example, keloids and scleroderma (Do and Eming, 2016). Tissue rearrangements are thereby driven by several growth factors, such as TGF-β, FGF, PDGF, VEGF, and POSTN (Andrews *et al.*, 2016; Deng *et al.*, 2021; Murota *et al.*, 2017). In 2021, Deng *et al.* analyzed keloids by scRNA-seq and compared them to normal scar tissue (Deng *et al.*, 2021). In both sample types, the four fibroblast subpopulations, that were previously defined in PH skin (Solé-Boldo *et al.*, 2020), could be detected. Similar to the cSCC samples analyzed in this thesis, the proportion of mesenchymal fibroblasts was significantly increased in keloids compared to normal scars, and these cells were also observed to secrete an excessive amount of collagen (Deng *et al.*, 2021). Interestingly, significantly more mesenchymal fibroblasts in keloids than in normal scars showed expression of the CAF-associated gene *ACTA2*. Furthermore, interaction analyses revealed increased TGF-β, POSTN, and NOTCH signaling in keloids (Deng *et al.*, 2021), which are pathways that are also known to play a role in CAF activation and cSCC tumorigenesis

(Chhabra and Weeraratna, 2023; South *et al.*, 2012; Yilmaz *et al.*, 2017). Therefore, similar molecular mechanisms might be involved in the establishment of fibrotic tissue and a pro-tumorigenic TME for carcinomas, that mimic "non-healing wounds" (Chandler *et al.*, 2019; Dvorak, 1986). This may indicate fibrosis as a premalignant stage for tumors in different organs, such as liver and lung (Kaps and Schuppan, 2020; Li *et al.*, 2023).

4.5 CAFs promote cSCC tumorigenesis via common and subpopulation-specific cellular communication

Computational scRNA-seq analyses of BDs and cSCCs allowed detailed characterization of how CAFs affect tumorigenesis. Therefore, cellular interaction tools were used and identified CAFs as the most important sender cell type, secreting signaling ligands into the TME. One of the receiving cell types that are influenced by CAFs, are malignant keratinocytes. Detailed signaling analyses showed that especially the collagen and FN1 networks are active with cSCC-derived CAFs secreting mostly collagen type I and VI, as well as FN1 and cancer cells presenting the receptors CD44 and SDC1/4 on their surfaces. Importantly, CD44 is known to activate, for example the PI3K/AKT and SRC/MAPK pathways, which are involved in the proliferation and invasion of tumor cells (Chen *et al.*, 2018). In epithelial ovarian carcinoma, enriched CD44 levels were associated with more advanced cancer stages and poor prognosis (Sacks and Barbolina, 2015). Furthermore, CD44 surface expression correlates with cancer stem cell maintenance, as well as chemoresistance (Foster *et al.*, 2013; Martincuks *et al.*, 2020). In breast cancer, it was shown that activated SDC1 further stimulated STAT3 and NOTCH signaling, modulating inflammation and cancer stemness. Interestingly, SDC1 silencing in breast cancer cell lines resulted in a significantly reduced 3D spheroid and colony formation, and a significant downregulation of EGFR signaling, which is also known to be aberrant activated in cSCC (Ibrahim *et al.*, 2017; Kolev *et al.*, 2008).

CAFs not only influence tumorigenesis by cellular interactions with cancer cells, but also different non-malignant cell types in the TME are affected. Interestingly, in the latter case, subpopulation-dependent differences were observed. For cSCC-derived iCAFs, the computational interaction tools used in this thesis predicted high activity for CALCR and CXCL networks, including the interaction pairs ADM-CALCRL and CXCL12-CXCR4, respectively. ADM is already known to bind to CALCRL on the surface of vascular ECs, modulating EC survival, proliferation, and vessel permeability in physiological and pathological states (Karpinich *et al.*, 2011). In breast cancer, it was shown that CAF-secreted ADM promoted tumor growth and angiogenesis (Benyahia *et al.*, 2017). Interestingly, Zudaire *et al.* observed also a receptor-independent chemotaxis for ADM, modulating mast cells and finally promoting human lung cancer growth *in vitro* (Zudaire *et al.*, 2006). This finding further supports the

predicted immunoregulatory functions of cSCC-related iCAFs. Moreover, CXCL12-related signaling was found to regulate cancer stem cell features in oral SCC (OSCC) and recruited monocytes displaying the M2 macrophage phenotype (Li *et al.*, 2019b). These M2 macrophages are known to be involved in anti-inflammatory processes, as well as in tumor promotion, supporting the predicted immunosuppressive functions of iCAFs (Saqib *et al.*, 2018). In addition, it has been observed that CXCL12 also fulfills an anti-inflammatory role with respect to T cells by binding to CXCR4, regulating their polarization towards Tregs, which again promotes an immunosuppressive TME (Santagata *et al.*, 2021). Importantly, for skin cancer it has been already shown that the inhibition of the CXCL12-CXCR4 pathway by AMD3100 indeed prevented tumor formation (Sarchio *et al.*, 2014).

On the other hand, for cSCC-derived myCAFs the computational interaction tools predicted active cellular communication with mainly vascular ECs and pericytes by the secretion of ANGPTL2 and WNT5A. For ANGPTL2 it was already reported that it binds to integrin α5β1 (ITGA5/ITGB1) on vascular ECs in the TME, accelerating angiogenesis and leading to an increased vessel permeability (Kadomatsu *et al.*, 2014; Tabata *et al.*, 2009). Interestingly, in osteosarcoma ANGPTL2-integrin α5β1 signaling was involved in p38 MAPK activation and MMP upregulation, leading to enriched ECM remodeling and tumor metastasis (Odagiri *et al.*, 2014). This might suggest further myCAF-derived ANGPTL2 functions with respect to not only vascular ECs but also cancer cells, supporting their predicted role in matrix-related processes. Furthermore, the myCAF-secreted ligand WNT5A was predicted to bind to MCAM on the surface of vascular ECs and pericytes. In general, it was shown already that MCAM is important for pericyte recruitment and vessel stabilization (Leroyer *et al.*, 2019). In breast cancer, WNT5A was observed to promote VEGF-independent angiogenesis in the TME (Wan *et al.*, 2021). Moreover, WNT5A-MCAM signaling showed regulatory functions for cell motility and even contributed to tumor invasion in KCs (Pourreyron *et al.*, 2012; Ye *et al.*, 2013), further confirming the important role of myCAFs in the establishment of a pro-tumorigenic TME.

4.6 cSCC-related CAF characteristics differ in BCCs

In order to check if CAF features identified in BD and cSCC could be transferred to other KCs, CAFs in the second main KC type BCC were investigated. Therefore, two publicly available scRNA-seq datasets were analyzed (Guerrero-Juarez *et al.*, 2022; Yerly *et al.*, 2022). Overall, BCC-derived fibroblasts could be divided into four distinct groups but showed only low expression levels for commonly used CAF marker genes (*FAP*, *ACTA2*), as well as pancreatic- and cSCC-related CAF genes. This observation suggests the presence of a mixed group of stromal cells in the samples with fibroblasts and CAFs. This might be caused by the sampling process for the tumor biopsies. For this thesis all scRNA-seq samples were taken from the

carcinoma center to ensure a high degree of cancer cells and TME. In contrast, for both analyzed BCC datasets the authors only mentioned that tissue pieces were taken from residual biopsy specimens (Guerrero-Juarez *et al.*, 2022; Yerly *et al.*, 2022). This may imply that not only cancerous BCC tissue was pre-processed and sequenced but also parts of unremarkable skin, for example from the periphery of the removed lesion. This could lead to overall lower CAF-related expression values and also to the observed high variability in gene expression between the four fibroblast clusters.

In order to compensate for this potential fibroblast and CAF mixture, only cells showing high CAF-related gene expression were isolated and used for further analyses. Unsupervised clustering revealed again four subpopulations for these putative BCC CAFs. Nevertheless, a high variability in expression was again detected between the groups with respect to general cSCC-related CAF genes, as well as specific iCAF- and myCAF-associated genes. However, one BCC-derived CAF group showed enriched expression for some CAF marker genes and a GO analysis with the most representative genes of this cluster indicated functions in collagen synthesis and ECM organization.

These observations indeed matches the observations made by the two original studies since both of them identified four CAF subpopulations with distinct gene expression patterns and functions (Guerrero-Juarez *et al.*, 2022; Yerly *et al.*, 2022). Guerrero-Juarez *et al.* detected in total four fibroblast and two fibroblast-like clusters by analyzing four BCCs and two peritumoral skin samples (Guerrero-Juarez *et al.*, 2022). The authors reported that all four fibroblast subpopulations were present in the tumor tissue samples, as well as in the normal skin, potentially suggesting indeed mixed samples as previously described. However, one fibroblast group was observed to be enriched in the TME, compared to peritumoral skin, showing upregulation of ECM-related genes and WNT5A. Therefore, they might represent myCAF-like cells in BCC, involved in ECM organization.

Also Yerly *et al.* identified four fibroblast subpopulations when analyzing five BCC samples by scRNA-seq (Yerly *et al.*, 2022). Interestingly, the authors observed upregulation of CAF-related genes only in two groups, whereas one fibroblast subpopulation even showed an enrichment of quiescent cells. Furthermore, similarly to the BCC-related observations in this thesis, high expression of ECM-related genes were only detected in one fibroblast cluster (Yerly *et al.*, 2022). However, further studies will be required to investigate CAFs in BCC in greater detail.

Although CAF heterogeneity in cSCC and BCC seem to differ at least to some extent, several studies analyzing melanoma suggest the presence of iCAF- and myCAF-like subpopulations. In murine melanoma, three CAF groups were identified with functions in inflammation, ECM remodeling, and cytoskeleton organization, respectively (Davidson *et al.*, 2020). An integrated analyses of head and neck carcinoma, lung carcinoma, and melanoma

also detected six CAF subpopulations, including myCAFs and iCAFs (Galbo *et al.*, 2021). Moreover, an interesting study from 2020 dissected melanoma spheroids by scRNA-seq (Novotný *et al.*, 2020). They were generated with melanoma cells and either old and chronically UVR-exposed fibroblasts or young and UVR-protected fibroblasts. Three different CAF subpopulations were identified with an overall more extensive deregulation of gene expression in the TME containing the photodamaged cells, which may indicate age- and UVR-dependent CAF features (Novotný *et al.*, 2020). For example, CAFs developed from UVR-exposed fibroblasts showed upregulation of *POSTN* and *FAP*, as well as enriched activity for the TNF signaling pathway, known to be involved in tumor invasion (Novotný *et al.*, 2020; Stuelten *et al.*, 2005).

5. Conclusion and Outlook

Taken together, this thesis provides an extensive characterization of CAFs during human cSCC progression (Figure 38). CAF heterogeneity was investigated and scRNA-seq, as well as multiplexed RNA FISH, revealed the presence of two functionally distinct subpopulations originating from different healthy fibroblast subtypes. Findings from different computational analyses and *in situ* assays indicate that the cancer-related activation of pro-inflammatory fibroblasts lead to the development of iCAFs, which are involved in inflammation-associated processes. That includes, for example, cellular interactions with T cells and macrophages, modulating their phenotypic state and finally resulting in an establishment of an immunosuppressive and therefore pro-tumorigenic TME. Furthermore, the second major CAF group detected in BDs and cSCCs showed matrix-related functions, such as collagen synthesis and ECM organization. These myCAFs seem to originate from mesenchymal fibroblasts and were found to actively communicate with pericytes. This may lead to further TME remodeling and potentially facilitates cancer cell migration, ultimately supporting tumor invasion. In addition, the subpopulation-specific ways to establish a pro-tumorigenic TME, were complemented by cellular interactions of all CAFs with vascular ECs, which stimulates angiogenesis and by the direct promotion of cancer cell survival and proliferation via collagen and FN1 signaling.

Although this thesis provides novel and important insights into CAF heterogeneity and their functional roles during cSCC tumorigenesis, further studies will be required to verify these findings and to analyze several aspects of CAF development in greater detail. For example, with scRNA-seq and multiplexed RNA FISH assays different proportions of iCAFs and myCAFs were detected in BDs and cSCCs, probably due to the limited availability of RNA FISH probes to clearly classify both CAF subpopulations *in situ*. Therefore, further scRNA-seq studies will be required, incorporating more samples throughout the cSCC disease continuum to precisely determine iCAF and myCAF proportions in the different cancer stages. For this purpose, studies including spatial transcriptomic assays might be also beneficial to obtain transcriptomic and spatial information simultaneously for multiple samples.

In addition, further data on CAF origins and their exact activation timing will be required. In this thesis, scRNA-seq analyses suggested pro-inflammatory and mesenchymal fibroblasts as the origins for iCAFs and myCAFs, respectively, which could be also validated *in situ*. However, to definitely confirm these findings, *in vivo* cell tracing approaches could be used and combined with live imaging techniques, to follow CAF activation from unremarkable skin towards invasive cSCC. Also, CAF activation mechanisms need to be investigated in cSCC. Since this thesis detected CAFs already in the *in situ* carcinoma BD, paracrine signaling seem to be essential

for CAF activation. However, further studies will be needed to dissect the exact pathways involved, as well as source cell types, such as malignant keratinocytes and/or immune cells.

Moreover, additional studies to characterize CAFs in BCC will be required. This thesis showed that information about CAF heterogeneity and subpopulation-specific gene expression patterns cannot be directly transferred from cSCC. To verify these findings, further BCC scRNA-seq studies should be performed, ensuring pure samples from the TME without contaminations from adjacent non-tumoral tissue. This may be achieved by sampling from the center of the tumors.

For this thesis, all samples were retrieved from immunocompetent patients to ensure data compatibility. However, it has been shown that mutational patterns in cSCC-derived keratinocytes were affected by the patient's immune status and their medication (Inman *et al.*, 2018). Accordingly, future scRNA-seq studies should include tumors from immunosuppressed patients, in order to investigate if immunosuppressive drugs also cause transcriptomic differences in malignant keratinocytes and non-malignant cell types, like CAFs.

Furthermore, additional studies will be required to potentially correlate CAF heterogeneity and their subpopulation-specific functions with clinicopathological features in BDs and cSCCs. Therefore, long-term data from patients with tumors along the disease continuum are likely to be needed.
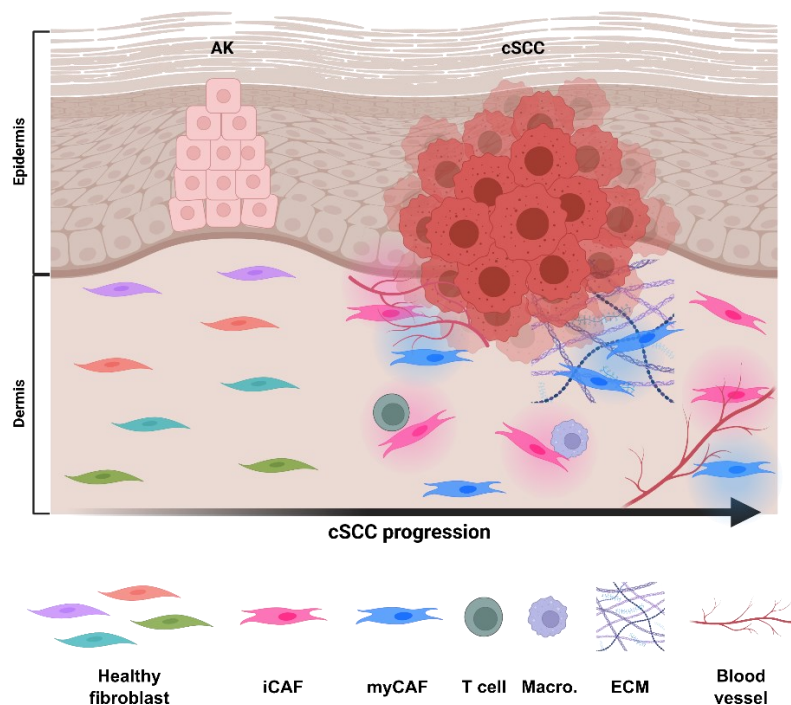
Figure 38. Cancer-associated fibroblast heterogeneity in cutaneous squamous cell carcinoma. AK: actinic keratosis, cSCC: cutaneous squamous cell carcinoma, iCAF: inflammatory cancer-associated fibroblast, myCAF: myofibroblastic cancer-associated fibroblast, Macro.: macrophage, ECM: extracellular matrix. Created with BioRender.

6. Material and Methods

6.1 Material

6.1.1 Software and computational tools

All software and computational tools used in this thesis are listed in Table 2.

Software or tool	Version	Reference
BioRender		BioRender.com
CellChat	1.4	Jin *et al.*, 2021
Cell Ranger	4.0.0	10x Genomics
CopyKAT	1.1	Gao *et al.*, 2021
DAVID Bioinformatics Database	6.8	Huang da *et al.*, 2009; Sherman *et al.*, 2022
Fiji	2.3.0	Schindelin *et al.*, 2012
ggplot2	3.3.5	Wickham, 2016
GSEA software & Molecular Signature Database	4.3.2	Liberzon *et al.*, 2011; Subramanian *et al.*, 2005
HiPlex Image Registration Software	2.0.1	Bio-Techne
InferCNV	1.6	Patel *et al.*, 2014; Tirosh *et al.*, 2016
Inkscape	1.1.1	Inkscape Project, 2021
LIANA	0.1.11	Dimitrov *et al.*, 2022
QuPath	0.3.2	Bankhead *et al.*, 2017
R	4.0.3	R Core Team, 2020
RStudio	1.2.5033	RStudio Team, 2020
Seurat	4.0.5	Hao *et al.*, 2021
SigmaPlot	14.0	Systat Software Inc.
Slingshot	1.8	Street *et al.*, 2018

Table 2. Software and computational tools.

6.1.2 Chemicals and reagents

All chemicals and reagents used in this thesis are listed in Table 3.

Chemical or reagent	Company	Reference #
D1000 Reagent	Agilent Technologies	5067-5583
Distilled water	Invitrogen	10977
Ethanol	Merck	1.00983.1011
MACS Tissue Storage Solution	Miltenyi Biotec	130-100-008
Paraffin	Leica	N/A
Paraformaldehyde	Roth	0335.3
Phosphate-buffered saline (PBS)	Gibco	70011
ProLong Gold Antifade mounting medium	Thermo Fisher Scientific	P36930
SSC buffer (20x)	Thermo Fisher Scientific	J60839.K2
Tween-20	Merck	P9416
Xylene	VWR chemicals	28975.325

Table 3. Chemicals and reagents.

6.1.3 Devices and laboratory consumables

All devices and laboratory consumables used in this thesis are listed in Table 4.

Device or laboratory consumables	Company	Reference #
4200 TapeStation System	Agilent Technologies	G2991BA
Biopsy embedding cassette	Simport	E478.1
Chromium Controller	10x Genomics	N/A
Chromium Next GEM Chip G	10x Genomics	PN-1000127
Coverslips	Thermo Fisher Scientific	11708701
D1000 ScreenTape	Agilent Technologies	5067-5582
Filter (70µm)	Corning	352350
Freezer (-20°C)	Liebherr	N/A
Fridge (4°C)	Liebherr	N/A
Fume hood	Waldner	N/A
gentleMACS Dissociator	Miltenyi Biotec	130-093-235

HistoCore Arcadia H (paraffin embedding station)	Leica	14039357258
HybEZ II oven	Bio-Techne	321710
HybEZ Humidity Control tray	Bio-Techne	310012
ImmEdge pen	Vector Laboratories	H-4000
Microm HM 355S	Thermo Fisher Scientific	N/A
Micropipettes	Gilson	N/A
MiniMACS Separator	Miltenyi Biotec	130-042-102
MS Separation Column	Miltenyi Biotec	130-042-201
NovaSeq 6000 sequencing system	Illumina	N/A
Pipette tips	Nerbe plus	N/A
Qubit 4 fluorometer	Invitrogen	Q33226
Reaction tubes 1.5ml	Sarstedt	72.690.001
Reaction tubes 2ml	Sarstedt	72.691
Scalpel No 21	Feather	530032
Slide scanning microscope Slideview VS200	Olympus	N/A
Superfrost ultra plus microscopy slides	Thermo Fisher Scientific	J3800AMNZ
Tissue processor ASP300S	Leica	N/A
Tubes 15ml	Greiner Bio-One	188 271-N
Tubes 50ml	Greiner Bio-One	227 261
Water bath	Julabo	3884

Table 4. Devices and laboratory consumables.

6.1.4 Commercial kits

All commercial kits used in this thesis are listed in Table 5.

Commercial kit	Company	Reference #
Chromium Next GEM Single Cell 3' Reagent kit	10x Genomics	PN-1000128
Dead Cell Removal kit	Miltenyi Biotec	130-090-101
Qubit dsDNA HS Assay kit	Invitrogen	Q32851
RNAscope HiPlex12 Reagents v2 kit	Bio-Techne	324409
Whole Skin Dissociation kit (human)	Miltenyi Biotec	130-101-540

Table 5. Commercial kits.

6.1.5 RNA FISH probes

All RNAscope HiPlex probes used for multiplexed RNA FISH assays in this thesis are listed in Table 6.

Probe	Company	Reference #
Hs-APCDD1-T1[1]	Bio-Techne	535851-T1
Hs-APOE-T5[1]	Bio-Techne	433091-T5
Hs-C3-T8[1,2]	Bio-Techne	430701-T8
Hs-CCN5-T7[1]	Bio-Techne	888111-T7
Hs-CD3D-T9[2]	Bio-Techne	599391-T9
Hs-COL3A1-T4[1,2]	Bio-Techne	549431-T4
Hs-CXCL12-T3[2]	Bio-Techne	422991-T3
Hs-CXCR4-T2[2]	Bio-Techne	310511-T2
Hs-DIO2-T11[1]	Bio-Techne	562211-T11
Hs-IGF1-T6[1]	Bio-Techne	313031-T6
Hs-KRT14-T12[1,2]	Bio-Techne	310191-T12
Hs-MCAM-T7[2]	Bio-Techne	601731-T7
Hs-MMP11-T3[1]	Bio-Techne	479741-T3
Hs-POSTN-T2[1]	Bio-Techne	409181-T2
Hs-VWF-T11[2]	Bio-Techne	560461-T11
Hs-WNT5A-T10[1,2]	Bio-Techne	604921-T10

Table 6. RNA FISH probes. [1]: used for multiplexed RNA FISH assays to detect cSCC-related iCAFs and myCAFs (see Results, sections 3.3.1-3.3.3), [2]: used for multiplexed RNA FISH assays to detect iCAF/myCAF-related cellular interactions (see Results, section 3.3.4).

6.1.6 Clinical samples

All clinical samples used for multiplexed RNA FISH assays and scRNA-seq analyses are listed in Table 7 and 8, respectively.

Sample ID	Gender	Age (years)	Localization	Immune status	Grading & tumor thickness	Biopsy
EH 1	male	65	face	IC	N/A	incisional
EH 2	male	66	head	IC	N/A	incisional
EH 3	male	83	face	IC	N/A	incisional
AK 1	male	84	head	IC	N/A	incisional
AK 2	male	88	face	IC	N/A	shave

AK 3	male	82	head	IC	N/A	shave
BD 1	male	77	head	IC	N/A	shave
BD 2	male	82	head	IC	N/A	shave
BD 3	male	79	head	IC	N/A	shave
cSCC 1	male	71	head	IC	G2 / 4.0mm	incisional
cSCC 2	male	85	head	IC	G1 / 2.0mm	incisional
cSCC 3	male	81	head	IC	G2 / 1.2mm	incisional
cSCC 4*	male	72	face	IC	G2 / 5.0mm	incisional
cSCC 5*	male	81	face	IC	G2 / 3.6mm	incisional

Table 7. Overview of the clinical samples used for multiplexed RNA FISH assays. EH: chronically ultraviolet radiation (UVR)-exposed healthy skin, AK: actinic keratosis, BD: Bowen's disease, cSCC: cutaneous squamous cell carcinoma, IC: immunocompetent, N/A: not available, *: samples used for additional assays to visualize cellular interactions.

Sample ID	Gender	Age (years)	Localization	Chronic UVR exposure	Immune status	Diagnosis	Grading & tumor thickness	Number of cells
PH 1*	male	53	inguinal	no	IC	healthy	N/A	2,592
PH 2*	male	70	inguinal	no	IC	healthy	N/A	1,833
PH 3*	male	69	inguinal	no	IC	healthy	N/A	4,386
EH 1	male	47	temple	yes	IC	healthy	N/A	13,439
EH 2	male	87	cheek	yes	IC	healthy	N/A	8,757
EH 3	male	71	head	yes	IC	healthy	N/A	7,380
BD 1	male	65	head	yes	IC	BD	N/A	10,047
BD 2**	male	85	upper arm	yes	IC	BD	early invasive	7,183
BD 3**	male	85	shoulder	yes	IC	BD	early invasive	18,988
cSCC 1	male	72	head	yes	IC	cSCC	G3-4 / 6.0mm	18,336
cSCC 2	male	72	head	yes	IC	cSCC	G2 / 3.6mm	4,054
cSCC 3	male	91	head	yes	IC	cSCC	G2 / 6.0mm	4,533
cSCC 4	male	93	head	yes	IC	cSCC	G1 / 8.0mm	4,536
cSCC 5	male	84	head	yes	IC	cSCC	G1-2 / 3.2mm	8,989

Table 8. Overview of the clinical samples used for scRNA-seq. UVR: ultraviolet radiation, PH: UVR-protected healthy skin, EH: chronically UVR-exposed healthy skin, BD: Bowen's disease, cSCC: cutaneous squamous cell carcinoma, IC: immunocompetent, N/A: not available, * raw data obtained from Solé-Boldo et al., 2020, ** samples obtained from the same patient.

6.2 Methods

6.2.1 Clinical samples

All clinical samples used in this thesis were part of residual human skin tissue from patients undergoing routine surgery at the Department of Dermatology from University Hospital in Heidelberg. They were obtained after written informed consent by the patients, and the study was approved by the Ethics Committee of Heidelberg University (S-091/2011) in compliance with the current legislation and institutional guidelines. All samples were evaluated by a dermatohistopathologist and/or a pathologist, and were not required for further diagnostic purposes.

For multiplexed RNA FISH, either fresh human skin biopsies (three EH skin samples) were obtained from the Department of Dermatology from University Hospital in Heidelberg, or 4µm FFPE skin sections (three AK, three BD and five cSCC samples) were obtained from the NCT tissue bank in Heidelberg. For better compatibility, only samples from chronically UVR-exposed body areas of male patients between 65 and 88 years old were included into the assays. Clinicopathological characteristics are summarized in Table 7.

For scRNA-seq, 3mm skin punch biopsies were obtained from different stages within the cSCC disease continuum, including three EH skin samples, three BDs and five cSCCs. To minimize the effect of potential confounding factors, all samples were taken from chronically UVR-exposed body areas of male patients between 47 and 93 years old. Clinicopathological characteristics are summarized in Table 8.

6.2.2 Sample preparation for scRNA-seq

Directly after removal, the fresh human skin biopsy was kept in MACS Tissue Storage Solution (Miltenyi Biotec) and stored at 4°C. At the same or following day, the sample was dissociated using the Whole Skin Dissociation kit for human tissue (Miltenyi Biotec), following the manufacturer's instructions. Briefly, the punch biopsy was cut into smaller pieces using a sterile scalpel and subcutaneous fat tissue was removed. Then, enzymatic digestion was performed in a water bath at 37°C for three hours, followed by a mechanical dissociation using the gentleMACS Dissociator device (Miltenyi Biotec) with a specific program for human skin. After applying the cell suspension to a 70µm separation filter (Corning), alive cells were enriched using the Dead Cell Removal kit (Miltenyi Biotec), following the manufacturer's instructions. First, cells were incubated with Dead Cell Removal MicroBeads for 15min at room temperature (RT) and then this mixture was applied to a MS separation column (Miltenyi Biotec) that was placed in the magnetic field of a MiniMACS Separator (Miltenyi Biotec). The magnetically

labeled dead or apoptotic cells were kept in the column while alive cells could be collected in the flow-through.

Library preparation was then performed in the DKFZ scOpen Lab, using the previously prepared single cell suspension and the Chromium Next GEM Single Cell 3' Reagent kit v2/v3.1 (10x Genomics), following the manufacturer's instructions. Briefly, Gel Beads-in-emulsion (GEMs), each containing one cell, were generated with the 10x Genomics Chromium Controller via loading around 20,000 single cells together with barcoded gel beads onto the Chromium Next GEM Chip G (10x Genomics). Afterwards, cells within the GEMs were lysed and poly-adenylated mRNAs were reverse transcribed into barcoded, full-length cDNA. Then, GEMs were broken up and the pooled and purified cDNA was amplified, as well as subsequently used for library construction, including enzymatic fragmentation and size selection to optimize the cDNA amplicon size. Furthermore, sequencing adaptors and sample indices were ligated to library fragments. Quality control to check cDNA concentration and integrity was then performed using the Qubit dsDNA HS Assay kit (Invitrogen) and D1000 ScreenTapes (Agilent Technologies), with the Qubit fluorometer (Invitrogen) and the TapeStation System (Agilent Technologies), respectively. Finally, the library was submitted to the DKFZ NGS core facility and pairwise sequencing (26 + 96bp) was performed using the NovaSeq 6000 Sequencing System (Illumina).

Library preparation for one EH skin sample was performed by employees of the DKFZ scOpen Lab, since the access to the laboratory was temporary prohibited for external users, due to the COVID-19 pandemic.

6.2.3 Computational data analysis for scRNA-seq

After sequencing all scRNA-seq libraries, the CellRanger v4.0.0 software (10x Genomics) was used to process the raw reads, including their demultiplexing and alignment to the human genome. These steps were performed by Dr. Günter Raddatz.

Then, the main part of computational analyses was performed using the Seurat v4.0.5 package (Hao *et al.*, 2021) in RStudio v1.2.5033 (RStudio Team, 2020) with R v4.0.3 (R Core Team, 2020). First, the dataset was extended with sequencing reads from three PH skin samples from Solé-Boldo *et al.*, 2020, and then Seurat objects for each sample were generated. During quality control steps, cells expressing less than 200 and more than 2,000 unique genes were discarded for each sample. Furthermore, only cells with less than 5% mitochondrial reads were selected for subsequent analyses.

Afterwards, the standard integration protocol from Seurat was applied, starting with log-normalization of unique molecular identifier (UMI) counts and selection of the 2,000 most variable genes across all samples using the functions *NormalizeData* and

FindVariableFeatures with default parameters. After determining anchor genes for the first 80 dimensions of canonical correlation analysis (CCA) with the function *FindIntegrationAnchors*, these genes were used to integrate the data for all samples (*IntegrateData*). Next, the integrated dataset was scaled using the function *ScaleData* to achieve equal weights for all genes in downstream analyses, without highly expressed genes dominating. Subsequently, the dimensional reduction technique principal component analysis (PCA) was performed via *RunPCA*, and the resulting first 130 dimensions were used to construct a K-nearest neighbor (KNN) plot. This plot was then used for unsupervised clustering of all cells, including modulatory optimization via the Louvain algorithm and a resolution of 0.9 (*FindNeighbors* and *FindClusters*). To finally visualize the integrated dataset, the non-linear dimension reduction technique UMAP was performed, using the function *RunUMAP* with the first 130 PCA dimensions.

Afterwards, differentially expressed genes detected in at least 25% of the cells, were determined with *FindAllMarkers* (min.pct = 0.25) to identify the most representative genes for each cell cluster. These genes together with well-known marker genes from the literature (Solé-Boldo *et al.*, 2020) were then used to annotate skin-related cell types in the integrated dataset.

6.2.3.1 Cell cycle analysis

In Seurat several gene signatures are deposited, including genes related to different cell cycle phases, according to Tirosh *et al.*, 2016. With the function *CellCycleScoring*, expression levels for 54 G2/M phase-related genes and 43 S phase-related genes were determined. High expression values for one or the other gene signature led to the automatic assignment of cells to either the G2/M or S phase. For cells showing no enriched expression for both of them, the algorithm assumed that these cells belong to the G1 cell cycle phase.

6.2.3.2 CNV inference

To distinguish healthy and malignant keratinocytes, CNVs were inferred from scRNA-seq data using the R packages InferCNV v1.6 (Patel *et al.*, 2014; Tirosh *et al.*, 2016) and CopyKAT v1.1 (Gao *et al.*, 2021), following the provided tutorials.

Briefly, to work with InferCNV, the raw count matrix for keratinocytes of all samples were extracted from the integrated dataset and then used to create an InferCNV object via the function *CreateInfercnvObject*. After assigning cells from PH skin samples as reference, CNVs for EH, BD and cSCC samples were calculated using the function *run* by the comparison of

gene expression intensities between cancer cells and healthy keratinocytes across all chromosomes.

For CopyKAT, also the raw gene expression matrices of keratinocytes from all samples were used as input. Similar to InferCNV, the function *copycat* classified keratinocytes as aneuploid or diploid, based on PH-derived cells as reference. For some keratinocytes no clear assignment was possible, leading to a third group of non defined cells.

6.2.3.3 GO analysis

For GO analyses, the most representative genes (*p*-value < 0.05 and fold change ≥ 1.5) for each target cell group were selected. Then, these genes were submitted to the Gene Functional Annotation Tool from the DAVID Bioinformatics Database v6.8 (Huang da *et al.*, 2009; Sherman *et al.*, 2022), and involved biological processes were analyzed with the option GOTERM_BP_DIRECT. For visualization of the top significant (*p*-value < 0.05) GO terms, the R package ggplot2 v3.3.5 (Wickham, 2016) was used to create bar plots, sorted according to their *p*-values.

6.2.3.4 GSEA

GSEA were performed using the GSEA software with gene sets from the Molecular Signature Database (MSigDB) (Liberzon *et al.*, 2011; Subramanian *et al.*, 2005). For keratinocyte analyses, the gene sets HALLMARK_G2M_CHECKPOINT, HALLMARK_IL6_JAK_STAT3_SIGNALING, HALLMARK_HEDGEHOG_SIGNALING, HALLMARK_OXIDATIVE_PHOSPHORYLATION and HALLMARK_DNA_REPAIR from MSigDB (Liberzon *et al.*, 2015) were used, and CAF analyses were performed with PDAC-derived iCAF/myCAF gene signatures (Elyada *et al.*, 2019; Öhlund *et al.*, 2017). Besides the gene sets, further input data comprised the normalized scRNA-seq gene expression matrices of target cells and their classification into two distinct groups.

6.2.3.5 Trajectory inference

To study CAF development during cSCC progression, trajectory inference from scRNA-seq gene expression data was performed with the R package Slingshot v1.8 (Street *et al.*, 2018), following the provided tutorial.

Input data included PH-derived fibroblasts and CAFs from BD samples and cSCCs. For CAF trajectory inference, Slingshot required a dataset with two clusters, one containing healthy fibroblasts and the other one including CAFs. Therefore, the previously generated integrated

dataset could not be used since the integration workflow resulted in mixed fibroblast/CAF clusters, requiring alternative data preparation. First, quality control steps and normalization were performed with Seurat as previously described (see Material and Methods, section 6.2.3) Subsequently, datasets of samples from the same entity were merged in each case. Batch correction was then performed with extracted gene expression matrices of all patients within each sample type using the Combat method (Johnson *et al.*, 2007), and corrected matrices were re-transferred into the particular Seurat objects. After merging all sample types, the regular data processing, described previously, was performed. This included the determination of variable genes, data scaling, running PCA and UMAP (first 20 PCA dimensions), as well as unsupervised clustering with the first 20 PCA dimensions and a resolution of 0.1. Afterwards, cell type information was transferred from the previously generated integrated dataset and data for the fibroblast and CAF clusters were extracted.

Finally, to use Slingshot, the fibroblast/CAF Seurat object was first converted into a single cell experiment object. Then, unsupervised trajectory inference was performed using the function *slingshot*. In addition, the tool assigned each cell along an arbitrary pseudotime axis, reflecting CAF development from healthy fibroblasts.

6.2.3.6 Cellular interaction analysis

The R packages CellChat v1.4 (Jin *et al.*, 2021) and LIANA v0.1.11 (Dimitrov *et al.*, 2022) were used to analyze cellular interactions between cell types in the scRNA-seq datasets of BD and cSCC samples, following the provided tutorials. CellChat is based on the comparison of scRNA-seq gene expression data with a database of known interacting signaling ligands, receptors and co-factors. LIANA works in a similar way, but combines several cellular interaction tools and databases. Predicted results represent the consensus of the methods and resources behind.

For CellChat, first, cells from either BD or cSCC samples were extracted from the integrated dataset, and melanocytes, Schwann cells, as well as erythrocytes were removed due to low cell numbers. Then, the function *createCellChat* was used to build a new object and an appropriate database was assigned (CellChatDB.human). Afterwards, highly expressed genes for ligands and receptors and their interactions were determined in all cell types (*identifyOverExpressedGenes* and *identifyOverExpressedInteractions*). Communication probabilities between cell types were then calculated with the function *computeCommunProb*. To compare total interaction networks between BD and cSCC samples regarding number and importance of interactions, all communication probabilities were summed up into an aggregated cellular network using the function *aggregateNet*. In addition, general communication probabilities were determined by summarizing single probabilities for each

signaling pathway between all cell types (*computeCommunProbPathway*). For visualization of the overall interaction activity between all cell types in each sample type, scatter plots were generated with the function *netAnalysis_signalingRole_scatter*. To study the most important signaling pathways involving CAFs, heatmaps (*netAnalysis_signalingRole_network*), dot plots (*netVisual_bubble*) and hierarchy plots (*netVisual*) were used.

For LIANA, again data from BD samples or cSCCs were isolated from the integrated scRNA-seq dataset and the minor cell types melanocytes, Schwann cells and erythrocytes were removed. Afterwards, interaction analyses were performed using the function *liana_wrap*, which returned a list with results corresponding to the different deposited resources. This list was then ranked based on the consensus of all methods and underlying *p*-values for the predicted interaction pairs (*liana_aggregate*). Dot plots visualizing target interaction pairs, as previously defined with CellChat, were generated using the function *liana_dotplot*.

6.2.4 Tissue preparation for chronically UVR-exposed healthy skin

Fresh human EH skin biopsies were fixed with 4% formalin at RT overnight and then placed in biopsy embedding cassettes (Simport). Then, they were washed with distilled water and stored in 50% ethanol at 4°C up to several days. For tissue dehydration and infiltration with paraffin, a tissue processor (Leica) in the DKFZ Light Microscopy core facility was used, that automatically performed several incubation steps (Table 9).

Chemical	Incubation time (h)	Temperature
50% ethanol	1	RT
70% ethanol	2	RT
80% ethanol	2	RT
96% ethanol	1	RT
100% ethanol	1	RT
100% ethanol	2	RT
xylene	1	RT
xylene	2	37°C
xylene	2	37°C
paraffin	1	62°C
paraffin	2	62°C
paraffin	2	62°C

Table 9. Incubation steps for tissue dehydration and paraffin infiltration. All steps were performed automatically by the Tissue Processor ASP300S (Leica) in the DKFZ Light Microscopy core facility. h: hour, RT: room temperature.

Afterwards, each skin biopsy was removed from the cassette and placed into a metal container. The tissue was completely covered with melted paraffin using the HistoCore Arcadia H paraffin embedding station (Leica) in the DKFZ Light Microscopy core facility, and closed with a plastic lid. The metal container was then removed as soon as the paraffin got solid, obtaining a FFPE sample block. All FFPE blocks were stored at -20°C. For multiplexed RNA FISH assays, the rotary microtome Microm HM 355S (Thermo Fisher Scientific) in the DKFZ Light Microscopy core facility was used to generate 4µm sections on Superfrost ultra plus microscopy slides (Thermo Fisher Scientific) for all FFPE samples.

6.2.5 Multiplexed RNA FISH

To perform multiplexed RNA FISH analyses, the RNAscope HiPlex12 Reagents v2 kit (Bio-Techne) was used. For the assays detecting iCAFs and myCAFs at different disease stages, the following probes targeting genes of interest were specifically designed: *APCDD1*, *POSTN*, *MMP11*, *COL3A1*, *APOE*, *IGF1*, *CCN5* (also known as *WISP2*), *C3*, *WNT5A*, *DIO2* and *KRT14* (Bio-Techne, Table 6). For multiplexed RNA FISH assays visualizing CAF-related cellular interactions, probes hybridizing with mRNA molecules of *CXCR4*, *CXCL12*, *COL3A1*, *C3*, *CD3D*, *WNT5A*, *VWF* and *KRT14* were used (Bio-Techne, Table 6).

The NCT tissue bank kindly provided 4µm FFPE skin sections of three suitable AKs, three BDs and five cSCCs, and performed hematoxylin and eosin (H&E) staining for one section per sample. The stained sections were then reviewed by PD Dr. med. Anke Lonsdorf and Prof. Dr. med. Jochen Hoffmann to confirm sample diagnosis and to subdivide tissue sections into regions of different disease stages.

Multiplexed RNA FISH assays to detect CAF subpopulations were performed in three rounds in the DKFZ scOpen Lab, following the kit manufacturer's instructions. They included one EH skin sample (see Material and Methods, section 6.2.4), one AK, one BD and one cSCC sample in each round. Furthermore, two additional EH skin sections were used as positive and negative control slides.

For visualizing interactions between CAFs and non-malignant cell types, one multiplexed RNA FISH assay was conducted in the DKFZ scOpen Lab with two cSCC sections, also following the kit manufacturer's instructions. Also here, two additional EH skin sections were used as positive and negative control slides.

First, FFPE sections were dried at 60°C for 1h and deparaffinized using xylene incubation twice for 5min each, followed by incubation with 100% ethanol twice for 2min each and another drying step at 60°C for 5min. Then, the sections were incubated in boiling RNAscope 1x Target Retrieval Reagents solution for 15min, and washed with distilled water and 100% ethanol. After drying them, RNAscope Protease III treatment was performed at 40°C for 30min using the

HybEZ II oven (Bio-Techne) with the HybEZ Humidity Control tray (Bio-Techne). Subsequently, the sections were washed twice with distilled water and incubated with either the combined target probe mixture or positive/negative probe mixtures, at 40°C (HybEZ II oven) for 2h. Then, they were washed twice with 1x RNAscope Wash Buffer at RT for 2min, and stored in 5x SSC buffer at RT overnight.

The next day, signal amplification for the first four probes was performed by incubation with RNAscope HiPlex Amp 1 solution at 40°C (HybEZ II oven) for 30min, with subsequent washing using 1x RNAscope Wash Buffer. These steps were then repeated twice using RNAscope HiPlex Amp 2 & 3 solutions to amplify the signal of all probes. To reduce autofluorescence, sections were incubated with 5% RNAscope HiPlex FFPE Reagent at RT for 30min, followed by two washing steps with 1x RNAscope Wash Buffer. Afterwards, fluorophores (Alexa Fluor 488, Dylight 550, Dylight 650, Alexa Fluor 750) for the first four probes were hybridized using the RNAscope HiPlex Fluoro T1-T4 solution at 40°C (HybEZ II oven) for 15min, with subsequent washing using 1x RNAscope Wash Buffer. Cell nuclei were then stained with DAPI and slides were mounted using ProLong Gold Antifade mounting medium (Thermo Fisher Scientific). For visualization of the first four probes, the slide scanner microscope Slideview VS200 (Olympus) was used (40x objective). After imaging, the sections were stored in a dark humid chamber at 4°C overnight.

The following day, the slides were soaked in 4x SSC buffer until all coverslips fell off and fluorophores were cleaved, by incubating the sections with 10% RNAscope cleaving solution v2 at RT for 15min. After washing twice with PBST (0.5% Tween), the incubation step with 10% RNAscope cleaving solution v2 and washing with PBST (0.5% Tween) were repeated once. Then, the sections were again incubated with 5% RNAscope HiPlex FFPE Reagent, as described before, and fluorophores were hybridized to the next four probes by incubation with RNAscope HiPlex Fluoro T5-T8 solution at 40°C (HybEZ II oven) for 15min. The slides were mounted and imaged as described before.

After removing the coverslips and cleaving the fluorophores, as described before, the sections were again incubated with 5% RNAscope HiPlex FFPE Reagent and RNAscope HiPlex Fluoro T9-T12 solution to hybridize fluorophores to the last four probes. Finally, slides were mounted and imaged for the third time, as described before.

6.2.5.1 Image analysis and quantification

The HiPlex Image Registration Software v2.0.1 (Bio-Techne) was used to overlay the channels for DAPI and all probes per section, according to the developer's instructions. The images were then processed and analyzed using the software QuPath v0.3.2 (Bankhead *et al.*, 2017) and Fiji v2.3.0 (Schindelin *et al.*, 2012).

General CAF quantification in BDs and cSCCs was performed by counting CAFs (*COL3A1*[+]) in several dermal regions. The number of iCAFs and myCAFs was then determined by the co-expression of *COL3A1* with *C3* and/or *IGF1* or *MMP11* and/or *WNT5A*, respectively. Like this, double- and also triple-positive CAFs were considered for quantitative analyses. In contrast, *COL3A1*-positive CAFs showing mixed co-expression of iCAF and myCAF marker genes simultaneously, were neglected during the quantification since a clear subpopulation classification was not possible. The same is true for CAFs without expression of any of the subpopulation-specific marker genes. In addition, potential CAF origins were analyzed by quantifying cells co-expressing iCAF/myCAF marker genes and the fibroblast subpopulation marker genes *APOE* or *POSTN*. Also here, CAFs showing simultaneous co-expression of *APOE* and *POSTN* were not considered for analyses.

In order to quantify specific iCAF and myCAF interactions with different non-malignant cell types, T cells (*CD3D*^{+}) and vascular ECs (*VWF*[+]) were counted in several dermal regions. Then, the amount of T cells and vascular ECs expressing the respective interaction receptors *CXCR4* and *MCAM* were determined. In addition, iCAFs (*COL3A1*[+], *C3*[+]) and myCAFs (*COL3A1*[+], *WNT5A*^{+}) in the direct surrounding of T cells and vascular ECs were counted. For neighboring iCAFs, the expression of the interaction ligand *CXCL12* was also quantified.

6.2.6 Statistics

The software CellRanger v4.0.0 (10x Genomics) and the R package Seurat v4.0.5 (Hao *et al.*, 2021) were used for general statistical analyses of scRNA-seq data and violin plots (Wilcoxon Rank Sum tests). For specific comparisons of fibroblast proportions and cell cycle proportions of mesenchymal fibroblasts within the different scRNA-seq sample types, one-way ANOVA tests with pairwise comparisons were performed using the Holm-Sidak test in SigmaPlot v14.0 (Systat Software Inc.). In addition, two-sided unpaired and paired t-tests were performed with SigmaPlot, and were used to analyze CAF proportions in tumor samples (scRNA-seq data), the correlation of CAF subtypes with healthy fibroblast subpopulations (scRNA-seq data), CAF proportions in each cell cycle phase (scRNA-seq data) and image quantification results (multiplexed RNA FISH).

7. Appendix

7.1 Data availability

The results of this thesis have been incorporated into the manuscript "Cancer-associated fibroblasts with distinct origins and functions establish a pro-tumorigenic environment in squamous cell carcinoma", which was recently submitted (Schütz *et al.*, 2023).

Publicly available datasets used in this thesis are accessible from the Gene Expression Omnibus (GEO) database through the codes GSE130973 (Solé-Boldo *et al.*, 2020), GSE181907 (Yerly *et al.*, 2022) and GSE141526 (Guerrero-Juarez *et al.*, 2022).

7.2 List of publications

Solé-Boldo, L., Raddatz, G., **Schütz, S.**, Mallm, J.P., Rippe, K., Lonsdorf, A.S., Rodríguez-Paredes, M., and Lyko, F. (2020). Single-cell transcriptomes of the human skin reveal age-related loss of fibroblast priming. *Communications biology* 3, 188, doi:10.1038/s42003-020-0922-4.

Ahlers, J.M.D., Falckenhayn, C., Holzscheck, N., Solé-Boldo, L., **Schütz, S.**, Wenck, H., Winnefeld, M., Lyko, F., Grönniger, E., and Siracusa, A. (2021). Single-Cell RNA Profiling of Human Skin Reveals Age-Related Loss of Dermal Sheath Cells and Their Contribution to a Juvenile Phenotype. *Front Genet* 12, 797747, doi:10.3389/fgene.2021.797747.

Schütz, S., Solé-Boldo, L., Lucena-Porcel, C., Hoffmann, J., Brobeil, A., Lonsdorf, A.S., Rodríguez-Paredes, M., and Lyko, F. (2023). Cancer-associated fibroblasts with distinct origins and functions establish a pro-tumorigenic environment in squamous cell carcinoma. Submitted.

8. References

Affo, S., Yu, L.X., and Schwabe, R.F. (2017). The Role of Cancer-Associated Fibroblasts and Fibrosis in Liver Cancer. *Annu Rev Pathol* 12, 153-186, doi:10.1146/annurev-pathol-052016-100322.

Aggarwal, V., Montoya, C.A., Donnenberg, V.S., and Sant, S. (2021). Interplay between tumor microenvironment and partial EMT as the driver of tumor progression. *iScience* 24, 102113, doi:10.1016/j.isci.2021.102113.

Ahadiat, O., Higgins, S., Sutton, A., Ly, A., and Wysong, A. (2017). SLNB in cutaneous SCC: A review of the current state of literature and the direction for the future. *J Surg Oncol* 116, 344-350, doi:10.1002/jso.24675.

Ahlers, J.M.D., Falckenhayn, C., Holzscheck, N., Solé-Boldo, L., Schütz, S., Wenck, H., Winnefeld, M., Lyko, F., Grönniger, E., and Siracusa, A. (2021). Single-Cell RNA Profiling of Human Skin Reveals Age-Related Loss of Dermal Sheath Cells and Their Contribution to a Juvenile Phenotype. *Front Genet* 12, 797747, doi:10.3389/fgene.2021.797747.

Andrews, J.P., Marttala, J., Macarak, E., Rosenbloom, J., and Uitto, J. (2016). Keloids: The paradigm of skin fibrosis - Pathomechanisms and treatment. *Matrix biology : journal of the International Society for Matrix Biology* 51, 37-46, doi:10.1016/j.matbio.2016.01.013.

Apalla, Z., Lallas, A., Sotiriou, E., Lazaridou, E., and Ioannides, D. (2017). Epidemiological trends in skin cancer. *Dermatology practical & conceptual* 7, 1-6, doi:10.5826/dpc.0702a01.

Arda, O., Göksügür, N., and Tüzün, Y. (2014). Basic histological structure and functions of facial skin. *Clin Dermatol* 32, 3-13, doi:10.1016/j.clindermatol.2013.05.021.

Arina, A., Idel, C., Hyjek, E.M., Alegre, M.L., Wang, Y., Bindokas, V.P., Weichselbaum, R.R., and Schreiber, H. (2016). Tumor-associated fibroblasts predominantly come from local and not circulating precursors. *Proc Natl Acad Sci U S A* 113, 7551-7556, doi:10.1073/pnas.1600363113.

Arnold, J.N., Magiera, L., Kraman, M., and Fearon, D.T. (2014). Tumoral immune suppression by macrophages expressing fibroblast activation protein-α and heme oxygenase-1. *Cancer Immunol Res* 2, 121-126, doi:10.1158/2326-6066.Cir-13-0150.

Athar, M., Tang, X., Lee, J.L., Kopelovich, L., and Kim, A.L. (2006). Hedgehog signalling in skin development and cancer. *Exp Dermatol* 15, 667-677, doi:10.1111/j.1600-0625.2006.00473.x.

Auepemkiate, S., Boonyaphiphat, P., and Thongsuksai, P. (2002). p53 expression related to the aggressive infiltrative histopathological feature of basal cell carcinoma. *Histopathology* 40, 568-573, doi:10.1046/j.1365-2559.2002.01393.x.

Bachelor, M.A., and Bowden, G.T. (2004). UVA-mediated activation of signaling pathways involved in skin tumor promotion and progression. *Semin Cancer Biol* 14, 131-138, doi:10.1016/j.semcancer.2003.09.017.

Bankhead, P., Loughrey, M.B., Fernández, J.A., Dombrowski, Y., McArt, D.G., Dunne, P.D., McQuaid, S., Gray, R.T., Murray, L.J., Coleman, H.G. *et al.* (2017). QuPath: Open source software for digital pathology image analysis. *Sci Rep* 7, 16878, doi:10.1038/s41598-017-17204-5.

Barallobre-Barreiro, J., Woods, E., Bell, R.E., Easton, J.A., Hobbs, C., Eager, M., Baig, F., Ross, A.M., Mallipeddi, R., Powell, B. *et al.* (2019). Cartilage-like composition of keloid scar extracellular matrix suggests fibroblast mis-differentiation in disease. *Matrix Biol Plus* 4, 100016, doi:10.1016/j.mbplus.2019.100016.

Bartoschek, M., Oskolkov, N., Bocci, M., Lovrot, J., Larsson, C., Sommarin, M., Madsen, C.D., Lindgren, D., Pekar, G., Karlsson, G. *et al.* (2018). Spatially and functionally distinct subclasses of breast cancer-associated fibroblasts revealed by single cell RNA sequencing. *Nat Commun* 9, 5150, doi:10.1038/s41467-018-07582-3.

Beebe, E., Motamed, Z., Opitz, L., Cheng, P.F., Levesque, M.P., Markkanen, E., and Feldmeyer, L. (2022). Defining the Molecular Landscape of Cancer-Associated Stroma in Cutaneous Squamous Cell Carcinoma. *The Journal of investigative dermatology* 142, 3304-3312.e3305, doi:10.1016/j.jid.2022.06.017.

Benyahia, Z., Dussault, N., Cayol, M., Sigaud, R., Berenguer-Daizé, C., Delfino, C., Tounsi, A., Garcia, S., Martin, P.M., Mabrouk, K. *et al.* (2017). Stromal fibroblasts present in breast carcinomas promote tumor growth and angiogenesis through adrenomedullin secretion. *Oncotarget* 8, 15744-15762, doi:10.18632/oncotarget.14999.

Bernard, V., Semaan, A., Huang, J., San Lucas, F.A., Mulu, F.C., Stephens, B.M., Guerrero, P.A., Huang, Y., Zhao, J., Kamyabi, N. *et al.* (2019). Single-Cell Transcriptomics of Pancreatic Cancer Precursors Demonstrates Epithelial and Microenvironmental Heterogeneity as an Early Event in Neoplastic Progression. *Clin Cancer Res* 25, 2194-2205, doi:10.1158/1078-0432.Ccr-18-1955.

Bhattacharjee, S., Hamberger, F., Ravichandra, A., Miller, M., Nair, A., Affo, S., Filliol, A., Chin, L., Savage, T.M., Yin, D. *et al.* (2021). Tumor restriction by type I collagen opposes tumor-promoting effects of cancer-associated fibroblasts. *The Journal of clinical investigation* 131, doi:10.1172/jci146987.

Biffi, G., Oni, T.E., Spielman, B., Hao, Y., Elyada, E., Park, Y., Preall, J., and Tuveson, D.A. (2019). IL1-Induced JAK/STAT Signaling Is Antagonized by TGFβ to Shape CAF Heterogeneity in Pancreatic Ductal Adenocarcinoma. *Cancer discovery* 9, 282-301, doi:10.1158/2159-8290.Cd-18-0710.

Biffi, G., and Tuveson, D.A. (2021). Diversity and Biology of Cancer-Associated Fibroblasts. *Physiol Rev* 101, 147-176, doi:10.1152/physrev.00048.2019.

Bocheva, G., Slominski, R.M., and Slominski, A.T. (2019). Neuroendocrine Aspects of Skin Aging. *International journal of molecular sciences* 20, doi:10.3390/ijms20112798.

Boeckmann, L., Martens, M.C., and Emmert, S. (2020). Molecular Biology of Basal and Squamous Cell Carcinomas. *Advances in experimental medicine and biology* 1268, 171-191, doi:10.1007/978-3-030-46227-7_9.

Bosch, R., Philips, N., Suárez-Pérez, J.A., Juarranz, A., Devmurari, A., Chalensouk-Khaosaat, J., and González, S. (2015). Mechanisms of Photoaging and Cutaneous Photocarcinogenesis, and Photoprotective Strategies with Phytochemicals. *Antioxidants (Basel)* 4, 248-268, doi:10.3390/antiox4020248.

Brash, D.E., Rudolph, J.A., Simon, J.A., Lin, A., McKenna, G.J., Baden, H.P., Halperin, A.J., and Pontén, J. (1991). A role for sunlight in skin cancer: UV-induced p53 mutations in squamous cell carcinoma. *Proc Natl Acad Sci U S A* 88, 10124-10128, doi:10.1073/pnas.88.22.10124.

Breiteneder-Geleff, S., Soleiman, A., Kowalski, H., Horvat, R., Amann, G., Kriehuber, E., Diem, K., Weninger, W., Tschachler, E., Alitalo, K. *et al.* (1999). Angiosarcomas express mixed endothelial phenotypes of blood and lymphatic capillaries: podoplanin as a specific marker for lymphatic endothelium. *Am J Pathol* 154, 385-394, doi:10.1016/s0002-9440(10)65285-6.

Burton, K.A., Ashack, K.A., and Khachemoune, A. (2016). Cutaneous Squamous Cell Carcinoma: A Review of High-Risk and Metastatic Disease. *American journal of clinical dermatology* 17, 491-508, doi:10.1007/s40257-016-0207-3.

Calcinotto, A., Kohli, J., Zagato, E., Pellegrini, L., Demaria, M., and Alimonti, A. (2019). Cellular Senescence: Aging, Cancer, and Injury. *Physiol Rev* 99, 1047-1078, doi:10.1152/physrev.00020.2018.

Cammareri, P., Rose, A.M., Vincent, D.F., Wang, J., Nagano, A., Libertini, S., Ridgway, R.A., Athineos, D., Coates, P.J., McHugh, A. *et al.* (2016). Inactivation of TGFβ receptors in stem cells drives cutaneous squamous cell carcinoma. *Nat Commun* 7, 12493, doi:10.1038/ncomms12493.

Campbell, I., Polyak, K., and Haviv, I. (2009). Clonal mutations in the cancer-associated fibroblasts: the case against genetic coevolution. *Cancer research* 69, 6765-6768; discussion 6769, doi:10.1158/0008-5472.Can-08-4253.

Cavinato, M., and Jansen-Dürr, P. (2017). Molecular mechanisms of UVB-induced senescence of dermal fibroblasts and its relevance for photoaging of the human skin. *Exp Gerontol* 94, 78-82, doi:10.1016/j.exger.2017.01.009.

Chakravarthy, A., Khan, L., Bensler, N.P., Bose, P., and De Carvalho, D.D. (2018). TGF-β-associated extracellular matrix genes link cancer-associated fibroblasts to immune evasion and immunotherapy failure. *Nat Commun* 9, 4692, doi:10.1038/s41467-018-06654-8.

Chandler, C., Liu, T., Buckanovich, R., and Coffman, L.G. (2019). The double edge sword of fibrosis in cancer. *Transl Res* 209, 55-67, doi:10.1016/j.trsl.2019.02.006.

Chang, P.H., Hwang-Verslues, W.W., Chang, Y.C., Chen, C.C., Hsiao, M., Jeng, Y.M., Chang, K.J., Lee, E.Y., Shew, J.Y., and Lee, W.H. (2012). Activation of Robo1 signaling of breast cancer cells by Slit2 from stromal fibroblast restrains tumorigenesis via blocking PI3K/Akt/β-catenin pathway. *Cancer research* 72, 4652-4661, doi:10.1158/0008-5472.Can-12-0877.

Chen, C., Zhao, S., Karnad, A., and Freeman, J.W. (2018). The biology and role of CD44 in cancer progression: therapeutic implications. *J Hematol Oncol* 11, 64, doi:10.1186/s13045-018-0605-5.

Chen, W., Thiboutot, D., and Zouboulis, C.C. (2002). Cutaneous androgen metabolism: basic research and clinical perspectives. *The Journal of investigative dermatology* 119, 992-1007, doi:10.1046/j.1523-1747.2002.00613.x.

Cheng, J.B., Sedgewick, A.J., Finnegan, A.I., Harirchian, P., Lee, J., Kwon, S., Fassett, M.S., Golovato, J., Gray, M., Ghadially, R. *et al.* (2018). Transcriptional Programming of Normal and Inflamed Human Epidermis at Single-Cell Resolution. *Cell reports* 25, 871-883, doi:10.1016/j.celrep.2018.09.006.

Chhabra, Y., and Weeraratna, A.T. (2023). Fibroblasts in cancer: Unity in heterogeneity. *Cell* 186, 1580-1609, doi:10.1016/j.cell.2023.03.016.

Collins, C.A., Kretzschmar, K., and Watt, F.M. (2011). Reprogramming adult dermis to a neonatal state through epidermal activation of beta-catenin. *Development (Cambridge, England)* 138, 5189-5199, doi:10.1242/dev.064592.

Comito, G., Giannoni, E., Segura, C.P., Barcellos-de-Souza, P., Raspollini, M.R., Baroni, G., Lanciotti, M., Serni, S., and Chiarugi, P. (2014). Cancer-associated fibroblasts and M2-polarized macrophages synergize during prostate carcinoma progression. *Oncogene* 33, 2423-2431, doi:10.1038/onc.2013.191.

Cranmer, L.D., Engelhardt, C., and Morgan, S.S. (2010). Treatment of unresectable and metastatic cutaneous squamous cell carcinoma. *Oncologist* 15, 1320-1328, doi:10.1634/theoncologist.2009-0210.

Dabrowska, A.K., Spano, F., Derler, S., Adlhart, C., Spencer, N.D., and Rossi, R.M. (2018). The relationship between skin function, barrier properties, and body-dependent factors. *Skin research and technology : official journal of International Society for Bioengineering and the Skin (ISBS) [and] International Society for Digital Imaging of Skin (ISDIS) [and] International Society for Skin Imaging (ISSI)* 24, 165-174, doi:10.1111/srt.12424.

Damian, D.L., Patterson, C.R., Stapelberg, M., Park, J., Barnetson, R.S., and Halliday, G.M. (2008). UV radiation-induced immunosuppression is greater in men and prevented by topical nicotinamide. *The Journal of investigative dermatology* 128, 447-454, doi:10.1038/sj.jid.5701058.

Dao, H., Jr., and Kazin, R.A. (2007). Gender differences in skin: a review of the literature. *Gend Med* 4, 308-328, doi:10.1016/s1550-8579(07)80061-1.

Davidson, S., Efremova, M., Riedel, A., Mahata, B., Pramanik, J., Huuhtanen, J., Kar, G., Vento-Tormo, R., Hagai, T., Chen, X. *et al.* (2020). Single-Cell RNA Sequencing Reveals a Dynamic Stromal Niche That Supports Tumor Growth. *Cell reports* 31, 107628, doi:10.1016/j.celrep.2020.107628.

de Groot, A.E., Roy, S., Brown, J.S., Pienta, K.J., and Amend, S.R. (2017). Revisiting Seed and Soil: Examining the Primary Tumor and Cancer Cell Foraging in Metastasis. *Molecular cancer research : MCR* 15, 361-370, doi:10.1158/1541-7786.Mcr-16-0436.

Deng, C.C., Hu, Y.F., Zhu, D.H., Cheng, Q., Gu, J.J., Feng, Q.L., Zhang, L.X., Xu, Y.P., Wang, D., Rong, Z. *et al.* (2021). Single-cell RNA-seq reveals fibroblast heterogeneity and increased mesenchymal fibroblasts in human fibrotic skin diseases. *Nat Commun* 12, 3709, doi:10.1038/s41467-021-24110-y.

Dimitrov, D., Türei, D., Garrido-Rodriguez, M., Burmedi, P.L., Nagai, J.S., Boys, C., Ramirez Flores, R.O., Kim, H., Szalai, B., Costa, I.G. *et al.* (2022). Comparison of methods and resources for cell-cell communication inference from single-cell RNA-Seq data. *Nat Commun* 13, 3224, doi:10.1038/s41467-022-30755-0.

Do, N.N., and Eming, S.A. (2016). Skin fibrosis: Models and mechanisms. *Curr Res Transl Med* 64, 185-193, doi:10.1016/j.retram.2016.06.003.

Dongre, A., and Weinberg, R.A. (2019). New insights into the mechanisms of epithelial-mesenchymal transition and implications for cancer. *Nat Rev Mol Cell Biol* 20, 69-84, doi:10.1038/s41580-018-0080-4.

Driskell, R.R., Lichtenberger, B.M., Hoste, E., Kretzschmar, K., Simons, B.D., Charalambous, M., Ferron, S.R., Herault, Y., Pavlovic, G., Ferguson-Smith, A.C. *et al.* (2013). Distinct fibroblast lineages determine dermal architecture in skin development and repair. *Nature* 504, 277-281, doi:10.1038/nature12783.

Duda, D.G., Duyverman, A.M., Kohno, M., Snuderl, M., Steller, E.J., Fukumura, D., and Jain, R.K. (2010). Malignant cells facilitate lung metastasis by bringing their own soil. *Proc Natl Acad Sci U S A* 107, 21677-21682, doi:10.1073/pnas.1016234107.

Durai, P.C., Thappa, D.M., Kumari, R., and Malathi, M. (2012). Aging in elderly: chronological versus photoaging. *Indian J Dermatol* 57, 343-352, doi:10.4103/0019-5154.100473.

Dvorak, H.F. (1986). Tumors: wounds that do not heal. Similarities between tumor stroma generation and wound healing. *N Engl J Med* 315, 1650-1659, doi:10.1056/nejm198612253152606.

Dziunycz, P., Iotzova-Weiss, G., Eloranta, J.J., Läuchli, S., Hafner, J., French, L.E., and Hofbauer, G.F. (2010). Squamous cell carcinoma of the skin shows a distinct microRNA profile modulated by UV radiation. *The Journal of investigative dermatology* 130, 2686-2689, doi:10.1038/jid.2010.169.

Eckhart, L., and Zeeuwen, P. (2018). The skin barrier: Epidermis vs environment. *Exp Dermatol* 27, 805-806, doi:10.1111/exd.13731.

Elenbaas, B., and Weinberg, R.A. (2001). Heterotypic signaling between epithelial tumor cells and fibroblasts in carcinoma formation. *Experimental cell research* 264, 169-184, doi:10.1006/excr.2000.5133.

Elyada, E., Bolisetty, M., Laise, P., Flynn, W.F., Courtois, E.T., Burkhart, R.A., Teinor, J.A., Belleau, P., Biffi, G., Lucito, M.S. *et al.* (2019). Cross-Species Single-Cell Analysis of Pancreatic Ductal Adenocarcinoma Reveals Antigen-Presenting Cancer-Associated Fibroblasts. *Cancer discovery* 9, 1102-1123, doi:10.1158/2159-8290.Cd-19-0094.

Entenberg, D., Oktay, M.H., and Condeelis, J.S. (2023). Intravital imaging to study cancer progression and metastasis. *Nature reviews Cancer* 23, 25-42, doi:10.1038/s41568-022-00527-5.

Epstein, E.H. (2008). Basal cell carcinomas: attack of the hedgehog. *Nature reviews Cancer* 8, 743-754, doi:10.1038/nrc2503.

Erdogan, B., Ao, M., White, L.M., Means, A.L., Brewer, B.M., Yang, L., Washington, M.K., Shi, C., Franco, O.E., Weaver, A.M. *et al.* (2017). Cancer-associated fibroblasts promote directional cancer cell migration by aligning fibronectin. *The Journal of cell biology* 216, 3799-3816, doi:10.1083/jcb.201704053.

Ewald, A.J., Werb, Z., and Egeblad, M. (2011). Dynamic, long-term in vivo imaging of tumor-stroma interactions in mouse models of breast cancer using spinning-disk confocal microscopy. *Cold Spring Harb Protoc* 2011, pdb.top97, doi:10.1101/pdb.top97.

Fania, L., Didona, D., Di Pietro, F.R., Verkhovskaia, S., Morese, R., Paolino, G., Donati, M., Ricci, F., Coco, V., Ricci, F. *et al.* (2021). Cutaneous Squamous Cell Carcinoma: From Pathophysiology to Novel Therapeutic Approaches. *Biomedicines* 9, doi:10.3390/biomedicines9020171.

Fitzmaurice, C., Abate, D., Abbasi, N., Abbastabar, H., Abd-Allah, F., Abdel-Rahman, O., Abdelalim, A., Abdoli, A., Abdollahpour, I., Abdulle, A.S.M. *et al.* (2019). Global, Regional, and National Cancer Incidence, Mortality, Years of Life Lost, Years Lived With Disability, and Disability-Adjusted Life-Years for 29 Cancer Groups, 1990 to 2017: A Systematic Analysis for the Global Burden of Disease Study. *JAMA Oncol* 5, 1749-1768, doi:10.1001/jamaoncol.2019.2996.

Foster, D.S., Januszyk, M., Delitto, D., Yost, K.E., Griffin, M., Guo, J., Guardino, N., Delitto, A.E., Chinta, M., Burcham, A.R. *et al.* (2022). Multiomic analysis reveals conservation of cancer-associated fibroblast phenotypes across species and tissue of origin. *Cancer Cell* 40, 1392-1406.e1397, doi:10.1016/j.ccell.2022.09.015.

Foster, R., Buckanovich, R.J., and Rueda, B.R. (2013). Ovarian cancer stem cells: working towards the root of stemness. *Cancer Lett* 338, 147-157, doi:10.1016/j.canlet.2012.10.023.

Franco-Barraza, J., Beacham, D.A., Amatangelo, M.D., and Cukierman, E. (2016). Preparation of Extracellular Matrices Produced by Cultured and Primary Fibroblasts. *Curr Protoc Cell Biol* 71, 10.19.11-10.19.34, doi:10.1002/cpcb.2.

Friedman, O. (2005). Changes associated with the aging face. *Facial Plast Surg Clin North Am* 13, 371-380, doi:10.1016/j.fsc.2005.04.004.

Fuchs, E. (2007). Scratching the surface of skin development. *Nature* 445, 834-842, doi:10.1038/nature05659.

Gailani, M.R., Ståhle-Bäckdahl, M., Leffell, D.J., Glynn, M., Zaphiropoulos, P.G., Pressman, C., Undén, A.B., Dean, M., Brash, D.E., Bale, A.E. *et al.* (1996). The role of the human homologue of Drosophila patched in sporadic basal cell carcinomas. *Nature genetics* 14, 78-81, doi:10.1038/ng0996-78.

Galbo, P.M., Jr., Zang, X., and Zheng, D. (2021). Molecular Features of Cancer-associated Fibroblast Subtypes and their Implication on Cancer Pathogenesis, Prognosis, and Immunotherapy Resistance. *Clin Cancer Res* 27, 2636-2647, doi:10.1158/1078-0432.Ccr-20-4226.

Gallego-Rentero, M., Gutiérrez-Pérez, M., Fernández-Guarino, M., Mascaraque, M., Portillo-Esnaola, M., Gilaberte, Y., Carrasco, E., and Juarranz, Á. (2021). TGFβ1 Secreted by Cancer-Associated Fibroblasts as an Inductor of Resistance to Photodynamic Therapy in Squamous Cell Carcinoma Cells. *Cancers* 13, doi:10.3390/cancers13225613.

Gao, R., Bai, S., Henderson, Y.C., Lin, Y., Schalck, A., Yan, Y., Kumar, T., Hu, M., Sei, E., Davis, A. *et al.* (2021). Delineating copy number and clonal substructure in human tumors from single-cell transcriptomes. *Nature biotechnology* 39, 599-608, doi:10.1038/s41587-020-00795-2.

Gerling, M., Büller, N.V., Kirn, L.M., Joost, S., Frings, O., Englert, B., Bergström, Å., Kuiper, R.V., Blaas, L., Wielenga, M.C. *et al.* (2016). Stromal Hedgehog signalling is downregulated in colon cancer and its restoration restrains tumour growth. *Nat Commun* 7, 12321, doi:10.1038/ncomms12321.

Giacomoni, P.U., Mammone, T., and Teri, M. (2009). Gender-linked differences in human skin. *J Dermatol Sci* 55, 144-149, doi:10.1016/j.jdermsci.2009.06.001.

Giglia-Mari, G., and Sarasin, A. (2003). TP53 mutations in human skin cancers. *Hum Mutat* 21, 217-228, doi:10.1002/humu.10179.

Gilliver, S.C., Ashworth, J.J., and Ashcroft, G.S. (2007). The hormonal regulation of cutaneous wound healing. *Clin Dermatol* 25, 56-62, doi:10.1016/j.clindermatol.2006.09.012.

Gonzales, K.A.U., Polak, L., Matos, I., Tierney, M.T., Gola, A., Wong, E., Infarinato, N.R., Nikolova, M., Luo, S., Liu, S. *et al.* (2021). Stem cells expand potency and alter tissue fitness by accumulating diverse epigenetic memories. *Science* 374, eabh2444, doi:10.1126/science.abh2444.

Göppner, D., Nekwasil, S., Franke, I., Gollnick, H., and Leverkus, M. (2010). Successful combination therapy of a locally advanced squamous cell carcinoma of the skin with cetuximab and γ-irradiation. *J Dtsch Dermatol Ges* 8, 826-828, doi:10.1111/j.1610-0387.2010.07526.x.

Gorchs, L., Hellevik, T., Bruun, J.A., Camilio, K.A., Al-Saad, S., Stuge, T.B., and Martinez-Zubiaurre, I. (2015). Cancer-associated fibroblasts from lung tumors maintain their immunosuppressive abilities after high-dose irradiation. *Frontiers in oncology* 5, 87, doi:10.3389/fonc.2015.00087.

Green, J.M., Bishop, P.A., Muir, I.H., and Lomax, R.G. (2000). Gender differences in sweat lactate. *Eur J Appl Physiol* 82, 230-235, doi:10.1007/s004210050676.

Gu, Y., Han, J., Jiang, C., and Zhang, Y. (2020). Biomarkers, oxidative stress and autophagy in skin aging. *Ageing Res Rev* 59, 101036, doi:10.1016/j.arr.2020.101036.

Guerrero-Juarez, C.F., Dedhia, P.H., Jin, S., Ruiz-Vega, R., Ma, D., Liu, Y., Yamaga, K., Shestova, O., Gay, D.L., Yang, Z. *et al.* (2019). Single-cell analysis reveals fibroblast heterogeneity and myeloid-derived adipocyte progenitors in murine skin wounds. *Nat Commun* 10, 650, doi:10.1038/s41467-018-08247-x.

Guerrero-Juarez, C.F., Lee, G.H., Liu, Y., Wang, S., Karikomi, M., Sha, Y., Chow, R.Y., Nguyen, T.T.L., Iglesias, V.S., Aasi, S. *et al.* (2022). Single-cell analysis of human basal cell carcinoma reveals novel regulators of tumor growth and the tumor microenvironment. *Sci Adv* 8, eabm7981, doi:10.1126/sciadv.abm7981.

Guy, G.P., Jr., Machlin, S.R., Ekwueme, D.U., and Yabroff, K.R. (2015). Prevalence and costs of skin cancer treatment in the U.S., 2002-2006 and 2007-2011. *Am J Prev Med* 48, 183-187, doi:10.1016/j.amepre.2014.08.036.

Haensel, D., Jin, S., Sun, P., Cinco, R., Dragan, M., Nguyen, Q., Cang, Z., Gong, Y., Vu, R., MacLean, A.L. *et al.* (2020). Defining Epidermal Basal Cell States during Skin Homeostasis and Wound Healing Using Single-Cell Transcriptomics. *Cell reports* 30, 3932-3947.e3936, doi:10.1016/j.celrep.2020.02.091.

Hameetman, L., Commandeur, S., Bavinck, J.N., Wisgerhof, H.C., de Gruijl, F.R., Willemze, R., Mullenders, L., Tensen, C.P., and Vrieling, H. (2013). Molecular profiling of cutaneous squamous cell carcinomas and actinic keratoses from organ transplant recipients. *BMC cancer* 13, 58, doi:10.1186/1471-2407-13-58.

Hao, Y., Hao, S., Andersen-Nissen, E., Mauck, W.M., 3rd, Zheng, S., Butler, A., Lee, M.J., Wilk, A.J., Darby, C., Zager, M. *et al.* (2021). Integrated analysis of multimodal single-cell data. *Cell* 184, 3573-3587.e3529, doi:10.1016/j.cell.2021.04.048.

Harwood, C.A., Proby, C.M., Inman, G.J., and Leigh, I.M. (2016). The Promise of Genomics and the Development of Targeted Therapies for Cutaneous Squamous Cell Carcinoma. *Acta Derm Venereol* 96, 3-16, doi:10.2340/00015555-2181.

Haydont, V., Neiveyans, V., Fortunel, N.O., and Asselineau, D. (2019). Transcriptome profiling of human papillary and reticular fibroblasts from adult interfollicular dermis pinpoints the 'tissue skeleton' gene network as a component of skin chrono-ageing. *Mech Ageing Dev* 179, 60-77, doi:10.1016/j.mad.2019.01.003.

Heitman, N., Sennett, R., Mok, K.W., Saxena, N., Srivastava, D., Martino, P., Grisanti, L., Wang, Z., Ma'ayan, A., Rompolas, P. *et al.* (2020). Dermal sheath contraction powers stem cell niche relocation during hair cycle regression. *Science* 367, 161-166, doi:10.1126/science.aax9131.

Hiebert, P., Wietecha, M.S., Cangkrama, M., Haertel, E., Mavrogonatou, E., Stumpe, M., Steenbock, H., Grossi, S., Beer, H.D., Angel, P. *et al.* (2018). Nrf2-Mediated Fibroblast Reprogramming Drives Cellular Senescence by Targeting the Matrisome. *Developmental cell* 46, 145-161.e110, doi:10.1016/j.devcel.2018.06.012.

Hoath, S.B., and Leahy, D.G. (2003). The organization of human epidermis: functional epidermal units and phi proportionality. *The Journal of investigative dermatology* 121, 1440-1446, doi:10.1046/j.1523-1747.2003.12606.x.

Hoeijmakers, J.H. (2001). Genome maintenance mechanisms for preventing cancer. *Nature* 411, 366-374, doi:10.1038/35077232.

Hornburg, M., Desbois, M., Lu, S., Guan, Y., Lo, A.A., Kaufman, S., Elrod, A., Lotstein, A., DesRochers, T.M., Munoz-Rodriguez, J.L. *et al.* (2021). Single-cell dissection of cellular components and interactions shaping the tumor immune phenotypes in ovarian cancer. *Cancer Cell* 39, 928-944.e926, doi:10.1016/j.ccell.2021.04.004.

Hosein, A.N., Livingstone, J., Buchanan, M., Reid, J.F., Hallett, M., and Basik, M. (2015). A functional in vitro model of heterotypic interactions reveals a role for interferon-positive carcinoma associated fibroblasts in breast cancer. *BMC cancer* 15, 130, doi:10.1186/s12885-015-1117-0.

Huang da, W., Sherman, B.T., and Lempicki, R.A. (2009). Systematic and integrative analysis of large gene lists using DAVID bioinformatics resources. *Nature protocols* 4, 44-57, doi:10.1038/nprot.2008.211.

Hussein, M.R. (2005). Ultraviolet radiation and skin cancer: molecular mechanisms. *J Cutan Pathol* 32, 191-205, doi:10.1111/j.0303-6987.2005.00281.x.

Ibrahim, S.A., Gadalla, R., El-Ghonaimy, E.A., Samir, O., Mohamed, H.T., Hassan, H., Greve, B., El-Shinawi, M., Mohamed, M.M., and Götte, M. (2017). Syndecan-1 is a novel molecular marker for triple negative inflammatory breast cancer and modulates the cancer stem cell phenotype via the IL-6/STAT3, Notch and EGFR signaling pathways. *Mol Cancer* 16, 57, doi:10.1186/s12943-017-0621-z.

Inman, G.J., Wang, J., Nagano, A., Alexandrov, L.B., Purdie, K.J., Taylor, R.G., Sherwood, V., Thomson, J., Hogan, S., Spender, L.C. *et al.* (2018). The genomic landscape of cutaneous SCC reveals drivers and a novel azathioprine associated mutational signature. *Nat Commun* 9, 3667, doi:10.1038/s41467-018-06027-1.

Jackson, H.W., Fischer, J.R., Zanotelli, V.R.T., Ali, H.R., Mechera, R., Soysal, S.D., Moch, H., Muenst, S., Varga, Z., Weber, W.P. *et al.* (2020). The single-cell pathology landscape of breast cancer. *Nature* 578, 615-620, doi:10.1038/s41586-019-1876-x.

Jacobi, U., Gautier, J., Sterry, W., and Lademann, J. (2005). Gender-related differences in the physiology of the stratum corneum. *Dermatology* 211, 312-317, doi:10.1159/000088499.

Jacobs, G.H., Rippey, J.J., and Altini, M. (1982). Prediction of aggressive behavior in basal cell carcinoma. *Cancer* 49, 533-537, doi:10.1002/1097-0142(19820201)49:3<533::aid-cncr2820490322>3.0.co;2-o.

Janson, D.G., Saintigny, G., van Adrichem, A., Mahe, C., and El Ghalbzouri, A. (2012). Different gene expression patterns in human papillary and reticular fibroblasts. *The Journal of investigative dermatology* 132, 2565-2572, doi:10.1038/jid.2012.192.

Ji, A.L., Rubin, A.J., Thrane, K., Jiang, S., Reynolds, D.L., Meyers, R.M., Guo, M.G., George, B.M., Mollbrink, A., Bergenstråhle, J. *et al.* (2020). Multimodal Analysis of Composition and Spatial Architecture in Human Squamous Cell Carcinoma. *Cell* 182, 497-514.e422, doi:10.1016/j.cell.2020.05.039.

Jin, S., Guerrero-Juarez, C.F., Zhang, L., Chang, I., Ramos, R., Kuan, C.H., Myung, P., Plikus, M.V., and Nie, Q. (2021). Inference and analysis of cell-cell communication using CellChat. *Nat Commun* 12, 1088, doi:10.1038/s41467-021-21246-9.

Johansson, A.C., Ansell, A., Jerhammar, F., Lindh, M.B., Grenman, R., Munck-Wikland, E., Ostman, A., and Roberg, K. (2012). Cancer-associated fibroblasts induce matrix metalloproteinase-mediated cetuximab resistance in head and neck squamous cell carcinoma cells. *Molecular cancer research : MCR* 10, 1158-1168, doi:10.1158/1541-7786.Mcr-12-0030.

Johnson, W.E., Li, C., and Rabinovic, A. (2007). Adjusting batch effects in microarray expression data using empirical Bayes methods. *Biostatistics* 8, 118-127, doi:10.1093/biostatistics/kxj037.

Ju, M.J., Qiu, S.J., Fan, J., Xiao, Y.S., Gao, Q., Zhou, J., Li, Y.W., and Tang, Z.Y. (2009). Peritumoral activated hepatic stellate cells predict poor clinical outcome in hepatocellular carcinoma after curative resection. *Am J Clin Pathol* 131, 498-510, doi:10.1309/ajcp86ppbngohnnl.

Kadomatsu, T., Endo, M., Miyata, K., and Oike, Y. (2014). Diverse roles of ANGPTL2 in physiology and pathophysiology. *Trends Endocrinol Metab* 25, 245-254, doi:10.1016/j.tem.2014.03.012.

Kammeyer, A., and Luiten, R.M. (2015). Oxidation events and skin aging. *Ageing Res Rev* 21, 16-29, doi:10.1016/j.arr.2015.01.001.

Kaps, L., and Schuppan, D. (2020). Targeting Cancer Associated Fibroblasts in Liver Fibrosis and Liver Cancer Using Nanocarriers. *Cells* 9, doi:10.3390/cells9092027.

Karpinich, N.O., Hoopes, S.L., Kechele, D.O., Lenhart, P.M., and Caron, K.M. (2011). Adrenomedullin Function in Vascular Endothelial Cells: Insights from Genetic Mouse Models. *Curr Hypertens Rev* 7, 228-239, doi:10.2174/157340211799304761.

Kato, T., Noma, K., Ohara, T., Kashima, H., Katsura, Y., Sato, H., Komoto, S., Katsube, R., Ninomiya, T., Tazawa, H. *et al.* (2018). Cancer-Associated Fibroblasts Affect Intratumoral CD8(+) and FoxP3(+) T Cells Via IL6 in the Tumor Microenvironment. *Clin Cancer Res* 24, 4820-4833, doi:10.1158/1078-0432.Ccr-18-0205.

Ke, Y., and Wang, X.J. (2021). TGFβ Signaling in Photoaging and UV-Induced Skin Cancer. *The Journal of investigative dermatology* 141, 1104-1110, doi:10.1016/j.jid.2020.11.007.

Kendall, R.T., and Feghali-Bostwick, C.A. (2014). Fibroblasts in fibrosis: novel roles and mediators. *Front Pharmacol* 5, 123, doi:10.3389/fphar.2014.00123.

Kieffer, Y., Hocine, H.R., Gentric, G., Pelon, F., Bernard, C., Bourachot, B., Lameiras, S., Albergante, L., Bonneau, C., Guyard, A. *et al.* (2020). Single-Cell Analysis Reveals Fibroblast Clusters Linked to Immunotherapy Resistance in Cancer. *Cancer discovery* 10, 1330-1351, doi:10.1158/2159-8290.Cd-19-1384.

Kolev, V., Mandinova, A., Guinea-Viniegra, J., Hu, B., Lefort, K., Lambertini, C., Neel, V., Dummer, R., Wagner, E.F., and Dotto, G.P. (2008). EGFR signalling as a negative regulator of Notch1 gene transcription and function in proliferating keratinocytes and cancer. *Nature cell biology* 10, 902-911, doi:10.1038/ncb1750.

Kolimi, P., Narala, S., Nyavanandi, D., Youssef, A.A.A., and Dudhipala, N. (2022). Innovative Treatment Strategies to Accelerate Wound Healing: Trajectory and Recent Advancements. *Cells* 11, doi:10.3390/cells11152439.

Koster, M.I., and Roop, D.R. (2007). Mechanisms regulating epithelial stratification. *Annu Rev Cell Dev Biol* 23, 93-113, doi:10.1146/annurev.cellbio.23.090506.123357.

Kypriotou, M., Huber, M., and Hohl, D. (2012). The human epidermal differentiation complex: cornified envelope precursors, S100 proteins and the 'fused genes' family. *Exp Dermatol* 21, 643-649, doi:10.1111/j.1600-0625.2012.01472.x.

Lambrechts, D., Wauters, E., Boeckx, B., Aibar, S., Nittner, D., Burton, O., Bassez, A., Decaluwé, H., Pircher, A., Van den Eynde, K. *et al.* (2018). Phenotype molding of stromal cells in the lung tumor microenvironment. *Nature medicine* 24, 1277-1289, doi:10.1038/s41591-018-0096-5.

Langer, E.M., Allen-Petersen, B.L., King, S.M., Kendsersky, N.D., Turnidge, M.A., Kuziel, G.M., Riggers, R., Samatham, R., Amery, T.S., Jacques, S.L. *et al.* (2019). Modeling Tumor Phenotypes In Vitro with Three-Dimensional Bioprinting. *Cell reports* 26, 608-623.e606, doi:10.1016/j.celrep.2018.12.090.

Lasithiotakis, K., Leiter, U., Meier, F., Eigentler, T., Metzler, G., Moehrle, M., Breuninger, H., and Garbe, C. (2008). Age and gender are significant independent predictors of survival in primary cutaneous melanoma. *Cancer* 112, 1795-1804, doi:10.1002/cncr.23359.

Lee, J.W., Ratnakumar, K., Hung, K.F., Rokunohe, D., and Kawasumi, M. (2020). Deciphering UV-induced DNA Damage Responses to Prevent and Treat Skin Cancer. *Photochem Photobiol* 96, 478-499, doi:10.1111/php.13245.

Lephart, E.D. (2016). Skin aging and oxidative stress: Equol's anti-aging effects via biochemical and molecular mechanisms. *Ageing Res Rev* 31, 36-54, doi:10.1016/j.arr.2016.08.001.

Leroyer, A.S., Blin, M.G., Bachelier, R., Bardin, N., Blot-Chabaud, M., and Dignat-George, F. (2019). CD146 (Cluster of Differentiation 146). *Arterioscler Thromb Vasc Biol* 39, 1026-1033, doi:10.1161/atvbaha.119.312653.

Levra Levron, C., Watanabe, M., Proserpio, V., Piacenti, G., Lauria, A., Kaltenbach, S., Tamburrini, A., Nohara, T., Anselmi, F., Duval, C. *et al.* (2023). Tissue memory relies on stem cell priming in distal undamaged areas. *Nature cell biology* 25, 740-753, doi:10.1038/s41556-023-01120-0.

Li, A., Wei, Y., Hung, C., and Vunjak-Novakovic, G. (2018). Chondrogenic properties of collagen type XI, a component of cartilage extracellular matrix. *Biomaterials* 173, 47-57, doi:10.1016/j.biomaterials.2018.05.004.

Li, H., Courtois, E.T., Sengupta, D., Tan, Y., Chen, K.H., Goh, J.J.L., Kong, S.L., Chua, C., Hon, L.K., Tan, W.S. *et al.* (2017). Reference component analysis of single-cell transcriptomes elucidates cellular heterogeneity in human colorectal tumors. *Nature genetics* 49, 708-718, doi:10.1038/ng.3818.

Li, H., Fan, X., and Houghton, J. (2007). Tumor microenvironment: the role of the tumor stroma in cancer. *Journal of cellular biochemistry* 101, 805-815, doi:10.1002/jcb.21159.

Li, H., Wang, W., Huang, Z., Zhang, P., Liu, L., Sha, X., Wang, S., Zhou, Y.L., and Shi, J. (2023). Exploration of the shared genes and signaling pathways between lung adenocarcinoma and idiopathic pulmonary fibrosis. *J Thorac Dis* 15, 3054-3068, doi:10.21037/jtd-22-1522.

Li, S., Wang, P., Zhang, G., Ji, J., Lv, T., Wang, X., and Wang, H. (2019a). The effect of ALA-PDT on reversing the activation of cancer-associated fibroblasts in cutaneous squamous cell carcinoma. *Photodiagnosis Photodyn Ther* 27, 234-240, doi:10.1016/j.pdpdt.2019.05.043.

Li, X., Bu, W., Meng, L., Liu, X., Wang, S., Jiang, L., Ren, M., Fan, Y., and Sun, H. (2019b). CXCL12/CXCR4 pathway orchestrates CSC-like properties by CAF recruited tumor associated macrophage in OSCC. *Experimental cell research* 378, 131-138, doi:10.1016/j.yexcr.2019.03.013.

Li, X., Zhao, S., Bian, X., Zhang, L., Lu, L., Pei, S., Dong, L., Shi, W., Huang, L., Zhang, X. *et al.* (2022). Signatures of EMT, immunosuppression, and inflammation in primary and recurrent human cutaneous squamous cell carcinoma at single-cell resolution. *Theranostics* 12, 7532-7549, doi:10.7150/thno.77528.

Liberzon, A., Birger, C., Thorvaldsdóttir, H., Ghandi, M., Mesirov, J.P., and Tamayo, P. (2015). The Molecular Signatures Database (MSigDB) hallmark gene set collection. *Cell Syst* 1, 417-425, doi:10.1016/j.cels.2015.12.004.

Liberzon, A., Subramanian, A., Pinchback, R., Thorvaldsdóttir, H., Tamayo, P., and Mesirov, J.P. (2011). Molecular signatures database (MSigDB) 3.0. *Bioinformatics* 27, 1739-1740, doi:10.1093/bioinformatics/btr260.

Lichtenberger, B.M., Mastrogiannaki, M., and Watt, F.M. (2016). Epidermal beta-catenin activation remodels the dermis via paracrine signalling to distinct fibroblast lineages. *Nat Commun* 7, 10537, doi:10.1038/ncomms10537.

Lim, C.H., Sun, Q., Ratti, K., Lee, S.H., Zheng, Y., Takeo, M., Lee, W., Rabbani, P., Plikus, M.V., Cain, J.E. *et al.* (2018). Hedgehog stimulates hair follicle neogenesis by creating inductive dermis during murine skin wound healing. *Nat Commun* 9, 4903, doi:10.1038/s41467-018-07142-9.

Lincoln, V., Chao, L., Woodley, D.T., Murrell, D., Kim, M., O'Toole, E.A., Ly, A., Cogan, J., Mosallaei, D., Wysong, A. *et al.* (2021). Over-expression of stromal periostin correlates with poor prognosis of cutaneous squamous cell carcinomas. *Exp Dermatol* 30, 698-704, doi:10.1111/exd.14281.

Lippens, S., Denecker, G., Ovaere, P., Vandenabeele, P., and Declercq, W. (2005). Death penalty for keratinocytes: apoptosis versus cornification. *Cell Death Differ* 12 Suppl 2, 1497-1508, doi:10.1038/sj.cdd.4401722.

Liu, X.Y., Liu, Y.B., Xu, J.C., Zhang, Y.F., Ruan, Y.Y., Zhao, Y., Wu, L.F., Hu, J.W., Zhang, Z., He, M.J. *et al.* (2023). Single-cell transcriptomic analysis deciphers key transitional signatures associated with oncogenic evolution in human intramucosal oesophageal squamous cell carcinoma. *Clin Transl Med* 13, e1203, doi:10.1002/ctm2.1203.

Liu, Z.Q., Fang, J.M., Xiao, Y.Y., Zhao, Y., Cui, R., Hu, F., and Xu, Q. (2015). Prognostic role of vascular endothelial growth factor in prostate cancer: a systematic review and meta-analysis. *International journal of clinical and experimental medicine* 8, 2289-2298.

Longley, D.B., Harkin, D.P., and Johnston, P.G. (2003). 5-fluorouracil: mechanisms of action and clinical strategies. *Nature reviews Cancer* 3, 330-338, doi:10.1038/nrc1074.

López-Otín, C., Blasco, M.A., Partridge, L., Serrano, M., and Kroemer, G. (2023a). Hallmarks of aging: An expanding universe. *Cell* 186, 243-278, doi:10.1016/j.cell.2022.11.001.

López-Otín, C., Pietrocola, F., Roiz-Valle, D., Galluzzi, L., and Kroemer, G. (2023b). Meta-hallmarks of aging and cancer. *Cell Metab* 35, 12-35, doi:10.1016/j.cmet.2022.11.001.

Lotti, F., Jarrar, A.M., Pai, R.K., Hitomi, M., Lathia, J., Mace, A., Gantt, G.A., Jr., Sukhdeo, K., DeVecchio, J., Vasanji, A. *et al.* (2013). Chemotherapy activates cancer-associated fibroblasts to maintain colorectal cancer-initiating cells by IL-17A. *The Journal of experimental medicine* 210, 2851-2872, doi:10.1084/jem.20131195.

Louault, K., Bonneaud, T.L., Séveno, C., Gomez-Bougie, P., Nguyen, F., Gautier, F., Bourgeois, N., Loussouarn, D., Kerdraon, O., Barillé-Nion, S. *et al.* (2019). Interactions between cancer-associated fibroblasts and tumor cells promote MCL-1 dependency in

estrogen receptor-positive breast cancers. *Oncogene* 38, 3261-3273, doi:10.1038/s41388-018-0635-z.

Louault, K., Li, R.R., and DeClerck, Y.A. (2020). Cancer-Associated Fibroblasts: Understanding Their Heterogeneity. *Cancers* 12, doi:10.3390/cancers12113108.

Luo, H., Xia, X., Huang, L.B., An, H., Cao, M., Kim, G.D., Chen, H.N., Zhang, W.H., Shu, Y., Kong, X. *et al.* (2022). Pan-cancer single-cell analysis reveals the heterogeneity and plasticity of cancer-associated fibroblasts in the tumor microenvironment. *Nat Commun* 13, 6619, doi:10.1038/s41467-022-34395-2.

Lynch, M.D., and Watt, F.M. (2018). Fibroblast heterogeneity: implications for human disease. *The Journal of clinical investigation* 128, 26-35, doi:10.1172/jci93555.

Mariathasan, S., Turley, S.J., Nickles, D., Castiglioni, A., Yuen, K., Wang, Y., Kadel, E.E., III, Koeppen, H., Astarita, J.L., Cubas, R. *et al.* (2018). TGFβ attenuates tumour response to PD-L1 blockade by contributing to exclusion of T cells. *Nature* 554, 544-548, doi:10.1038/nature25501.

Maris, P., Blomme, A., Palacios, A.P., Costanza, B., Bellahcène, A., Bianchi, E., Gofflot, S., Drion, P., Trombino, G.E., Di Valentin, E. *et al.* (2015). Asporin Is a Fibroblast-Derived TGF-β1 Inhibitor and a Tumor Suppressor Associated with Good Prognosis in Breast Cancer. *PLoS Med* 12, e1001871, doi:10.1371/journal.pmed.1001871.

Marples, R.R. (1982). Sex, constancy, and skin bacteria. *Arch Dermatol Res* 272, 317-320, doi:10.1007/bf00509062.

Martincuks, A., Li, P.C., Zhao, Q., Zhang, C., Li, Y.J., Yu, H., and Rodriguez-Rodriguez, L. (2020). CD44 in Ovarian Cancer Progression and Therapy Resistance-A Critical Role for STAT3. *Frontiers in oncology* 10, 589601, doi:10.3389/fonc.2020.589601.

Mentlein, R., Hattermann, K., Hemion, C., Jungbluth, A.A., and Held-Feindt, J. (2011). Expression and role of the cell surface protease seprase/fibroblast activation protein-alpha (FAP-alpha) in astroglial tumors. *Biological chemistry* 392, 199-207, doi:10.1515/bc.2010.119.

Mesa, K.R., Kawaguchi, K., Cockburn, K., Gonzalez, D., Boucher, J., Xin, T., Klein, A.M., and Greco, V. (2018). Homeostatic Epidermal Stem Cell Self-Renewal Is Driven by Local Differentiation. *Cell Stem Cell* 23, 677-686.e674, doi:10.1016/j.stem.2018.09.005.

Mescher, A.L. (2017). Macrophages and fibroblasts during inflammation and tissue repair in models of organ regeneration. *Regeneration (Oxf)* 4, 39-53, doi:10.1002/reg2.77.

Mitra, A.K., Zillhardt, M., Hua, Y., Tiwari, P., Murmann, A.E., Peter, M.E., and Lengyel, E. (2012). MicroRNAs reprogram normal fibroblasts into cancer-associated fibroblasts in ovarian cancer. *Cancer discovery* 2, 1100-1108, doi:10.1158/2159-8290.Cd-12-0206.

Moreci, R.S., and Lechler, T. (2020). Epidermal structure and differentiation. *Curr Biol* 30, R144-r149, doi:10.1016/j.cub.2020.01.004.

Mudigonda, T., Pearce, D.J., Yentzer, B.A., Williford, P., and Feldman, S.R. (2010). The economic impact of non-melanoma skin cancer: a review. *J Natl Compr Canc Netw* 8, 888-896, doi:10.6004/jnccn.2010.0066.

Murota, H., Lingli, Y., and Katayama, I. (2017). Periostin in the pathogenesis of skin diseases. *Cellular and molecular life sciences : CMLS* 74, 4321-4328, doi:10.1007/s00018-017-2647-1.

Mutgan, A.C., Besikcioglu, H.E., Wang, S., Friess, H., Ceyhan, G.O., and Demir, I.E. (2018). Insulin/IGF-driven cancer cell-stroma crosstalk as a novel therapeutic target in pancreatic cancer. *Mol Cancer* 17, 66, doi:10.1186/s12943-018-0806-0.

Nagarajan, P., Asgari, M.M., Green, A.C., Guhan, S.M., Arron, S.T., Proby, C.M., Rollison, D.E., Harwood, C.A., and Toland, A.E. (2019). Keratinocyte Carcinomas: Current Concepts and Future Research Priorities. *Clin Cancer Res* 25, 2379-2391, doi:10.1158/1078-0432.Ccr-18-1122.

Naik, S., Larsen, S.B., Gomez, N.C., Alaverdyan, K., Sendoel, A., Yuan, S., Polak, L., Kulukian, A., Chai, S., and Fuchs, E. (2017). Inflammatory memory sensitizes skin epithelial stem cells to tissue damage. *Nature* 550, 475-480, doi:10.1038/nature24271.

Nakazawa, H., English, D., Randell, P.L., Nakazawa, K., Martel, N., Armstrong, B.K., and Yamasaki, H. (1994). UV and skin cancer: specific p53 gene mutation in normal skin as a biologically relevant exposure measurement. *Proc Natl Acad Sci U S A* 91, 360-364, doi:10.1073/pnas.91.1.360.

Nauroy, P., Barruche, V., Marchand, L., Nindorera-Badara, S., Bordes, S., Closs, B., and Ruggiero, F. (2017). Human Dermal Fibroblast Subpopulations Display Distinct Gene Signatures Related to Cell Behaviors and Matrisome. *The Journal of investigative dermatology* 137, 1787-1789, doi:10.1016/j.jid.2017.03.028.

Neal, J.T., Li, X., Zhu, J., Giangarra, V., Grzeskowiak, C.L., Ju, J., Liu, I.H., Chiou, S.H., Salahudeen, A.A., Smith, A.R. *et al.* (2018). Organoid Modeling of the Tumor Immune Microenvironment. *Cell* 175, 1972-1988.e1916, doi:10.1016/j.cell.2018.11.021.

Novotný, J., Strnadová, K., Dvořánková, B., Kocourková, Š., Jakša, R., Dundr, P., Pačes, V., Smetana, K., Jr., Kolář, M., and Lacina, L. (2020). Single-Cell RNA Sequencing Unravels Heterogeneity of the Stromal Niche in Cutaneous Melanoma Heterogeneous Spheroids. *Cancers* 12, doi:10.3390/cancers12113324.

Obrador, E., Liu-Smith, F., Dellinger, R.W., Salvador, R., Meyskens, F.L., and Estrela, J.M. (2019). Oxidative stress and antioxidants in the pathophysiology of malignant melanoma. *Biological chemistry* 400, 589-612, doi:10.1515/hsz-2018-0327.

Odagiri, H., Kadomatsu, T., Endo, M., Masuda, T., Morioka, M.S., Fukuhara, S., Miyamoto, T., Kobayashi, E., Miyata, K., Aoi, J. *et al.* (2014). The secreted protein ANGPTL2 promotes metastasis of osteosarcoma cells through integrin α5β1, p38 MAPK, and matrix metalloproteinases. *Sci Signal* 7, ra7, doi:10.1126/scisignal.2004612.

Öhlund, D., Handly-Santana, A., Biffi, G., Elyada, E., Almeida, A.S., Ponz-Sarvise, M., Corbo, V., Oni, T.E., Hearn, S.A., Lee, E.J. *et al.* (2017). Distinct populations of inflammatory fibroblasts and myofibroblasts in pancreatic cancer. *The Journal of experimental medicine* 214, 579-596, doi:10.1084/jem.20162024.

Ootani, A., Li, X., Sangiorgi, E., Ho, Q.T., Ueno, H., Toda, S., Sugihara, H., Fujimoto, K., Weissman, I.L., Capecchi, M.R. *et al.* (2009). Sustained in vitro intestinal epithelial culture within a Wnt-dependent stem cell niche. *Nature medicine* 15, 701-706, doi:10.1038/nm.1951.

Orimo, A., and Weinberg, R.A. (2007). Heterogeneity of stromal fibroblasts in tumors. *Cancer biology & therapy* 6, 618-619.

Özdemir, B.C., Pentcheva-Hoang, T., Carstens, J.L., Zheng, X., Wu, C.C., Simpson, T.R., Laklai, H., Sugimoto, H., Kahlert, C., Novitskiy, S.V. *et al.* (2015). Depletion of Carcinoma-Associated Fibroblasts and Fibrosis Induces Immunosuppression and Accelerates Pancreas Cancer with Reduced Survival. *Cancer Cell* 28, 831-833, doi:10.1016/j.ccell.2015.11.002.

Pallangyo, C.K., Ziegler, P.K., and Greten, F.R. (2015). IKKβ acts as a tumor suppressor in cancer-associated fibroblasts during intestinal tumorigenesis. *The Journal of experimental medicine* 212, 2253-2266, doi:10.1084/jem.20150576.

Paraiso, K.H., and Smalley, K.S. (2013). Fibroblast-mediated drug resistance in cancer. *Biochemical pharmacology* 85, 1033-1041, doi:10.1016/j.bcp.2013.01.018.

Parker, A.L., and Cox, T.R. (2020). The Role of the ECM in Lung Cancer Dormancy and Outgrowth. *Frontiers in oncology* 10, 1766, doi:10.3389/fonc.2020.01766.

Patel, A.P., Tirosh, I., Trombetta, J.J., Shalek, A.K., Gillespie, S.M., Wakimoto, H., Cahill, D.P., Nahed, B.V., Curry, W.T., Martuza, R.L. *et al.* (2014). Single-cell RNA-seq highlights intratumoral heterogeneity in primary glioblastoma. *Science* 344, 1396-1401, doi:10.1126/science.1254257.

Pellegrini, C., Maturo, M.G., Di Nardo, L., Ciciarelli, V., Gutiérrez García-Rodrigo, C., and Fargnoli, M.C. (2017). Understanding the Molecular Genetics of Basal Cell Carcinoma. *International journal of molecular sciences* 18, doi:10.3390/ijms18112485.

Philippeos, C., Telerman, S.B., Oules, B., Pisco, A.O., Shaw, T.J., Elgueta, R., Lombardi, G., Driskell, R.R., Soldin, M., Lynch, M.D. *et al.* (2018). Spatial and Single-Cell Transcriptional Profiling Identifies Functionally Distinct Human Dermal Fibroblast Subpopulations. *The Journal of investigative dermatology* 138, 811-825, doi:10.1016/j.jid.2018.01.016.

Plikus, M.V., Guerrero-Juarez, C.F., Ito, M., Li, Y.R., Dedhia, P.H., Zheng, Y., Shao, M., Gay, D.L., Ramos, R., Hsi, T.C. *et al.* (2017). Regeneration of fat cells from myofibroblasts during wound healing. *Science* 355, 748-752, doi:10.1126/science.aai8792.

Poljšak, B., Dahmane, R.G., and Godić, A. (2012). Intrinsic skin aging: the role of oxidative stress. *Acta Dermatovenerol Alp Pannonica Adriat* 21, 33-36.

Pourreyron, C., Reilly, L., Proby, C., Panteleyev, A., Fleming, C., McLean, K., South, A.P., and Foerster, J. (2012). Wnt5a is strongly expressed at the leading edge in non-melanoma skin cancer, forming active gradients, while canonical Wnt signalling is repressed. *PLoS One* 7, e31827, doi:10.1371/journal.pone.0031827.

Prasad, R.R., Paudel, S., Raina, K., and Agarwal, R. (2020). Silibinin and non-melanoma skin cancers. *J Tradit Complement Med* 10, 236-244, doi:10.1016/j.jtcme.2020.02.003.

Qiu, W., Hu, M., Sridhar, A., Opeskin, K., Fox, S., Shipitsin, M., Trivett, M., Thompson, E.R., Ramakrishna, M., Gorringe, K.L. *et al.* (2008). No evidence of clonal somatic genetic alterations in cancer-associated fibroblasts from human breast and ovarian carcinomas. *Nature genetics* 40, 650-655, doi:10.1038/ng.117.

Que, S.K.T., Zwald, F.O., and Schmults, C.D. (2018). Cutaneous squamous cell carcinoma: Management of advanced and high-stage tumors. *Journal of the American Academy of Dermatology* 78, 249-261, doi:10.1016/j.jaad.2017.08.058.

Rahmani, W., Abbasi, S., Hagner, A., Raharjo, E., Kumar, R., Hotta, A., Magness, S., Metzger, D., and Biernaskie, J. (2014). Hair follicle dermal stem cells regenerate the dermal sheath, repopulate the dermal papilla, and modulate hair type. *Developmental cell* 31, 543-558, doi:10.1016/j.devcel.2014.10.022.

Rahrovan, S., Fanian, F., Mehryan, P., Humbert, P., and Firooz, A. (2018). Male versus female skin: What dermatologists and cosmeticians should know. *Int J Womens Dermatol* 4, 122-130, doi:10.1016/j.ijwd.2018.03.002.

Ratushny, V., Gober, M.D., Hick, R., Ridky, T.W., and Seykora, J.T. (2012). From keratinocyte to cancer: the pathogenesis and modeling of cutaneous squamous cell carcinoma. *The Journal of clinical investigation* 122, 464-472, doi:10.1172/jci57415.

Ravikanth, M., Soujanya, P., Manjunath, K., Saraswathi, T.R., and Ramachandran, C.R. (2011). Heterogenecity of fibroblasts. *J Oral Maxillofac Pathol* 15, 247-250, doi:10.4103/0973-029x.84516.

Regitz-Zagrosek, V., and Kararigas, G. (2017). Mechanistic Pathways of Sex Differences in Cardiovascular Disease. *Physiol Rev* 97, 1-37, doi:10.1152/physrev.00021.2015.

Reynolds, A.J., Lawrence, C., Cserhalmi-Friedman, P.B., Christiano, A.M., and Jahoda, C.A. (1999). Trans-gender induction of hair follicles. *Nature* 402, 33-34, doi:10.1038/46938.

Reynolds, G., Vegh, P., Fletcher, J., Poyner, E.F.M., Stephenson, E., Goh, I., Botting, R.A., Huang, N., Olabi, B., Dubois, A. *et al.* (2021). Developmental cell programs are co-opted in inflammatory skin disease. *Science* 371, doi:10.1126/science.aba6500.

Rice, G., and Rompolas, P. (2020). Advances in resolving the heterogeneity and dynamics of keratinocyte differentiation. *Current opinion in cell biology* 67, 92-98, doi:10.1016/j.ceb.2020.09.004.

Richardson, M.R., Robbins, E.P., Vemula, S., Critser, P.J., Whittington, C., Voytik-Harbin, S.L., and Yoder, M.C. (2014). Angiopoietin-like protein 2 regulates endothelial colony forming cell vasculogenesis. *Angiogenesis* 17, 675-683, doi:10.1007/s10456-014-9423-8.

Rinkevich, Y., Walmsley, G.G., Hu, M.S., Maan, Z.N., Newman, A.M., Drukker, M., Januszyk, M., Krampitz, G.W., Gurtner, G.C., Lorenz, H.P. *et al.* (2015). Skin fibrosis. Identification and isolation of a dermal lineage with intrinsic fibrogenic potential. *Science* 348, aaa2151, doi:10.1126/science.aaa2151.

Rinn, J.L., Bondre, C., Gladstone, H.B., Brown, P.O., and Chang, H.Y. (2006). Anatomic demarcation by positional variation in fibroblast gene expression programs. *PLoS genetics* 2, e119, doi:10.1371/journal.pgen.0020119.

Rittié, L., and Fisher, G.J. (2015). Natural and sun-induced aging of human skin. *Cold Spring Harb Perspect Med* 5, a015370, doi:10.1101/cshperspect.a015370.

Rockey, D.C., Weymouth, N., and Shi, Z. (2013). Smooth muscle α actin (Acta2) and myofibroblast function during hepatic wound healing. *PLoS One* 8, e77166, doi:10.1371/journal.pone.0077166.

Rognoni, E., Gomez, C., Pisco, A.O., Rawlins, E.L., Simons, B.D., Watt, F.M., and Driskell, R.R. (2016). Inhibition of beta-catenin signalling in dermal fibroblasts enhances hair follicle regeneration during wound healing. *Development (Cambridge, England)* 143, 2522-2535, doi:10.1242/dev.131797.

Rognoni, E., and Watt, F.M. (2018). Skin Cell Heterogeneity in Development, Wound Healing, and Cancer. *Trends in cell biology* 28, 709-722, doi:10.1016/j.tcb.2018.05.002.

Rojahn, T.B., Vorstandlechner, V., Krausgruber, T., Bauer, W.M., Alkon, N., Bangert, C., Thaler, F.M., Sadeghyar, F., Fortelny, N., Gernedl, V. *et al.* (2020). Single-cell transcriptomics combined with interstitial fluid proteomics defines cell type-specific immune regulation in atopic dermatitis. *The Journal of allergy and clinical immunology* 146, 1056-1069, doi:10.1016/j.jaci.2020.03.041.

Rompolas, P., Mesa, K.R., Kawaguchi, K., Park, S., Gonzalez, D., Brown, S., Boucher, J., Klein, A.M., and Greco, V. (2016). Spatiotemporal coordination of stem cell commitment during epidermal homeostasis. *Science* 352, 1471-1474, doi:10.1126/science.aaf7012.

Rønnov-Jessen, L., Petersen, O.W., Koteliansky, V.E., and Bissell, M.J. (1995). The origin of the myofibroblasts in breast cancer. Recapitulation of tumor environment in culture unravels diversity and implicates converted fibroblasts and recruited smooth muscle cells. *The Journal of clinical investigation* 95, 859-873, doi:10.1172/jci117736.

Rosenstein, B.S., Phelps, R.G., Weinstock, M.A., Bernstein, J.L., Gordon, M.L., Rudikoff, D., Kantor, I., Shelton, R., and Lebwohl, M.G. (1999). p53 mutations in basal cell carcinomas arising in routine users of sunscreens. *Photochem Photobiol* 70, 798-806.

Sacks, J.D., and Barbolina, M.V. (2015). Expression and Function of CD44 in Epithelial Ovarian Carcinoma. *Biomolecules* 5, 3051-3066, doi:10.3390/biom5043051.

Sahai, E., Astsaturov, I., Cukierman, E., DeNardo, D.G., Egeblad, M., Evans, R.M., Fearon, D., Greten, F.R., Hingorani, S.R., Hunter, T. *et al.* (2020). A framework for advancing our understanding of cancer-associated fibroblasts. *Nature reviews Cancer* 20, 174-186, doi:10.1038/s41568-019-0238-1.

Sahovaler, A., Krishnan, R.J., Yeh, D.H., Zhou, Q., Palma, D., Fung, K., Yoo, J., Nichols, A., and MacNeil, S.D. (2019). Outcomes of Cutaneous Squamous Cell Carcinoma in the Head and Neck Region With Regional Lymph Node Metastasis: A Systematic Review and Meta-analysis. *JAMA Otolaryngol Head Neck Surg* 145, 352-360, doi:10.1001/jamaoto.2018.4515.

Salgado, R., Toll, A., Alameda, F., Baró, T., Martín-Ezquerra, G., Sanmartín, O., Martorell-Calatayud, A., Salido, M., Almenar, S., Solé, F. *et al.* (2010). CKS1B amplification is a frequent event in cutaneous squamous cell carcinoma with aggressive clinical behaviour. *Genes Chromosomes Cancer* 49, 1054-1061, doi:10.1002/gcc.20814.

Salzer, M.C., Lafzi, A., Berenguer-Llergo, A., Youssif, C., Castellanos, A., Solanas, G., Peixoto, F.O., Stephan-Otto Attolini, C., Prats, N., Aguilera, M. *et al.* (2018). Identity Noise and Adipogenic Traits Characterize Dermal Fibroblast Aging. *Cell* 175, 1575-1590.e1522, doi:10.1016/j.cell.2018.10.012.

Santagata, S., Ieranò, C., Trotta, A.M., Capiluongo, A., Auletta, F., Guardascione, G., and Scala, S. (2021). CXCR4 and CXCR7 Signaling Pathways: A Focus on the Cross-Talk Between Cancer Cells and Tumor Microenvironment. *Frontiers in oncology* 11, 591386, doi:10.3389/fonc.2021.591386.

Saqib, U., Sarkar, S., Suk, K., Mohammad, O., Baig, M.S., and Savai, R. (2018). Phytochemicals as modulators of M1-M2 macrophages in inflammation. *Oncotarget* 9, 17937-17950, doi:10.18632/oncotarget.24788.

Sarchio, S.N.E., Scolyer, R.A., Beaugie, C., McDonald, D., Marsh-Wakefield, F., Halliday, G.M., and Byrne, S.N. (2014). Pharmacologically antagonizing the CXCR4-CXCL12 chemokine pathway with AMD3100 inhibits sunlight-induced skin cancer. *The Journal of investigative dermatology* 134, 1091-1100, doi:10.1038/jid.2013.424.

Schindelin, J., Arganda-Carreras, I., Frise, E., Kaynig, V., Longair, M., Pietzsch, T., Preibisch, S., Rueden, C., Saalfeld, S., Schmid, B. *et al.* (2012). Fiji: an open-source platform for biological-image analysis. *Nature methods* 9, 676-682, doi:10.1038/nmeth.2019.

Schlichthorst, M., Sanci, L.A., Pirkis, J., Spittal, M.J., and Hocking, J.S. (2016). Why do men go to the doctor? Socio-demographic and lifestyle factors associated with healthcare utilisation among a cohort of Australian men. *BMC Public Health* 16, 1028, doi:10.1186/s12889-016-3706-5.

Schütz, S., Solé-Boldo, L., Lucena-Porcel, C., Hoffmann, J., Brobeil, A., Lonsdorf, A.S., Rodríguez-Paredes, M., and Lyko, F. (2023). Cancer-associated fibroblasts with distinct origins and functions establish a pro-tumorigenic environment in squamous cell carcinoma. Submitted.

Shaw, T.J., and Rognoni, E. (2020). Dissecting Fibroblast Heterogeneity in Health and Fibrotic Disease. *Curr Rheumatol Rep* 22, 33, doi:10.1007/s11926-020-00903-w.

Sherman, B.T., Hao, M., Qiu, J., Jiao, X., Baseler, M.W., Lane, H.C., Imamichi, T., and Chang, W. (2022). DAVID: a web server for functional enrichment analysis and functional annotation of gene lists (2021 update). *Nucleic Acids Res* 50, W216-221, doi:10.1093/nar/gkac194.

Shiga, K., Hara, M., Nagasaki, T., Sato, T., Takahashi, H., and Takeyama, H. (2015). Cancer-Associated Fibroblasts: Their Characteristics and Their Roles in Tumor Growth. *Cancers* 7, 2443-2458, doi:10.3390/cancers7040902.

Shin, K., Lim, A., Zhao, C., Sahoo, D., Pan, Y., Spiekerkoetter, E., Liao, J.C., and Beachy, P.A. (2014). Hedgehog signaling restrains bladder cancer progression by eliciting stromal production of urothelial differentiation factors. *Cancer Cell* 26, 521-533, doi:10.1016/j.ccell.2014.09.001.

Shin, W., Rosin, N.L., Sparks, H., Sinha, S., Rahmani, W., Sharma, N., Workentine, M., Abbasi, S., Labit, E., Stratton, J.A. *et al.* (2020). Dysfunction of Hair Follicle Mesenchymal Progenitors Contributes to Age-Associated Hair Loss. *Developmental cell* 53, 185-198.e187, doi:10.1016/j.devcel.2020.03.019.

Shook, B.A., Wasko, R.R., Rivera-Gonzalez, G.C., Salazar-Gatzimas, E., López-Giráldez, F., Dash, B.C., Muñoz-Rojas, A.R., Aultman, K.D., Zwick, R.K., Lei, V. *et al.* (2018). Myofibroblast proliferation and heterogeneity are supported by macrophages during skin repair. *Science* 362, doi:10.1126/science.aar2971.

Shuster, S., Black, M.M., and McVitie, E. (1975). The influence of age and sex on skin thickness, skin collagen and density. *Br J Dermatol* 93, 639-643, doi:10.1111/j.1365-2133.1975.tb05113.x.

Simon, T., and Salhia, B. (2022). Cancer-Associated Fibroblast Subpopulations With Diverse and Dynamic Roles in the Tumor Microenvironment. *Molecular cancer research : MCR* 20, 183-192, doi:10.1158/1541-7786.Mcr-21-0282.

Soikkeli, J., Podlasz, P., Yin, M., Nummela, P., Jahkola, T., Virolainen, S., Krogerus, L., Heikkilä, P., von Smitten, K., Saksela, O. *et al.* (2010). Metastatic outgrowth encompasses COL-I, FN1, and POSTN up-regulation and assembly to fibrillar networks regulating cell adhesion, migration, and growth. *Am J Pathol* 177, 387-403, doi:10.2353/ajpath.2010.090748.

Solé-Boldo, L., Raddatz, G., Gutekunst, J., Gilliam, O., Bormann, F., Liberio, M.S., Hasche, D., Antonopoulos, W., Mallm, J.P., Lonsdorf, A.S. *et al.* (2022). Differentiation-related epigenomic changes define clinically distinct keratinocyte cancer subclasses. *Molecular systems biology* 18, e11073, doi:10.15252/msb.202211073.

Solé-Boldo, L., Raddatz, G., Schütz, S., Mallm, J.P., Rippe, K., Lonsdorf, A.S., Rodríguez-Paredes, M., and Lyko, F. (2020). Single-cell transcriptomes of the human skin reveal age-related loss of fibroblast priming. *Communications biology* 3, 188, doi:10.1038/s42003-020-0922-4.

Sorge, R.E., and Totsch, S.K. (2017). Sex Differences in Pain. *J Neurosci Res* 95, 1271-1281, doi:10.1002/jnr.23841.

Sorrell, J.M., and Caplan, A.I. (2004). Fibroblast heterogeneity: more than skin deep. *J Cell Sci* 117, 667-675, doi:10.1242/jcs.01005.

South, A.P., Cho, R.J., and Aster, J.C. (2012). The double-edged sword of Notch signaling in cancer. *Semin Cell Dev Biol* 23, 458-464, doi:10.1016/j.semcdb.2012.01.017.

South, A.P., Purdie, K.J., Watt, S.A., Haldenby, S., den Breems, N., Dimon, M., Arron, S.T., Kluk, M.J., Aster, J.C., McHugh, A. *et al.* (2014). NOTCH1 mutations occur early during cutaneous squamous cell carcinogenesis. *The Journal of investigative dermatology* 134, 2630-2638, doi:10.1038/jid.2014.154.

Steele, C.D., Abbasi, A., Islam, S.M.A., Bowes, A.L., Khandekar, A., Haase, K., Hames-Fathi, S., Ajayi, D., Verfaillie, A., Dhami, P. *et al.* (2022). Signatures of copy number alterations in human cancer. *Nature* 606, 984-991, doi:10.1038/s41586-022-04738-6.

Stone, R.C., Pastar, I., Ojeh, N., Chen, V., Liu, S., Garzon, K.I., and Tomic-Canic, M. (2016). Epithelial-mesenchymal transition in tissue repair and fibrosis. *Cell Tissue Res* 365, 495-506, doi:10.1007/s00441-016-2464-0.

Straub, J.M., New, J., Hamilton, C.D., Lominska, C., Shnayder, Y., and Thomas, S.M. (2015). Radiation-induced fibrosis: mechanisms and implications for therapy. *J Cancer Res Clin Oncol* 141, 1985-1994, doi:10.1007/s00432-015-1974-6.

Street, K., Risso, D., Fletcher, R.B., Das, D., Ngai, J., Yosef, N., Purdom, E., and Dudoit, S. (2018). Slingshot: cell lineage and pseudotime inference for single-cell transcriptomics. *BMC Genomics* 19, 477, doi:10.1186/s12864-018-4772-0.

Stuelten, C.H., DaCosta Byfield, S., Arany, P.R., Karpova, T.S., Stetler-Stevenson, W.G., and Roberts, A.B. (2005). Breast cancer cells induce stromal fibroblasts to express MMP-9 via secretion of TNF-alpha and TGF-beta. *J Cell Sci* 118, 2143-2153, doi:10.1242/jcs.02334.

Stunova, A., and Vistejnova, L. (2018). Dermal fibroblasts-A heterogeneous population with regulatory function in wound healing. *Cytokine & growth factor reviews* 39, 137-150, doi:10.1016/j.cytogfr.2018.01.003.

Subramanian, A., Tamayo, P., Mootha, V.K., Mukherjee, S., Ebert, B.L., Gillette, M.A., Paulovich, A., Pomeroy, S.L., Golub, T.R., Lander, E.S. *et al.* (2005). Gene set enrichment analysis: a knowledge-based approach for interpreting genome-wide expression profiles. *Proc Natl Acad Sci U S A* 102, 15545-15550, doi:10.1073/pnas.0506580102.

Sun, Y., Campisi, J., Higano, C., Beer, T.M., Porter, P., Coleman, I., True, L., and Nelson, P.S. (2012). Treatment-induced damage to the tumor microenvironment promotes prostate cancer therapy resistance through WNT16B. *Nature medicine* 18, 1359-1368, doi:10.1038/nm.2890.

Tabata, M., Kadomatsu, T., Fukuhara, S., Miyata, K., Ito, Y., Endo, M., Urano, T., Zhu, H.J., Tsukano, H., Tazume, H. *et al.* (2009). Angiopoietin-like protein 2 promotes chronic adipose

tissue inflammation and obesity-related systemic insulin resistance. *Cell Metab* 10, 178-188, doi:10.1016/j.cmet.2009.08.003.

Tabib, T., Morse, C., Wang, T., Chen, W., and Lafyatis, R. (2018). SFRP2/DPP4 and FMO1/LSP1 Define Major Fibroblast Populations in Human Skin. *The Journal of investigative dermatology* 138, 802-810, doi:10.1016/j.jid.2017.09.045.

Tabs, S., and Avci, O. (2004). Induction of the differentiation and apoptosis of tumor cells in vivo with efficiency and selectivity. *Eur J Dermatol* 14, 96-102.

Takahashi, K., and Yamanaka, S. (2006). Induction of pluripotent stem cells from mouse embryonic and adult fibroblast cultures by defined factors. *Cell* 126, 663-676, doi:10.1016/j.cell.2006.07.024.

Talbott, H.E., Mascharak, S., Griffin, M., Wan, D.C., and Longaker, M.T. (2022). Wound healing, fibroblast heterogeneity, and fibrosis. *Cell Stem Cell* 29, 1161-1180, doi:10.1016/j.stem.2022.07.006.

Thiboutot, D., Jabara, S., McAllister, J.M., Sivarajah, A., Gilliland, K., Cong, Z., and Clawson, G. (2003). Human skin is a steroidogenic tissue: steroidogenic enzymes and cofactors are expressed in epidermis, normal sebocytes, and an immortalized sebocyte cell line (SEB-1). *The Journal of investigative dermatology* 120, 905-914, doi:10.1046/j.1523-1747.2003.12244.x.

Thomson, J., Bewicke-Copley, F., Anene, C.A., Gulati, A., Nagano, A., Purdie, K., Inman, G.J., Proby, C.M., Leigh, I.M., Harwood, C.A. *et al.* (2021). The Genomic Landscape of Actinic Keratosis. *The Journal of investigative dermatology* 141, 1664-1674.e1667, doi:10.1016/j.jid.2020.12.024.

Thulabandu, V., Chen, D., and Atit, R.P. (2018). Dermal fibroblast in cutaneous development and healing. *Wiley interdisciplinary reviews Developmental biology* 7, doi:10.1002/wdev.307.

Tirosh, I., Izar, B., Prakadan, S.M., Wadsworth, M.H., 2nd, Treacy, D., Trombetta, J.J., Rotem, A., Rodman, C., Lian, C., Murphy, G. *et al.* (2016). Dissecting the multicellular ecosystem of metastatic melanoma by single-cell RNA-seq. *Science* 352, 189-196, doi:10.1126/science.aad0501.

Tobin, D.J. (2017). Introduction to skin aging. *J Tissue Viability* 26, 37-46, doi:10.1016/j.jtv.2016.03.002.

Tsuboi, R., Niiyama, S., Irisawa, R., Harada, K., Nakazawa, Y., and Kishimoto, J. (2020). Autologous cell-based therapy for male and female pattern hair loss using dermal sheath cup cells: A randomized placebo-controlled double-blinded dose-finding clinical study. *Journal of the American Academy of Dermatology* 83, 109-116, doi:10.1016/j.jaad.2020.02.033.

Veit, G., Zwolanek, D., Eckes, B., Niland, S., Käpylä, J., Zweers, M.C., Ishada-Yamamoto, A., Krieg, T., Heino, J., Eble, J.A. *et al.* (2011). Collagen XXIII, novel ligand for integrin alpha2beta1 in the epidermis. *J Biol Chem* 286, 27804-27813, doi:10.1074/jbc.M111.220046.

Vennin, C., Mélénec, P., Rouet, R., Nobis, M., Cazet, A.S., Murphy, K.J., Herrmann, D., Reed, D.A., Lucas, M.C., Warren, S.C. *et al.* (2019). CAF hierarchy driven by pancreatic cancer cell p53-status creates a pro-metastatic and chemoresistant environment via perlecan. *Nat Commun* 10, 3637, doi:10.1038/s41467-019-10968-6.

von Gise, A., and Pu, W.T. (2012). Endocardial and epicardial epithelial to mesenchymal transitions in heart development and disease. *Circ Res* 110, 1628-1645, doi:10.1161/circresaha.111.259960.

Vorstandlechner, V., Laggner, M., Kalinina, P., Haslik, W., Radtke, C., Shaw, L., Lichtenberger, B.M., Tschachler, E., Ankersmit, H.J., and Mildner, M. (2020). Deciphering the functional heterogeneity of skin fibroblasts using single-cell RNA sequencing. *Faseb j* 34, 3677-3692, doi:10.1096/fj.201902001RR.

Waldman, A., and Schmults, C. (2019). Cutaneous Squamous Cell Carcinoma. *Hematol Oncol Clin North Am* 33, 1-12, doi:10.1016/j.hoc.2018.08.001.

Wan, X., Guan, S., Hou, Y., Qin, Y., Zeng, H., Yang, L., Qiao, Y., Liu, S., Li, Q., Jin, T. *et al.* (2021). FOSL2 promotes VEGF-independent angiogenesis by transcriptionnally activating Wnt5a in breast cancer-associated fibroblasts. *Theranostics* 11, 4975-4991, doi:10.7150/thno.55074.

Wang, B., Liu, X.M., Liu, Z.N., Wang, Y., Han, X., Lian, A.B., Mu, Y., Jin, M.H., and Liu, J.Y. (2020a). Human hair follicle-derived mesenchymal stem cells: Isolation, expansion, and differentiation. *World J Stem Cells* 12, 462-470, doi:10.4252/wjsc.v12.i6.462.

Wang, F.T., Sun, W., Zhang, J.T., and Fan, Y.Z. (2019a). Cancer-associated fibroblast regulation of tumor neo-angiogenesis as a therapeutic target in cancer. *Oncol Lett* 17, 3055-3065, doi:10.3892/ol.2019.9973.

Wang, S., Drummond, M.L., Guerrero-Juarez, C.F., Tarapore, E., MacLean, A.L., Stabell, A.R., Wu, S.C., Gutierrez, G., That, B.T., Benavente, C.A. *et al.* (2020b). Single cell transcriptomics of human epidermis identifies basal stem cell transition states. *Nat Commun* 11, 4239, doi:10.1038/s41467-020-18075-7.

Wang, W., Olson, D., Liang, G., Franceschi, R.T., Li, C., Wang, B., Wang, S.S., and Yang, S. (2012). Collagen XXIV (Col24alpha1) promotes osteoblastic differentiation and mineralization through TGF-beta/Smads signaling pathway. *International journal of biological sciences* 8, 1310-1322, doi:10.7150/ijbs.5136.

Wang, X., He, Y., Zhang, Q., Ren, X., and Zhang, Z. (2021a). Direct Comparative Analyses of 10X Genomics Chromium and Smart-seq2. *Genomics Proteomics Bioinformatics* 19, 253-266, doi:10.1016/j.gpb.2020.02.005.

Wang, Y., Hunt, K., Nazareth, I., Freemantle, N., and Petersen, I. (2013). Do men consult less than women? An analysis of routinely collected UK general practice data. *BMJ Open* 3, e003320, doi:10.1136/bmjopen-2013-003320.

Wang, Y., Liang, Y., Xu, H., Zhang, X., Mao, T., Cui, J., Yao, J., Wang, Y., Jiao, F., Xiao, X. *et al.* (2021b). Single-cell analysis of pancreatic ductal adenocarcinoma identifies a novel fibroblast subtype associated with poor prognosis but better immunotherapy response. *Cell Discov* 7, 36, doi:10.1038/s41421-021-00271-4.

Wang, Y., Wang, L., Wen, X., Hao, D., Zhang, N., He, G., and Jiang, X. (2019b). NF-κB signaling in skin aging. *Mech Ageing Dev* 184, 111160, doi:10.1016/j.mad.2019.111160.

Watt, F.M. (2014). Mammalian skin cell biology: at the interface between laboratory and clinic. *Science* 346, 937-940, doi:10.1126/science.1253734.

Weber, C.E., Kothari, A.N., Wai, P.Y., Li, N.Y., Driver, J., Zapf, M.A., Franzen, C.A., Gupta, G.N., Osipo, C., Zlobin, A. *et al.* (2015). Osteopontin mediates an MZF1-TGF-beta1-dependent transformation of mesenchymal stem cells into cancer-associated fibroblasts in breast cancer. *Oncogene* 34, 4821-4833, doi:10.1038/onc.2014.410.

Wen, S., Niu, Y., Yeh, S., and Chang, C. (2015). BM-MSCs promote prostate cancer progression via the conversion of normal fibroblasts to cancer-associated fibroblasts. *International journal of oncology* 47, 719-727, doi:10.3892/ijo.2015.3060.

Whitfield, M.L., George, L.K., Grant, G.D., and Perou, C.M. (2006). Common markers of proliferation. *Nature reviews Cancer* 6, 99-106, doi:10.1038/nrc1802.

Wickham, H. (2016). ggplot2: Elegant Graphics for Data Analysis (Springer-Verlag New York).

Wozel, G., Sticherling, M., and Schön, M.P. (2010). Cutaneous side effects of inhibition of VEGF signal transduction. *J Dtsch Dermatol Ges* 8, 243-249, doi:10.1111/j.1610-0387.2009.07268.x.

Wu, S.Z., Roden, D.L., Wang, C., Holliday, H., Harvey, K., Cazet, A.S., Murphy, K.J., Pereira, B., Al-Eryani, G., Bartonicek, N. *et al.* (2020). Stromal cell diversity associated with immune evasion in human triple-negative breast cancer. *Embo j* 39, e104063, doi:10.15252/embj.2019104063.

Xie, S., and Skotheim, J.M. (2020). A G1 Sizer Coordinates Growth and Division in the Mouse Epidermis. *Curr Biol* 30, 916-924.e912, doi:10.1016/j.cub.2019.12.062.

Ye, Z., Zhang, C., Tu, T., Sun, M., Liu, D., Lu, D., Feng, J., Yang, D., Liu, F., and Yan, X. (2013). Wnt5a uses CD146 as a receptor to regulate cell motility and convergent extension. *Nat Commun* 4, 2803, doi:10.1038/ncomms3803.

Yerly, L., Pich-Bavastro, C., Di Domizio, J., Wyss, T., Tissot-Renaud, S., Cangkrama, M., Gilliet, M., Werner, S., and Kuonen, F. (2022). Integrated multi-omics reveals cellular and molecular interactions governing the invasive niche of basal cell carcinoma. *Nat Commun* 13, 4897, doi:10.1038/s41467-022-32670-w.

Yilmaz, A.S., Ozer, H.G., Gillespie, J.L., Allain, D.C., Bernhardt, M.N., Furlan, K.C., Castro, L.T., Peters, S.B., Nagarajan, P., Kang, S.Y. *et al.* (2017). Differential mutation frequencies in

metastatic cutaneous squamous cell carcinomas versus primary tumors. *Cancer* 123, 1184-1193, doi:10.1002/cncr.30459.

Zhang, L., Stokes, N., Polak, L., and Fuchs, E. (2011). Specific microRNAs are preferentially expressed by skin stem cells to balance self-renewal and early lineage commitment. *Cell Stem Cell* 8, 294-308, doi:10.1016/j.stem.2011.01.014.

Zhang, S., and Duan, E. (2018). Fighting against Skin Aging: The Way from Bench to Bedside. *Cell Transplant* 27, 729-738, doi:10.1177/0963689717725755.

Zhu, L., Zhang, G., Wang, P., Zhang, L., Ji, J., Liu, X., Zhou, Z., Zhao, J., and Wang, X. (2019). The effect of C-X-C motif chemokine ligand 13 in cutaneous squamous cell carcinoma treated with aminolevulinic acid-photodynamic therapy. *Photodiagnosis Photodyn Ther* 26, 389-394, doi:10.1016/j.pdpdt.2019.04.018.

Zijl, S., Salameti, V., Louis, B., Negri, V.A., and Watt, F.M. (2022). Dynamic regulation of human epidermal differentiation by adhesive and mechanical forces. *Current topics in developmental biology* 150, 129-148, doi:10.1016/bs.ctdb.2022.03.004.

Zou, M.L., Teng, Y.Y., Wu, J.J., Liu, S.Y., Tang, X.Y., Jia, Y., Chen, Z.H., Zhang, K.W., Sun, Z.L., Li, X. *et al.* (2021). Fibroblasts: Heterogeneous Cells With Potential in Regenerative Therapy for Scarless Wound Healing. *Front Cell Dev Biol* 9, 713605, doi:10.3389/fcell.2021.713605.

Zudaire, E., Martínez, A., Garayoa, M., Pío, R., Kaur, G., Woolhiser, M.R., Metcalfe, D.D., Hook, W.A., Siraganian, R.P., Guise, T.A. *et al.* (2006). Adrenomedullin is a cross-talk molecule that regulates tumor and mast cell function during human carcinogenesis. *Am J Pathol* 168, 280-291, doi:10.2353/ajpath.2006.050291.

9. Acknowledgments

Llorenç, and Manolo for all their help, valuable feedback and most of all a great time in and around the office. I enjoyed every cake with them, solid or liquid and I will certainly remember this time forever.

Finally, I want to say a special thank you to the three most important people. I am more than grateful that you were always by my side during the whole time and for your unconditional support. Thank you so much for always standing behind me and being happy about successful experiments for me as much as you agreed when I complained about it when something did not work out. I can always count on the three of you and I certainly would not be where I am today without you. Also, special thanks to Refaat for keeping me alive with delicious food that made the others in the Casino jealous.